TITLE: **YAP controls cell migration and invasion through a Rho-GTPase switch**

AUTHORS: Sagar R. Shah[1,2a,b], Chunxiao Ren[7], Nathaniel D. Tippens[2c], JinSeok Park[1,6d], Ahmed Mohyeldin[2e], Shuyan Wang[5], Guillermo Vela[2f], Juan C. Martinez-Gutierrez[2g], Seth S. Margolis[3], Susanne Schmidt[6], Shuli Xia[5], *Alfredo Quiñones-Hinojosa[2,4h*]*, *Andre Levchenko[7*]*

AFFILIATIONS:

(At the time work was primarily conducted)

Departments of [1]Biomedical Engineering, [2]Neurosurgery, [3]Biological Chemistry, [4]Oncology, The Johns Hopkins University School of Medicine, Baltimore, MD 21231, USA.

[5]Department of Neurology, Kennedy Krieger Institute, Baltimore, MD 21231, USA.

[6]CRBM-CNRS, University of Montpellier, 1919 route de Mende, 34293 Montpellier, France.

[7]Department of Biomedical Engineering and Yale Systems Biology Institute, Yale University, New Haven, CT, USA.

(Current affiliation)

[a]Department of Molecular Biology and Genetics, Cornell University, Ithaca, NY, USA.

[b]Weill Institute for Cell and Molecular Biology, Cornell University, Ithaca, NY, USA.

[c]Laronde, Cambridge, MA, USA.

[d]Children's Hospital Los Angeles & University of Southern California, Los Angeles, CA, USA

[e]Department of Neurosurgery, University of California – Irvine, Irvine, CA, USA

[f]Nebulab Technologies, Inc., San Antonio, Tx, USA.

[g]The University of Texas Health Science Center at Houston, Houston, TX, USA.

[h]Department of Neurologic Surgery, Mayo Clinic, Jacksonville, FL, USA.

*To whom correspondence should be addressed: Andre Levchenko, Ph.D. (andre.levchenko@yale.edu), Alfredo Quiñones-Hinojosa, M.D. (Quinones-Hinojosa.Alfredo@mayo.edu).

SUMMARY:

Understanding the mechanisms controlling the invasive spread of normal and transformed cells is central to understanding diverse processes including cancer progression. Here, we report that Yes-associated protein (YAP), a central transcriptional regulator implicated in controlling organ and body size, modulates a Rho-GTPase switch that drives cellular migration by directly transactivating the Rac1-GEF protein TRIO. Additionally, YAP and TRIO activate the Rac1-STAT3 axis to promote invasive behavior. While we find this YAP-dependent infiltrative program in many cell types, it is particularly enhanced in a patient-specific way in the most common malignant brain tumor, glioblastoma (GBM), where hyperactivation of the YAP-mediated TRIO and STAT3 network also confers poor patient outcome and up-regulation of genes associated with the Mesenchymal subtype of GBM. Our analysis suggests that the YAP-TRIO-STAT3 signaling network identified in this study is a ubiquitous regulator of invasive cell spread in both normal and pathological contexts.

KEYWORDS:

YAP, glioblastoma, migration, invasion, Rho-GTPase, TRIO, Rac1, RhoA, STAT3, brain cancer

INTRODUCTION:

Cell migration is a tightly regulated process integrating multiple extracellular cues through intracellular signaling networks, which in turn defines the extent of cell polarization and the persistence and speed of locomotion. Extensive studies over the past two decades identified the Rho family of small GTPases, including Rac1 and RhoA, as key regulators of these processes. Ongoing analysis of the regulation of these GTPases and their interaction(*1*) suggests that they form a molecular circuit integrating the inputs from multiple other signaling networks. Insight into these mechanistic links can help identify important molecular components, whose activity can determine the outcome of cell migration-dependent events in development and disease. Ultimately, unraveling these converging pathways will clarify the determinants of cell migration, and may offer new therapeutic paradigms against the aberrant invasion seen in many cancers. Targeting migration pathways may be particularly effective against cancer where most deaths are caused by invasive and metastatic cells rather than the primary tumor mass.

Since many extracellular cues affecting cell migration also guide decisions such as cellular identity, it is likely that migratory behaviors are tightly integrated with transcriptional decision networks. Notably, Yes-associated protein (YAP) is known to integrate many inputs (Hippo signaling, E-Cadherin, mechanical cues, etc.) to orchestrate diverse cellular functions including growth, apoptosis, and migration, as well as cancer cell invasion and metastasis(*2–12*). From these studies, YAP has emerged as a proto-oncogene frequently overexpressed in a variety of cancers, including a particularly aggressive and infiltrative form of brain cancer, glioblastoma (GBM)(*7–9*, *13–19*). However, it is not fully understood how YAP expression and activity play a role in the regulation of the molecular networks controlling cell migration and invasion, and whether this role may enhance the progression of aggressive cancers. Here, we demonstrate that YAP binds an enhancer region to promote transcription of TRIO, a guanine nucleotide exchange factor (GEF) protein that regulates Rho GTPases function(*20*). YAP-mediated TRIO up-regulation activates Rac1, which in turn inhibits RhoA to increase migration speed. In addition, an increase in YAP-mediated TRIO expression leads to the activation of Rac1-STAT3 signaling to confer invasive

potential. These findings reveal YAP-TRIO signaling as a central regulator of cell dispersion that promotes mobility through a Rho-GTPase switch and invasion through STAT3. In addition, our work provides new insights into the biology of aggressive cancers, including the potential prognostic relevance of YAP-TRIO-STAT3 signaling in glioblastoma and its clinical significance to the Mesenchymal subtype.

RESULTS:

YAP regulates migratory capacity

To analyze putative mechanisms of YAP-mediated control of migration and invasion, we used primary patient-derived cultures of human glioblastoma (GBM) cells due to their highly aggressive and invasive spread *in vivo* that may be associated with YAP hyperactivity(*13*, *21–24*). We also tested another commonly used GBM cell line, GBMA172. In addition, we explored whether these YAP-driven migratory and invasive mechanisms are conserved in non-pathological systems using cells from two different tissues of origin: adult human brain astrocytes (NHA) and adult human breast cells (MCF10A).

Using intraoperatively obtained primary GBM tissues from patients, we found that YAP protein expression was indeed elevated and transcriptionally active in a majority of GBMs examined (**Fig. 1a, Suppl Table 1, Fig. S1a-b**). From these primary GBM tissues, we derived primary cultures (JHGBM612, JHGBM640, JHGBM651, JHGBM1A) and confirmed that these cell lines had similarly high YAP protein levels as the primary GBM tissues from which they were derived, particularly in the nucleus (**Fig. S1c**). To test whether this elevated YAP expression contributes to changes in cell migration in these GBM cells, we used multiple shRNA constructs to specifically inhibit YAP expression (**Fig. S1d-e**). We then used this perturbation to investigate the migration of cells plated at low density on laminin- (NHA and GBM cell lines) or collagen-coated (MCF10A) 2D surfaces. We followed the migratory response at 10-minute intervals for 8 hours. Following the shRNA-mediated stable knockdown of YAP (shYAP) using two different targeting sequences (shYAP/shYAP-1, shYAP-2), we observed a significant decrease in cell displacement and migration speed when compared to the control non-targeting vector (shCtrl) in all GBM

cell lines and non-neoplastic NHA and MCF10A cells (**Fig. 1b-c, Fig. S1f-g, Movie S1**). Conversely, stable overexpression of a constitutively active YAP (YAP OE) versus control vector (CONT) in GBM (JHGBM612 and JHGBM1A) and NHA cells showed that YAP up-regulation was sufficient to increase migration speed (**Fig. 1d, Fig. S1h-i**). To determine whether YAP affects infiltrative cell migration and spread *in vivo*, we used a murine intracranial xenograft tumor model of human brain cancer(*25*, *26*), which recapitulated the cellular infiltration along the corpus callosum seen in the donor patient tumor (**Fig. S1j**). To do this, we injected 150,000 shCtrl or shYAP JHGBM612 cells into the striatum of the right hemisphere (at pre-determined coordinates from the bregma; see Materials and Methods) of immunocompromised mice and quantified the number of human GBM cells infiltrating along the corpus callosum into the left hemisphere 5 weeks post-injection. Firstly, we confirmed the presence of tumor after the xenograft transplantation of GBM cells by performing a standard H&E staining. The images indeed display features commonly seen in murine xenograft models of human GBM (**Fig. S1k**). More importantly, we observed significantly fewer shYAP cells infiltrating the contralateral hemisphere than shCtrl JHGBM612 cells (**Fig. 1e-f, Fig. S1l**). These findings, coupled with our *in vitro* observations, suggest that YAP can enhance infiltrative cell migration in different micro-environmental contexts.

We then sought to identify the mechanism by which YAP modulates migratory behavior in non-neoplastic and cancer cells. To do so, we examined the regulation of small Rho GTPases, which are implicated as central regulators of cell motility(*1*). Interestingly, we found that YAP knockdown increased the number and area of focal adhesions, strongly affecting the shape of the cells (**Fig. 1g-h, Fig. S1m-n**) in a pattern reminiscent of the focal adhesion assembly phenotype observed upon RhoA hyperactivation(*27*). Consistent with pronounced focal adhesion assembly, an increase in absolute levels and ratio of phosphorylated and total LIM-kinase, a downstream target of Rho-associated protein kinase (ROCK), a major effector of RhoA(*1*), was observed in shYAP JHGBM651, JHGBM612, JHGBM1A, NHA, and MCF10A cells than their corresponding shCtrl cells (**Fig. 1i, Fig. S2a**). From these results, we

conclude that YAP regulates cytoskeletal organization and dynamics to potentiate cellular motility *in vitro* and *in vivo*.

YAP regulates migration through a Rho-GTPase switch

To better understand the regulation of RhoA by YAP, we measured its GTP load through G-LISA assays. We observed a significant increase in RhoA-GTP levels after YAP knockdown in JHGBM651 and NHA cells (**Fig. 2a, Fig. S2b**). Based on this data, we sought to test the relevance of RhoA-ROCK activity on cell speed. We found that pharmacologic inhibition of ROCK I/II using either Y27632 or H1152 restored the migration speed of shYAP-1 and -2 cells in a dose-dependent manner while having no effect on shCtrl cells (**Fig. 2b, Fig. S2c, Movie S2**). Furthermore, treatment with Y12732 or H1152 decreased the phosphorylation of Nonmuscle Myosin II (NMII), confirming the inhibition of ROCK activity (**Fig. S2d**). These results demonstrate that YAP can modulate RhoA-ROCK activity and that ROCK inhibition is sufficient to rescue the migratory speed of YAP knockdown cells. These results suggest that YAP promotes migration at least in part by suppressing RhoA-ROCK activity.

YAP can modulate the activity of RhoA either directly or indirectly. For instance, prior studies suggested that another small Rho-GTPase, Rac1, can antagonistically regulate RhoA(*28–30*), raising the possibility that modulation of RhoA activity by YAP might involve Rac1. We indeed found that Rac1-GTP levels were reduced after YAP knockdown (**Fig. 2c, Fig. S3a**). We also examined a downstream target of Rac1, p21-activated kinase (PAK), and found a pronounced decrease in phosphorylated PAK (p-PAK) level after normalizing to the total PAK protein level in shYAP cells compared to shCtrl cells (**Fig. S3b**). Thus, we inquired whether changes in Rac1 activity accounted for the decreased migratory speed of shYAP cells. We found that a pharmacological inhibitor of Rac1-GEFs, NSC23766, significantly decreased the migration speed of shCtrl cells in a dose-dependent manner, but not that of shYAP-1 or -2 cells (**Fig 2d, Fig. S3c, Movie S3**). Collectively, these findings demonstrate that YAP regulates the small

Rho-GTPase network governing cellular polarity and migration, leading to the activation of Rac1 and inhibition of RhoA in normal and cancer cells **(Fig. S3d**).

We next sought to clarify the precise regulatory mechanisms of YAP's interaction with Rac1 and RhoA given multiple scenarios of mutual regulation between the components. Our results suggest three possible hypotheses: 1) YAP activates Rac1 to inhibit RhoA, 2) YAP inhibits RhoA to activate Rac1, or 3) YAP independently modulates both Rac1 and RhoA. To test these hypotheses, we applied the logic of epistatic analysis by using pharmacological inhibitors of these small Rho-GTPases in lieu of dominant negative mutants. More specifically, we used sequential perturbation of the network components to deduce the regulatory hierarchy (further details and logic of the experiment are presented in **Fig. S4a**). Unlike the experiments described in **Fig. 2a-d** which explored the dose dependence of the inhibitors on the shCtrl and shYAP cells, our experiment here explores the time dependence of cell responses to either single inhibitor or sequential inhibitor application at fixed concentrations, high enough to achieve the maximal effect (10μM Y27632 or 250μM NSC23766). In addition, the time of the initiation of the experiment is when the first or only inhibitor used is already present long enough for the inhibition effect to be achieved (1 hour). Hence, the response of the cells can only change if the application of the second inhibitor has an added effect. Otherwise, the effects are expected to result in an unchanging response over time. Using this logic, we first verified that the migration speeds of shCtrl and shYAP-1or -2 cells were stable over a 6-hour period with or without treatment using Y27632 or NSC23766 (**Fig. 2e, Panels I-III, Fig. S4b**). These results are consistent with our prior observations in **Fig. 2a-d**. Next, we used one or both pharmacological inhibitors of Rac1 and ROCK to determine how these signaling intermediates regulate each other in these cells. Specifically, we treated shCtrl and shYAP-1 or -2 cells with either the Rac1-GEF inhibitor or the ROCK inhibitor for 3 hours, followed by the addition of the other inhibitor for the next 3 hours (**Fig. 2e, Panels IV-V, Fig. S4b**). The order of inhibitor treatments was indispensable in this analysis to ascertain which one of the aforementioned hypotheses is valid (**Fig. S4a**). Remarkably, we found that in cells treated to inhibit ROCK, subsequent inhibition of Rac1-GEF did not further alter the migration speed in either

shCtrl or shYAP cells (**Fig. 2e, Panel IV, Fig. S4b**). However, ROCK inhibition after the initial Rac1-GEF inhibition rescued the cell migration speed of both shCtrl and shYAP cells (**Fig. 2e, Panel V, Fig. S4b**). Altogether, these results strongly favored the model in which YAP activates Rac1 to inhibit ROCK signaling, resulting in the enhancement of cell migration.

We then investigated the effect of Rac1-GEF or ROCK inhibition on the activity of RhoA and Rac1 in shCtrl and shYAP cells. Our model predicts that Rac1 activity is not dependent on RhoA-ROCK signaling, and indeed we observed no change in Rac1-GTP or RhoA-GTP levels upon ROCK inhibition (**Fig. 2f, Fig. S4c, Fig S4d**). Again, consistent with our model, we observed a significant increase in RhoA-GTP levels in both shCtrl and shYAP cells following Rac1 inhibition with NSC23766 (**Fig. 2g**). As expected, Rac1 inhibition also significantly reduced Rac1-GTP levels in both shCtrl and shYAP cells (**Fig. S4e**). Finally, we tested whether RhoA perturbation was sufficient to restore the migratory speed of shYAP cells. Treatment with two RhoA siRNAs or a dominant-negative RhoA (DN-RhoA) rescued the migratory speed of shYAP cells, with no significant effect on the migration speed of shCtrl cells (**Fig. 2h-j**). Likewise, introducing a constitutively active Rac1 construct yields similar results (**Fig. 2k**). These findings demonstrate that YAP activates Rac1, resulting in the inhibition of RhoA-ROCK signaling, which altogether enhances cellular migration (**Fig. S4f**). Thus, YAP simultaneously and sequentially tunes Rac1 and RhoA activities to potentiate cell motility.

YAP directly transactivates the Rac1-GEF TRIO to modulate Rac1 activity

Next, we sought to determine how the transcriptional co-activator YAP regulates the activity of Rac1. Small GTPases can be regulated by GTPase activating proteins (GAPs) and guanine nucleotide exchange factors (GEFs)(*31*). Since NSC23766 disrupts the interaction of Rac1 with two Rac1-GEFs, TRIO, and TIAM1(*32*), we sought to determine if YAP regulates one or both of these Rac1-GEFs. We observed a decrease in TRIO protein and gene expression after YAP knockdown in all cell lines tested using two independent YAP-targeting shRNA sequences (**Fig. 3a-b, Fig. S5a, b**). Moreover, TRIO

expression increased following YAP overexpression both in GBM and MCF10A cells (**Fig. 3c, Fig. S5c**). However, we did not observe any changes in TIAM1 gene expression in shYAP cells compared to shCtrl cells (**Fig. S5d**). Given that YAP, a transcriptional co-activator, cooperates with TEAD family transcription factors to directly modulate gene expression(*6*), we examined whether TRIO is transcriptionally regulated by YAP and whether YAP is found at known enhancer and promoter regions of TRIO. Using published chromatin immunoprecipitation (ChIP) sequencing data for YAP and TEAD4 in MDA-MB-231 cells(*33*), we found that both YAP and TEAD4 bind an intronic element of TRIO (Site 1: 14265617 to 14266192 base pairs on chromosome 5) that bears histone modification patterns indicative of active enhancers(*34*) (**Fig. 3d**). Specifically, this locus bears enhancer-associated H3K4 monomethylation (H3K4me1) and H3K27 acetylation (H3K27ac), with less promoter-associated H3K4 trimethylation (H3K4me3)(*35*). Notably, this enhancer region was independently reported to physically interact with TRIO's promoter(*36*). In addition, we found a weaker enrichment of YAP-TEAD4 binding at a second, intronic binding site (Site 2: 14268225 to 14268865 bp on chromosome 5) (**Fig. 3d**). By contrast, we found no evidence of YAP or TEAD4 binding at TIAM1 enhancer and promoter elements. We tested the MDA-MB-231 YAP binding sites by ChIP-PCR on both intronic TRIO enhancer sites in GBM cells. Indeed, significant YAP binding was observed at both enhancer sites of TRIO (**Fig. 3e, Fig. S5e**). To evaluate the functional consequence of this binding, we performed an enhancer luciferase assay using a 150 bp sequence (centered on the peak of YAP binding) paired with the promoter region of TRIO in HEK293 cells, with or without overexpression of YAP. We found that this sequence increased reporter activity compared to negative control and showed increased activity upon YAP overexpression (**Fig. 3f**). To further confirm that YAP only interacts with the enhancer and not the promoter sequence of TRIO, we performed an additional control experiment using a 1470 bp promoter sequence of TRIO paired with a luciferase reporter, with or without overexpression of YAP. Since Zanconato *et al*, have previously shown that YAP's transcriptional regulation is largely restricted to direct enhancer binding with a few exceptions like CTGF where YAP occupies its promoter region, we also included a 612 bp sequence of CTGF's

minimal promoter linked to a luciferase reporter as a positive control. Unlike CTGF's promoter, TRIO's full-length promoter sequence did not increase reporter activity and showed no enhancement in activity upon YAP overexpression (**Fig. S5f**). All these results suggest that YAP directly activates TRIO transcription by binding to its enhancer region.

Next, we examined whether YAP-TRIO signaling was sufficient to regulate Rac1 activity. We found an increase in Rac1-GTP levels in YAP OE cells compared to CONT cells (**Fig. 3g, Fig. S5g)**. Furthermore, stable overexpression of wildtype TRIO (TRIO OE) was sufficient to increase Rac1-GTP levels (**Fig. 3h, Fig. S5h)**. Consistent with these findings, shRNA-mediated stable knockdown of TRIO (shTRIO) decreased Rac1-GTP levels (**Fig. 3i, Fig. S5i)**. Given the antagonistic relationship between Rac1 and RhoA signaling, we assessed the activity of RhoA-GTP in these cells. We observed decreased RhoA-GTP levels in YAP OE and TRIO OE cells vs. control cells (**Fig. S5j**), and increased RhoA-GTP levels in shTRIO cells vs. shCtrl cells, paralleling our observations in shYAP cells (**Fig. S5l**). Collectively, these results demonstrate that YAP directly transactivates the Rac1-GEF TRIO and that TRIO is necessary and sufficient to activate Rac1 and inhibit RhoA.

Given that there has been evidence suggesting that TRIO-Rac1 signaling can inhibit YAP phosphorylation in HEK293 cells(*37*), we explored this potential feedback regulation in GBM cells. Interestingly, we did not observe any significant change in either phospho-YAP or YAP protein levels when we knocked down TRIO (**Fig. S5k**), indicating that no potential direct feedback regulation between YAP and TRIO-Rac1 signaling exists in the context of GBM cells.

To test whether our *in vitro* observations were consistent with data from clinical samples, we assessed TRIO expression in intraoperatively obtained primary GBM tissues from patients (**Fig. S5m**). We found that the full-length TRIO protein was indeed expressed in a majority of the GBM tissues analyzed. More importantly, its expression positively correlated with YAP expression in these clinical samples (**Fig. 3j**). Next, we surveyed gene expression profiles from the Repository for Molecular Brain Neoplasia Data (REMBRANDT) and The Cancer Genome Atlas (TCGA). Specifically, we explored

whether there was a correlation between YAP and either TRIO or TIAM1 expression in these two GBM datasets. To enable this analysis, we first derived a list of genes significantly downregulated in shYAP compared to shCtrl mRNA samples from JHGBM651 and JHGBM612 cells (See Materials and Methods) (**Suppl Table 2**). We refer to these YAP-regulated genes as the GB-YAP signature. Gene signatures allow a more robust estimation of YAP activity from gene expression datasets than mRNA alone, since many transcriptional regulators, including YAP, undergo significant post-transcriptional regulation. We found that the GB-YAP signature of GBM cells correlated with YAP signatures derived from other cell types(*38*) (**Fig. S5n**). Furthermore, the REMBRANT data suggested that the patients with elevated GB-YAP signature genes also have significantly higher expression of TRIO, but not TIAM1 (**Fig. 3k**). Indeed, patients with TRIO overexpression were significantly overrepresented among patients with high GB-YAP signature expression in this dataset (comparing all observed patient group sizes to random expectation using Fisher's exact test (**Fig. 3l**). Taken together, these results derived from patient-derived tumor tissues support our *in vitro* observations that YAP modulates TRIO expression.

TRIO is necessary and sufficient for YAP-driven migration

Given our previous results, we sought to test whether TRIO was necessary and/or sufficient for YAP's control of cell migration. Consistent with its putative functional role, we found that silencing the expression of TRIO decreased the migration speed of GBM, NHA, and MCF10A cells (**Fig. 4a, Fig. S6a-b, Movie S5**). As a preliminary test, we used a specific pharmacological inhibitor of TRIO, ITX3(*39*). We confirmed ITX3 specificity by treating shTRIO cells with this compound and observed no further change in migration speed or Rac1-GTP levels (**Fig. S6c-d**). We then found that ITX3 reduced the migration speed of shCtrl cells in a dose-dependent manner without affecting shYAP-1 or -2 cells (**Fig. S6d, Fig. S7a, Movie S4**). Furthermore, higher doses of ITX3 also decreased the migration speed of YAP OE GBM cells to match the speed of CONT cells (**Fig. S7b)**. Furthermore, ITX3 treatment significantly reduced Rac1-GTP levels in shCtrl and shYAP cells (**Fig. S7c**). Conversely, upon treatment with ITX3, a

significant increase in RhoA-GTP level was observed in shCtrl, but not in shYAP cells (**Fig. S7d)**, demonstrating negative regulation of RhoA activity by TRIO-Rac1 signaling downstream of YAP. These results suggest that the effects of YAP on RhoA-GTPases and cell migration can be entirely explained by TRIO expression.

We further explored whether YAP-mediated Rac1 activation was largely driven by TRIO. Given that we found that, in contrast to TRIO, the gene expression of TIAM1 was not reduced in shYAP cells, combined TIAM1/TRIO inhibition using NSC23766 did not significantly alter the migration speed or Rac1-GTP level of shTRIO-1 or -2 cells (**Fig. S7e-f**). On the other hand, the introduction of constitutively active Rac1 (CA-Rac1) rescued the migration speed in shTRIO cells but not shCtrl cells (**Fig. S7g**). Furthermore, we found no significant change in RhoA-GTP level in shTRIO cells treated with NSC23766, which contrasted with the increase seen in shCtrl cells treated with the inhibitor compared to vehicle (**Fig. S7h**). These results confirmed the specific role of TRIO but not TIAM1 signaling in mediating YAP's control of cell migration.

We then explored the effect of perturbations of TRIO on RhoA-dependent signaling and its phenotypic consequences. We found that ITX3 treatment significantly increased the RhoA-GTP level of shCtrl, but not shTRIO cells (**Fig. S8a**), providing additional evidence of the inhibitory effect of TRIO-dependent signaling on RhoA. Furthermore, the introduction of a dominant-negative RhoA construct (DN-RhoA) rescued the migratory phenotype of shTRIO cells but not of shCtrl cells (**Fig. S8b**). Suppression of the downstream effector of RhoA with the ROCK inhibitors, Y27632 or H1152, rescued the migration speed of shTRIO cells, like our observations with shYAP cells (**Fig. S8c, Movie S6**). Consistent with our prior results, ROCK inhibitors did not significantly affect Rac1-GTP or RhoA-GTP levels (**Fig. S8d)**, suggesting no feedback from ROCK on these Rho-GTPases. These results further indicate that TRIO inhibits RhoA activity to enhance cellular migration.

Next, we inquired whether TRIO was sufficient to rescue the migration speed of shYAP cells. First, we confirmed that overexpression of TRIO increases migratory speed (**Fig. 4b, Fig. S8e**).

Remarkably, overexpression of a knockdown-resistant TRIO in shYAP-1 or -2 cells (shYAP-1 or -2 + TRIO OE) completely rescued migration speed to levels of shCtrl cells (**Fig. 4c, Fig. S8f)**. To further explore the molecular mechanisms of TRIO activity, we focused on its GEF function. TRIO has two distinct GEF domains, GEF1 and GEF2 that control Rac1 and RhoA activation, respectively. However, our findings indicate that TRIO activates Rac1 signaling while inhibiting RhoA to potentiate migration. Thus, we sought to determine whether one or both GEF domains are relevant for this TRIO-mediated migratory behavior in GBM cells. We monitored migration speed upon stable overexpression of wildtype TRIO (TRIO OE), TRIO with inactivating GEF1 (TRIO iGEF1 OE) or GEF2 (TRIO iGEF2 OE) mutations (**Fig. 4d**). Notably, we observed an increase in migration speed of TRIO iGEF2 cells, phenocopying the migratory behavior of TRIO OE cells (**Fig. 4d**). However, we observed no change in migratory speed of TRIO iGEF1 cells (**Fig. 4d**). These results demonstrate that the GEF1 domain of TRIO, responsible for activation of Rac1, is indispensable for TRIO's pro-migratory effect. Moreover, TRIO's RhoA-activating GEF2 domain appears dormant and is dispensable for YAP-TRIO-driven migration in GBM cells. Our results demonstrate that TRIO is necessary and sufficient to account for Rac1 activation by YAP, resulting in RhoA inhibition and increased cell migration.

YAP promotes invasion by activating STAT3

In addition to modulation of migration speed, infiltration of the surrounding stroma tissue requires enhanced invasive capacity, enabling cell navigation in structurally complex tissue environments. Interestingly, in both the TCGA and REMBRANDT tumor gene expression datasets, the GB-YAP signature is associated with higher expression of an invasive gene signature (IGS)(*40*) (**Fig. 5a, Fig. S9a**). In a reciprocal fashion, patients with elevated expression of the IGS were significantly overrepresented among patients with high GB-YAP signature expression (**Fig. S9b**). Consistent with these observations, we observed that fewer shYAP and more YAP OE cells invaded through Matrigel-coated Boyden chambers than their respective control cells *in vitro* (**Fig. 5b-c, Fig. S9c**). This led us to explore the

mechanisms of YAP-mediated regulation of invasion by surveying genes implicated in ECM remodeling, degradation, and proteolysis(*41*, *42*). We found that MMP2 and MMP9 (as well as the YAP-target control CTGF) mRNA expression was decreased in shYAP GBM cells (**Fig. S9d**). Given that these genes are transactivated by STAT3(*43–45*), a transcription factor known to promote invasion and metastasis(*46*), we hypothesized that YAP may modulate STAT3 activity. Indeed, we found evidence of an association between elevated expression of the GB-YAP signature and a published GB-STAT3 signature(*47*), with significant overrepresentation of patients with elevated expression of the two signatures in GBM samples from both clinical datasets (**Fig. 5d-e, Fig. S9e**). This prompted us to further investigate this correlation between YAP and STAT3 activity. *In vitro*, we observed decreased phosphorylation of STAT3 on Tyr705 in shYAP-1 or -2 cells (**Fig. 5f, Fig. S9f**). Moreover, YAP OE cells expressed higher levels of phosphorylated STAT3 than CONT cells **(Fig. 5g, Fig. S9f)**. Functionally, pharmacological inhibition of STAT3 using LLL12 impaired both the invasive and migratory capacity of shCtrl cells more than that of shYAP cells (**Fig. 5h, Fig. S9g-h, Movie S7**). These results suggest that YAP activates STAT3 to drive both migration and invasion.

We then surveyed primary GBM tissues for expression and phosphorylation of STAT3 to assess a possible clinical significance of this factor (**Fig. 5i**). We indeed observed both expression and phosphorylation of STAT3 in most patient-derived tumor samples and the majority of specimens with elevated YAP expression also exhibited high STAT3 phosphorylation levels **(Fig. 5i-j)**. Conversely, only a few tumor samples with low YAP levels had high STAT3 phosphorylation **(Fig. 5i-j)**. Taken together, these clinical results lend support to our observations *in vitro* that YAP increases STAT3 activity to potentiate invasion.

YAP potentiates invasion by activating the TRIO-mediated Rac1-STAT3 axis

What is the mechanism of YAP-mediated STAT3 regulation? We explored the possibility that it might depend on the TRIO-mediated activation of Rac1 because there is evidence suggesting that Rac1

can activate STAT3(*48*). It is reported that Rac1 can directly bind to and regulate STAT3 activity(*49*, *50*). Rac1 can also indirectly induce STAT3 activity through the autocrine production of cytokine IL-6(*51*, *52*). Various normal biological processes involve activation of the Rac1-STAT3 signaling such as gland involution(*53*), chondrogenesis(*54*), and primordial follicle pool production(*55*). Additionally, studies have shown that the Rac1-STAT3 axis is important in promoting invasion and epithelial-mesenchymal transition in colorectal cancer(*50*) and gastric cancer(*56*). However, few efforts have been put into exploring this signaling axis in GBM. Given its presentation in clinical specimens and datasets, we sought to investigate its connection to the YAP-TRIO-Rac1 network. Firstly, we observed a decrease in STAT3 phosphorylation and invasion following the silencing of TRIO expression vs. shCtrl cells, phenocopying the decreased invasive capacity of shYAP cells (**Fig. 6a-b, Fig. S10a-b**). Similarly, applying TRIO inhibitor ITX3 decreased STAT3 phosphorylation levels in a dose-dependent manner (**Fig. S10c**). In addition, we observed reduced invasion of shCtrl cells treated with this TRIO inhibitor, but not in shYAP and shTRIO cells after treatment (**Fig. S10d**). Furthermore, TRIO OE GBM cells exhibited an increase in STAT3 phosphorylation and invasion compared to CONT cells (**Fig. 6c-d**). Remarkably, stable overexpression of TRIO in shYAP cells (shYAP + TRIO OE) recovered the phosphorylation levels of STAT3 to shCtrl cell levels (**Fig. 6e**). To explore the link between Rac1 and STAT3, we treated the cells with the Rac1-GEF inhibitor, and we observed decreased phospho-STAT3 expression in a dose-dependent manner, mirroring our findings with TRIO inhibition (**Fig. S10c**). We also tested the involvement of RhoA in this YAP-STAT3-signaling cascade by applying the ROCK inhibitors, Y26732 and H1152, in shYAP and shTRIO cells. Not surprisingly, ROCK inhibition rescued the invasive capacity of shYAP and shTRIO cells without significantly altering the invasion of shCtrl cells (**Fig. S10e**). These results suggest that not only Rac1 activation but also RhoA inhibition is involved in this YAP-driven regulation of cell invasion. Finally, we confirmed that there was a significant decrease in MMP2 protein level after knocking down YAP, TRIO, or STAT3 compared to shCtrl cells indicating that MMP2 acts as a candidate downstream target of STAT3 to promote GBM cell invasion (**Fig. S10f**). Collectively, these findings suggest that there

exists a crosstalk between STAT3 and YAP-TRIO driven Rho-GTPase switch to modulate the invasive capacity of GBM cells.

Given the critical role of YAP-TRIO signaling in driving the migratory and invasive capacity of GBM cells, we sought to evaluate the relevance of this cascade *in vivo* using our murine intracranial xenograft model of GBM infiltration. Specifically, we sought to determine whether TRIO is necessary for YAP-driven cellular infiltration *in vivo*. To that end, we established control (CONT) and YAP overexpressing (YAP OE) JHGBM612 cells with or without TRIO knockdown. *In vitro*, we found decreased STAT3 phosphorylation in both CONT + shTRIO and YAP OE + shTRIO cells, compared to their respective controls, reinforcing the relevance of TRIO signaling in YAP-driven STAT3 activation (**Fig. 6f**). Next, we injected 50,000 CONT + shCtrl, CONT + shTRIO, YAP OE + shCtrl, or YAP OE + shTRIO JHGBM612 cells into the striatum (at pre-determined coordinates from the bregma; see Materials and Methods) of immunocompromised mice and quantified the number of human GBM cells infiltrating along the corpus callosum 5-weeks post-injection. We observed that overexpression of YAP was sufficient to increase invasion of JHGBM612 cells via the corpus callosum into the contralateral hemisphere (CONT + shCtrl vs YAP OE + shCtrl; **Fig. 6g-h**). Moreover, knocking down TRIO significantly attenuated the invasive potential of these GBM cells (CONT + shCtrl vs CONT + shTRIO; **Fig. 6g-h**). In addition, we found a significant reduction in the number of YAP OE + shTRIO cells vs. YAP OE + shCtrl cells migrating through the corpus callosum (**Fig. 6g-h**). Together, these results indicated that while YAP is sufficient to increase the invasive capacity of GBM cells, TRIO is necessary to promote YAP-driven cell dispersion *in vivo*. In summary, our *in vitro* and *in vivo* findings identify TRIO as a critical switch through which YAP activates Rac1 and STAT3 signaling to potentiate cellular infiltration in GBMs (**Fig. 6i**).

YAP-TRIO-STAT3 signaling predicts poor clinical outcome in glioblastoma

Our results suggest YAP-driven migration and invasion are critical for the biology of aggressive cancers. We, therefore, explored the clinical implications of these findings for gliomas, of which GBM is

the highest grade (Grade 4) tumor with a median survival of 14 months. We found that GB-YAP signature expression increased with glioma grade in the REMBRANDT dataset (**Fig. S11a**); notably, STAT3 and TRIO have also been reported to increase with glioma grade(*57*). Additionally, the percentage of glioma patients overexpressing the GB-YAP signature compared to non-cancer cortex increased with glioma grade (**Fig. 7a**). Having found that YAP is hyperactive in GBMs, we focused on its prognostic value for these patients as determined by Kaplan-Meier analyses. Strikingly, higher expression of the GB-YAP signature predicted poor prognosis of GBM patients from both TCGA (**Fig. 7b**) and REMBRANDT cohorts (**Fig. S11b**). In addition, the YAP gene signature was more predictive than 91.5% of 1 million simulated, size-matched gene sets (empirical $p = 0.085$), suggesting it is one of the most predictive gene sets of its size.

Due to the molecular heterogeneity of GBMs, we explored if YAP activity was associated with one or more of the GBM subtypes including proneural, classical, and mesenchymal subtypes recently described by Wang et al(*58*). Notably, Mesenchymal GBMs are distinguished by the invasion of brain parenchyma coupled with pronounced angiogenesis(*59*). Moreover, the transcription factors STAT3 and C/EBPβ have been proposed to synergistically drive Mesenchymal GBMs(*47*). Of interest, TAZ, a paralog of YAP, was also found to potentiate Mesenchymal differentiation and transformation, but in a fashion that is independent of STAT3- and C/EBPβ, through direct transcriptional activation(*60*). Consistently, Bhat *et al*(*60*) observed no modulation of STAT3 upon TAZ knockdown in GBM cells. These results raised the possibility that YAP might modulate the Mesenchymal phenotype associated with the eponymous sub-class in a way distinct from TAZ, through the activation of STAT3. Indeed, there was a significant over-representation of GB-YAP-high patients among the Mesenchymal GBMs, but not among other subclasses (**Fig. 7c**). Furthermore, our findings that YAP-TRIO signaling regulated the activity of STAT3 by promoting its phosphorylation (**Fig. 5, Fig. 6, Fig. S9, Fig. S10**) suggest that YAP may be a driver of mesenchymal reprogramming in GBMs. Consistent with this hypothesis, higher expression of the GB-YAP signature corresponded to higher expression of Mesenchymal subclass genes in both GBM

datasets (**Fig. 7d**). *In vitro*, we observed decreased expression levels of several Mesenchymal subclass genes after YAP knockdown in all three GBM cell lines (**Fig. 7e**). Taken together, these results demonstrate that YAP can drive Mesenchymal subclass-related genes in GBMs at least in part by modulating STAT3 activity.

Interestingly, we also found that YAP-low patients were significantly overrepresented among GBMs in the glioma CpG island methylator phenotype (G-CIMP) subclass, which exhibits hypermethylation at CpG islands and longer progression-free survival (**Fig. 7c**). This result suggested that patients with lower YAP activity would present a less aggressive subtype of GBM, and most patients in this group might not benefit from any potential therapies targeting YAP. To explore this idea further, we inquired whether the prognostic power associated with enhanced YAP activity was restricted to a particular subclass of patients. Using Kaplan-Meier analyses, we evaluated progression-free survival along with YAP signature expression in each GBM subclass individually. Strikingly, higher expression of the GB-YAP signature predicted rapid recurrence in all the GBM subclasses except the G-CIMP subtype (**Fig. S11c-e**). This suggests that YAP-targeted therapies may be effective for patients with non-G-CIMP tumors, and especially the Mesenchymal subclass.

We then investigated whether the YAP-TRIO-STAT3 signaling axis is clinically relevant in GBMs. First, using the TCGA dataset, we determined the distribution of patient groups with hyperactivation of either one, two, or all three of the network components (i.e., YAP, TRIO, and STAT3). Hyperactivation was determined using the GB-YAP signature, TRIO transcript, and GB-STAT3 signature (**Fig. 7f**). Indeed, we found a significant over-representation of GBM patients with hyperactivation of all the three members of the YAP-TRIO-STAT3 molecular network. Next, we stratified patients into 8 groups representing every possible combination of YAP, TRIO, and STAT3 co-activation, and performed Kaplan-Meier survival analyses. Notably, the groups that exhibited YAP co-activation with either TRIO or STAT3 had a significantly worse prognosis than the group without hyperactivation of any of these proteins (YAP^{LOW}, $TRIO^{LOW}$, $STAT3^{LOW}$) (**Fig. 7g-i, Fig. S11f-g, Fig. S12)**. Furthermore, the results

showed that YAP+TRIO or YAP+STAT3 co-activation was associated with a similarly poor prognosis as hyperactivation of all three regulators (i.e. YAP^{HIGH}, $TRIO^{HIGH}$, $STAT3^{HIGH}$). Importantly, hyperactivation of TRIO and STAT3 (i.e., TRIO+STAT3) without high YAP activity did not appear to be associated with poor patient prognosis in this dataset (**Fig. S12**), emphasizing the prognostic power of YAP-dependent signaling. Overall, these analyses emphasize the co-dependence of TRIO and STAT3 on YAP to confer poor patient prognosis. These results should be viewed as preliminary, as the tumor purity, mRNA degradation, and cohort size might be confounding factors in this analysis. Larger patient cohorts with matched expression data, which are currently unavailable, would help to validate these results. Nevertheless, collectively, our study provides important initial evidence of the clinical value of the YAP-driven pro-migratory and invasive genetic circuit in predicting patient outcomes (**Fig. 7j**).

DISCUSSION:

This study suggests a central and widespread role for YAP in controlling the migratory speed and invasiveness of several cancer and normal cell types through the modulation of a Rho-GTPase switch. Previous work has illustrated the function of cytoplasmic YAP in regulating endothelial cell migration(*61*). Our work uncovers a YAP-mediated signaling circuit focusing on the role of nuclear YAP as a transcriptional coactivator. Specifically, we demonstrate that YAP increases the expression of the Rac1-GEF TRIO, leading to activation of Rac1 and inhibition of RhoA small GTPases, and subsequently resulting in STAT3 activation. This intricate cascade simultaneously promotes cell motility and invasion, using both transcriptional and post-transcriptional mechanisms (**Fig. 7j**). Furthermore, we find that, although TRIO harbors two GEF domains, its YAP-driven functions are mediated by the GEF1 domain's activation of Rac1. This agrees with studies in different systems that demonstrate Rac1 is the major target of TRIO(*20*). One known example of RhoA activation by TRIO is Gaq signaling, where Gaq binds to the PH2 module within the GEF2 domain, releasing PH2-mediated inhibition of DH2, thereby stimulating GEFD2 activity on RhoA(*62*). Nevertheless, the activity of both Rac1 and RhoA was found

to be important in mediating the YAP-driven TRIO-dependent control of cell migration and invasion, suggesting the importance of the crosstalk between Rac1 and RhoA, downstream of TRIO activation.

Intriguingly, it has been reported that TRIO-mediated Rho-GTPase signaling can regulate YAP(*63–68*) which, coupled with our results, suggests that regulation between YAP and Rho-GTPases can be mutually enhancing, constituting a feedback loop that can stabilize migratory and invasive phenotypes. Recently, it has been shown that YAP regulates actin dynamics through the modulation of ARHGAP29 to promote metastasis of gastric cancer cells(*69*). Interestingly, unlike in GBM, YAP modulates Rac1 via transactivation of the Rac1-GEF, TIAM1, through an enhancer-mediated mechanism, during invadopodia formation in breast cancer, supporting the argument for disease-specific regulation(*70*). Since YAP expression and activity are controlled by a diverse range of stimuli and genetic alterations(*3*, *5*, *7*, *14*, *15*, *64*, *67*, *71*), the evidence of crosstalk between YAP, Rho-GTPases, and STAT3 establishes a wide spectrum of inputs and mechanisms that regulate cell locomotion. Furthermore, our results implicate YAP and STAT3 as key transcriptional regulators of cell migration and invasion, which could aid the development of metastatic gene expression signatures for cancer. A recent study reported the role of YAP signaling in the activation of the JAK-STAT3 pathway to regulate endothelial cell proliferation during angiogenesis(*72*), further establishing the significance of YAP-mediated activation of STAT3 in different phenotypic and cellular contexts. Similar to our findings, others have demonstrated the regulation of STAT3 by Rac1, further reinforcing the relationship between these signaling cascades. Likewise, additional studies have shown that STAT3 activation by YAP through other intermediatory regulators can be facilitated by direct interaction. Altogether, these findings support a model of crosstalk between multiple shared signaling components in a cell-type and context-specific manner.

Together with our previous study by Park *et al*(*73*), our results suggest that YAP-controlled cell migration and invasion are fundamental functions present in many cell types. This pathway may be particularly important in developmental and physiological contexts involving episodes of large-scale migration, such as wound healing and progenitor cell navigation during neural tissue development. In this

context, our study suggests that the central role of YAP in controlling cell and tissue growth is balanced by regulating cell dispersion required by many morphogenetic events.

Given the widespread hyperactivation of YAP in many cancers(*11*), our study further clarifies the mechanisms controlling invasive cancer cell phenotypes. One of the hallmarks of tumor malignancy and progression to higher pathological grades is the ability of cancer cells to invade their surrounding parenchyma, intravasate surrounding blood, and lymphatic vessels, and eventually, seed distant tissues as metastatic tumors(*74*). Tumor recurrence and lethality can be greatly aided by the migratory and invasive capacity of cells(*75*). While the YAP-TEAD interaction has been shown to promote metastasis in breast cancer(*6*), the downstream signals responsible for increased metastatic potential have remained poorly understood. As with metastatic cancers, GBMs often evade eradication because individual cells spread from the primary bulk tumor, thus making complete resection and localized radiation treatment virtually impossible. Clinically, more than half of metastatic tumors display pronounced local infiltration(*24*) and can recur in as little as 3 months despite radical surgery, chemo- and radiotherapy(*21–23*). Thus, understanding the molecular basis for cell dispersal can inform patient prognosis and facilitate the development of improved treatment modalities(*75–78*).

Our finding that YAP-TRIO signaling can promote STAT3 activity through activation of Rac1 establishes a novel pro-invasive signaling axis with possible therapeutic implications in glioblastoma and other cancers, where YAP and STAT3 can independently and synergistically confer malignancy and predict poor prognosis(*47*). Moreover, this YAP-TRIO-STAT3 network is found in multiple cell types and thus forms a general molecular framework for predicting clinical outcomes in aggressive cancers such as glioblastoma. Importantly, our work highlights the dependency of the downstream effects exercised by YAP on TRIO and/or STAT3 activation in conferring poor GBM patient prognosis. Therefore, our study suggests that a network, systems perspective on the etiology of aggressive cancers can benefit from explicit analysis of molecular cascades that integrate numerous signaling pathways, inform the design of

targeted and combination therapies, as well as augment our understanding of the drivers of transcriptionally distinct tumor subtypes.

ACKNOWLEDGEMENTS:

We thank the Department of Neurological Surgery and Oncology at Johns Hopkins Hospital for access to intraoperatively-obtained glioblastoma tissues; Lakesha Johnson and Liron Noiman for establishing primary cell cultures of these primary glioblastoma specimens; Colette Ap Rhys for designing and preparing lentiviruses; Conover Talbot Jr. for technical support and helpful discussions of microarray analysis; Tom Schaffer for technical support with the RhoA-GTP pull-down assay; and Kaisorn L. Chaichana for glioblastoma patient MRI images. This research was funded by NIH R01 NS070024 and NIH 5K08 NS055851 (A.Q.-H), and U54 CA209992 and U01 CA155758 (A.L). S.R.S. was supported by the National Science Foundation Graduate Research Fellowship. A.M. was supported by the Maryland Stem Cell Postdoctoral Research Fellowship.

AUTHOR CONTRIBUTIONS:

S.R.S. conceived and designed the project. S.R.S., N.D.T. performed the experiments. C.R. assisted with the experiments. N.D.T. performed bioinformatic analysis. J.P. tracked and analyzed migration time-lapse data. A.M. and G.V. assisted with early experiments. J.C.M-G assisted with YAP-TRIO *in vitro* rescue experiments. S.S. provided TRIO wildtype and mutant lentiviral and corresponding control constructs. S.W., and S. X. assisted with YAP-TRIO *in vivo* experiment. S.R.S., N.D.T., C.R., and J.P. interpreted the results. A.L. and A.Q.-H. supervised the project. S.R.S. and N.D.T. wrote the manuscript. S.R.S., C.R., S.M., A.L., and A.Q.-H. reviewed and revised the manuscript.

DECLARATION OF INTERESTS:

Microarray data of shCtrl and shYAP JHGBM651 and JHGBM612 cells have been deposited with NCBI Gene Expression Omnibus under accession code (*upon acceptance of manuscript*). Reprints and permissions information is available at www.nature.com/reprints. The authors declare no competing financial interests. Correspondence and requests for material should be addressed to A.L. (andre.levchenko@yale.edu) or A.Q.-H (Quinones-Hinojosa.Alfredo@mayo.edu).

REFERENCES:

1. E. Sahai, C. J. Marshall, RHO-GTPases and cancer. *Nat Rev Cancer*. **2**, 133–142 (2002).

2. F. Calvo, N. Ege, A. Grande-Garcia, S. Hooper, R. P. Jenkins, S. I. Chaudhry, K. Harrington, P. Williamson, E. Moeendarbary, G. Charras, E. Sahai, Mechanotransduction and YAP-dependent matrix remodelling is required for the generation and maintenance of cancer-associated fibroblasts. *Nat Cell Biol*. **15**, 637–646 (2013).

3. D. Chen, Y. Sun, Y. Wei, P. Zhang, A. H. Rezaeian, J. Teruya-Feldstein, S. Gupta, H. Liang, H.-K. Lin, M.-C. Hung, L. Ma, LIFR is a breast cancer metastasis suppressor upstream of the Hippo-YAP pathway and a prognostic marker. *Nat Med*. **18**, 1511–1517 (2012).

4. J. Dong, G. Feldmann, J. Huang, S. Wu, N. Zhang, S. A. Comerford, M. F. Gayyed, R. A. Anders, A. Maitra, D. Pan, Elucidation of a universal size-control mechanism in Drosophila and mammals. *Cell*. **130**, 1120–1133 (2007).

5. S. Dupont, L. Morsut, M. Aragona, E. Enzo, S. Giulitti, M. Cordenonsi, F. Zanconato, J. Le Digabel, M. Forcato, S. Bicciato, N. Elvassore, S. Piccolo, Role of YAP/TAZ in mechanotransduction. *Nature*. **474**, 179–183 (2011).

6. J. M. Lamar, P. Stern, H. Liu, J. W. Schindler, Z.-G. Jiang, R. O. Hynes, The Hippo pathway target, YAP, promotes metastasis through its TEAD-interaction domain. *Proceedings of the National Academy of Sciences*. **109**, E2441–E2450 (2012).

7. M. Overholtzer, J. Zhang, G. A. Smolen, B. Muir, W. Li, D. C. Sgroi, C.-X. Deng, J. S. Brugge, D. A. Haber, Transforming properties of YAP, a candidate oncogene on the chromosome 11q22 amplicon. *Proc Natl Acad Sci U S A*. **103**, 12405–12410 (2006).

8. S. R. Shah, J. M. David, N. D. Tippens, A. Mohyeldin, J. C. Martinez-Gutierrez, S. Ganaha, P. Schiapparelli, D. H. Hamilton, C. Palena, A. Levchenko, A. Quiñones-Hinojosa, Brachyury-YAP Regulatory Axis Drives Stemness and Growth in Cancer. *Cell Rep*. **21**, 495–507 (2017).

9. S. Wei, J. Wang, O. Oyinlade, D. Ma, S. Wang, L. Kratz, B. Lal, Q. Xu, S. Liu, S. R. Shah, H. Zhang, Y. Li, A. Quiñones-Hinojosa, H. Zhu, Z.-Y. Huang, L. Cheng, J. Qian, S. Xia, Heterozygous IDH1R132H/WT created by “single base editing” inhibits human astroglial cell growth by downregulating YAP. *Oncogene*. **37**, 5160–5174 (2018).

10. S. A. Mosaddad, Y. Salari, S. Amookhteh, R. S. Soufdoost, Response to Mechanical Cues by Interplay of YAP/TAZ Transcription Factors and Key Mechanical Checkpoints of the Cell:A Comprehensive Review. *Cell Physiol Biochem*. **55**, 33–60 (2021).

11. S. Piccolo, T. Panciera, P. Contessotto, M. Cordenonsi, YAP/TAZ as master regulators in cancer: modulation, function and therapeutic approaches. *Nat Cancer*, 1–18 (2022).

12. O. Kilic, A. Yoon, S. R. Shah, H. M. Yong, A. Ruiz-Valls, H. Chang, R. A. Panettieri, S. B. Liggett, A. Quiñones-Hinojosa, S. S. An, A. Levchenko, A microphysiological model of the bronchial airways reveals the interplay of mechanical and biochemical signals in bronchospasm. *Nat Biomed Eng*. **3**, 532–544 (2019).

13. B. A. Orr, H. Bai, Y. Odia, D. Jain, R. A. Anders, C. G. Eberhart, Yes-associated protein 1 is widely expressed in human brain tumors and promotes glioblastoma growth. *J Neuropathol Exp Neurol*. **70**, 568–577 (2011).

14. D. Pan, The hippo signaling pathway in development and cancer. *Dev Cell*. **19**, 491–505 (2010).

15. Y. Xu, I. Stamenkovic, Q. Yu, CD44 attenuates activation of the Hippo signaling pathway and is a prime therapeutic target for glioblastoma. *Cancer Res*. **70**, 2455–2464 (2010).

16. S. R. Shah, A. Quinones-Hinojosa, S. Xia, Advances in Brain Cancer: Creating Monoallelic Single Point Mutation in IDH1 by Single Base Editing. *J Oncol Res Ther*. **5**, 166 (2019).

17. L. Li, J. Luo, J.-Y. Fang, R. Zhang, J.-B. Ma, Z.-P. Zhu, Expression characteristics of the yes-associated protein in breast cancer: A meta-analysis. *Medicine (Baltimore)*. **101**, e30176 (2022).

18. X. Hu, Y. Zhang, H. Yu, Y. Zhao, X. Sun, Q. Li, Y. Wang, The role of YAP1 in survival prediction, immune modulation, and drug response: A pan-cancer perspective. *Front Immunol*. **13**, 1012173 (2022).

19. M. Castellan, A. Guarnieri, A. Fujimura, F. Zanconato, G. Battilana, T. Panciera, H. L. Sladitschek, P. Contessotto, A. Citron, A. Grilli, O. Romano, S. Bicciato, M. Fassan, E. Porcù, A. Rosato, M. Cordenonsi, S. Piccolo, Single-cell analyses reveal YAP/TAZ as regulators of stemness and cell plasticity in glioblastoma. *Nat Cancer*. **2**, 174–188 (2021).

20. S. Schmidt, A. Debant, Function and regulation of the Rho guanine nucleotide exchange factor Trio. *Small GTPases*. **5**, e29769 (2014).

21. E. Bell, L. J. Karnosh, Cerebral hemispherectomy; report of a case 10 years after operation. *J Neurosurg*. **6**, 285–293 (1949).

22. K. L. Chaichana, P. Zadnik, J. D. Weingart, A. Olivi, G. L. Gallia, J. Blakeley, M. Lim, H. Brem, A. Quiñones-Hinojosa, Multiple resections for patients with glioblastoma: prolonging survival. *J Neurosurg*. **118**, 812–820 (2013).

23. W. E. DANDY, REMOVAL OF RIGHT CEREBRAL HEMISPHERE FOR CERTAIN TUMORS WITH HEMIPLEGIA: PRELIMINARY REPORT. *Journal of the American Medical Association*. **90**, 823–825 (1928).

24. Y. Matsukado, C. S. Maccarty, J. W. Kernohan, The growth of glioblastoma multiforme (astrocytomas, grades 3 and 4) in neurosurgical practice. *J Neurosurg*. **18**, 636–644 (1961).

25. J. Lee, S. Kotliarova, Y. Kotliarov, A. Li, Q. Su, N. M. Donin, S. Pastorino, B. W. Purow, N. Christopher, W. Zhang, J. K. Park, H. A. Fine, Tumor stem cells derived from glioblastomas cultured in bFGF and EGF more closely mirror the phenotype and genotype of primary tumors than do serum-cultured cell lines. *Cancer Cell*. **9**, 391–403 (2006).

26. S. M. Pollard, K. Yoshikawa, I. D. Clarke, D. Danovi, S. Stricker, R. Russell, J. Bayani, R. Head, M. Lee, M. Bernstein, J. A. Squire, A. Smith, P. Dirks, Glioma stem cell lines expanded in adherent culture have tumor-specific phenotypes and are suitable for chemical and genetic screens. *Cell Stem Cell*. **4**, 568–580 (2009).

27. A. J. Ridley, A. Hall, The small GTP-binding protein rho regulates the assembly of focal adhesions and actin stress fibers in response to growth factors. *Cell*. **70**, 389–399 (1992).

28. M. Parri, P. Chiarugi, Rac and Rho GTPases in cancer cell motility control. *Cell Communication and Signaling*. **8**, 23 (2010).

29. G. A. Wildenberg, M. R. Dohn, R. H. Carnahan, M. A. Davis, N. A. Lobdell, J. Settleman, A. B. Reynolds, p120-catenin and p190RhoGAP regulate cell-cell adhesion by coordinating antagonism between Rac and Rho. *Cell*. **127**, 1027–1039 (2006).

30. L. K. Nguyen, B. N. Kholodenko, A. von Kriegsheim, Rac1 and RhoA: Networks, loops and bistability. *Small GTPases*. **9**, 316–321 (2018).

31. J. L. Bos, H. Rehmann, A. Wittinghofer, GEFs and GAPs: Critical Elements in the Control of Small G Proteins. *Cell*. **129**, 865–877 (2007).

32. Y. Gao, J. B. Dickerson, F. Guo, J. Zheng, Y. Zheng, Rational design and characterization of a Rac GTPase-specific small molecule inhibitor. *Proc Natl Acad Sci U S A*. **101**, 7618–7623 (2004).

33. F. Zanconato, M. Forcato, G. Battilana, L. Azzolin, E. Quaranta, B. Bodega, A. Rosato, S. Bicciato, M. Cordenonsi, S. Piccolo, Genome-wide association between YAP/TAZ/TEAD and AP-1 at enhancers drives oncogenic growth. *Nat Cell Biol*. **17**, 1218–1227 (2015).

34. N. D. Heintzman, R. K. Stuart, G. Hon, Y. Fu, C. W. Ching, R. D. Hawkins, L. O. Barrera, S. Van Calcar, C. Qu, K. A. Ching, W. Wang, Z. Weng, R. D. Green, G. E. Crawford, B. Ren, Distinct and predictive chromatin signatures of transcriptional promoters and enhancers in the human genome. *Nat Genet*. **39**, 311–318 (2007).

35. A. Sethi, M. Gu, E. Gumusgoz, L. Chan, K.-K. Yan, J. Rozowsky, I. Barozzi, V. Afzal, J. A. Akiyama, I. Plajzer-Frick, C. Yan, C. S. Novak, M. Kato, T. H. Garvin, Q. Pham, A. Harrington, B. J. Mannion, E. A. Lee, Y. Fukuda-Yuzawa, A. Visel, D. E. Dickel, K. Y. Yip, R. Sutton, L. A. Pennacchio, M. Gerstein, Supervised enhancer prediction with epigenetic pattern recognition and targeted validation. *Nat Methods*. **17**, 807–814 (2020).

36. F. Jin, Y. Li, J. R. Dixon, S. Selvaraj, Z. Ye, A. Y. Lee, C.-A. Yen, A. D. Schmitt, C. A. Espinoza, B. Ren, A high-resolution map of the three-dimensional chromatin interactome in human cells. *Nature*. **503**, 290–294 (2013).

37. J.-W. Jang, M.-K. Kim, Y.-S. Lee, J.-W. Lee, D.-M. Kim, S.-H. Song, J.-Y. Lee, B.-Y. Choi, B. Min, X.-Z. Chi, S.-C. Bae, RAC-LATS1/2 signaling regulates YAP activity by switching between the YAP-binding partners TEAD4 and RUNX3. *Oncogene*. **36**, 999–1011 (2017).

38. M. Cordenonsi, F. Zanconato, L. Azzolin, M. Forcato, A. Rosato, C. Frasson, M. Inui, M. Montagner, A. R. Parenti, A. Poletti, M. G. Daidone, S. Dupont, G. Basso, S. Bicciato, S. Piccolo, The Hippo Transducer TAZ Confers Cancer Stem Cell-Related Traits on Breast Cancer Cells. *Cell*. **147**, 759–772 (2011).

39. N. Bouquier, E. Vignal, S. Charrasse, M. Weill, S. Schmidt, J.-P. Léonetti, A. Blangy, P. Fort, A cell active chemical GEF inhibitor selectively targets the Trio/RhoG/Rac1 signaling pathway. *Chem Biol*. **16**, 657–666 (2009).

40. R. Liu, X. Wang, G. Y. Chen, P. Dalerba, A. Gurney, T. Hoey, G. Sherlock, J. Lewicki, K. Shedden, M. F. Clarke, The Prognostic Role of a Gene Signature from Tumorigenic Breast-Cancer Cells. *New England Journal of Medicine*. **356**, 217–226 (2007).

41. J.-I. Jun, L. F. Lau, Taking aim at the extracellular matrix: CCN proteins as emerging therapeutic targets. *Nat Rev Drug Discov*. **10**, 945–963 (2011).

42. C. M. Overall, C. López-Otín, Strategies for MMP inhibition in cancer: innovations for the post-trial era. *Nat Rev Cancer*. **2**, 657–672 (2002).

43. T. N. Dechow, L. Pedranzini, A. Leitch, K. Leslie, W. L. Gerald, I. Linkov, J. F. Bromberg, Requirement of matrix metalloproteinase-9 for the transformation of human mammary epithelial cells by Stat3-C. *Proc Natl Acad Sci U S A*. **101**, 10602–10607 (2004).

44. D. Hilfiker-Kleiner, A. Hilfiker, M. Fuchs, K. Kaminski, A. Schaefer, B. Schieffer, A. Hillmer, A. Schmiedl, Z. Ding, E. Podewski, E. Podewski, V. Poli, M. D. Schneider, R. Schulz, J.-K. Park, K. C. Wollert, H. Drexler, Signal transducer and activator of transcription 3 is required for myocardial capillary growth, control of interstitial matrix deposition, and heart protection from ischemic injury. *Circ Res*. **95**, 187–195 (2004).

45. T.-X. Xie, D. Wei, M. Liu, A. C. Gao, F. Ali-Osman, R. Sawaya, S. Huang, Stat3 activation regulates the expression of matrix metalloproteinase-2 and tumor invasion and metastasis. *Oncogene*. **23**, 3550–3560 (2004).

46. H. Yu, D. Pardoll, R. Jove, STATs in cancer inflammation and immunity: a leading role for STAT3. *Nat Rev Cancer*. **9**, 798–809 (2009).

47. M. S. Carro, W. K. Lim, M. J. Alvarez, R. J. Bollo, X. Zhao, E. Y. Snyder, E. P. Sulman, S. L. Anne, F. Doetsch, H. Colman, A. Lasorella, K. Aldape, A. Califano, A. Iavarone, The transcriptional network for mesenchymal transformation of brain tumours. *Nature*. **463**, 318–325 (2010).

48. J. Corry, H. R. Mott, D. Owen, Activation of STAT transcription factors by the Rho-family GTPases. *Biochemical Society Transactions*. **48**, 2213–2227 (2020).

49. A. R. Simon, H. G. Vikis, S. Stewart, B. L. Fanburg, B. H. Cochran, K.-L. Guan, Regulation of STAT3 by Direct Binding to the Rac1 GTPase. *Science*. **290**, 144–147 (2000).

50. K. Zhou, J. Rao, Z. Zhou, X. Yao, F. Wu, J. Yang, L. Yang, X. Zhang, Y. Cui, X.-W. Bian, Y. Shi, Y. Ping, RAC1-GTP promotes epithelial-mesenchymal transition and invasion of colorectal cancer by activation of STAT3. *Laboratory Investigation*. **98**, 989–998 (2018).

51. T. R. Faruqi, D. Gomez, X. R. Bustelo, D. Bar-Sagi, N. C. Reich, Rac1 mediates STAT3 activation by autocrine IL-6. *Proc Natl Acad Sci U S A*. **98**, 9014–9019 (2001).

52. E. L. Morgan, A. Macdonald, Autocrine STAT3 activation in HPV positive cervical cancer through a virus-driven Rac1—NFκB—IL-6 signalling axis. *PLOS Pathogens*. **15**, e1007835 (2019).

53. H. Bagci, M. Laurin, J. Huber, W. J. Muller, J.-F. Côté, Impaired cell death and mammary gland involution in the absence of Dock1 and Rac1 signaling. *Cell Death Dis*. **5**, e1375–e1375 (2014).

54. H. Kim, J. K. Sonn, Rac1 promotes chondrogenesis by regulating STAT3 signaling pathway. *Cell Biology International*. **40**, 976–983 (2016).

55. L. Zhao, X. Du, K. Huang, T. Zhang, Z. Teng, W. Niu, C. Wang, G. Xia, Rac1 modulates the formation of primordial follicles by facilitating STAT3-directed Jagged1, GDF9 and BMP15 transcription in mice. *Sci Rep*. **6**, 23972 (2016).

56. G. Liu, Y. Xia, H. Wang, X. Jin, S. Chen, W. Chen, C. Zhang, Y. He, Downregulation of CYRI-B promotes migration, invasion and EMT by activating the Rac1-STAT3 pathway in gastric cancer. *Experimental Cell Research*. **423**, 113453 (2023).

57. B. Salhia, N. L. Tran, A. Chan, A. Wolf, M. Nakada, F. Rutka, M. Ennis, W. S. McDonough, M. E. Berens, M. Symons, J. T. Rutka, The guanine nucleotide exchange factors trio, Ect2, and Vav3 mediate the invasive behavior of glioblastoma. *Am J Pathol*. **173**, 1828–1838 (2008).

58. Q. Wang, B. Hu, X. Hu, H. Kim, M. Squatrito, L. Scarpace, A. C. deCarvalho, S. Lyu, P. Li, Y. Li, F. Barthel, H. J. Cho, Y.-H. Lin, N. Satani, E. Martinez-Ledesma, S. Zheng, E. Chang, C.-E. G. Sauvé, A. Olar, Z. D. Lan, G. Finocchiaro, J. J. Phillips, M. S. Berger, K. R. Gabrusiewicz, G. Wang, E. Eskilsson, J. Hu, T. Mikkelsen, R. A. DePinho, F. Muller, A. B. Heimberger, E. P. Sulman, D.-H. Nam, R. G. W. Verhaak, Tumor Evolution of Glioma-Intrinsic Gene Expression Subtypes Associates with Immunological Changes in the Microenvironment. *Cancer Cell*. **32**, 42-56.e6 (2017).

59. H. S. Phillips, S. Kharbanda, R. Chen, W. F. Forrest, R. H. Soriano, T. D. Wu, A. Misra, J. M. Nigro, H. Colman, L. Soroceanu, P. M. Williams, Z. Modrusan, B. G. Feuerstein, K. Aldape, Molecular subclasses of high-grade glioma predict prognosis, delineate a pattern of disease progression, and resemble stages in neurogenesis. *Cancer Cell*. **9**, 157–173 (2006).

60. K. P. L. Bhat, K. L. Salazar, V. Balasubramaniyan, K. Wani, L. Heathcock, F. Hollingsworth, J. D. James, J. Gumin, K. L. Diefes, S. H. Kim, A. Turski, Y. Azodi, Y. Yang, T. Doucette, H. Colman, E. P. Sulman, F. F. Lang, G. Rao, S. Copray, B. D. Vaillant, K. D. Aldape, The transcriptional coactivator TAZ regulates mesenchymal differentiation in malignant glioma. *Genes Dev*. **25**, 2594–2609 (2011).

61. M. Sakabe, J. Fan, Y. Odaka, N. Liu, A. Hassan, X. Duan, P. Stump, L. Byerly, M. Donaldson, J. Hao, M. Fruttiger, Q. R. Lu, Y. Zheng, R. A. Lang, M. Xin, YAP/TAZ-CDC42 signaling regulates vascular tip cell migration. *Proceedings of the National Academy of Sciences*. **114**, 10918–10923 (2017).

62. J. P. Vaqué, R. T. Dorsam, X. Feng, R. Iglesias-Bartolome, D. J. Forsthoefel, Q. Chen, A. Debant, M. A. Seeger, B. R. Ksander, H. Teramoto, J. S. Gutkind, A genome-wide RNAi screen reveals a Trio-regulated Rho GTPase circuitry transducing mitogenic signals initiated by G protein-coupled receptors. *Mol Cell*. **49**, 94–108 (2013).

63. J. Cai, X. Song, W. Wang, T. Watnick, Y. Pei, F. Qian, D. Pan, A RhoA-YAP-c-Myc signaling axis promotes the development of polycystic kidney disease. *Genes Dev*. **32**, 781–793 (2018).

64. X. Feng, M. S. Degese, R. Iglesias-Bartolome, J. P. Vaque, A. A. Molinolo, M. Rodrigues, M. R. Zaidi, B. R. Ksander, G. Merlino, A. Sodhi, Q. Chen, J. S. Gutkind, Hippo-independent activation of YAP by the GNAQ uveal melanoma oncogene through a trio-regulated rho GTPase signaling circuitry. *Cancer Cell*. **25**, 831–845 (2014).

65. R. Gargini, M. Escoll, E. García, R. García-Escudero, F. Wandosell, I. M. Antón, WIP Drives Tumor Progression through YAP/TAZ-Dependent Autonomous Cell Growth. *Cell Rep*. **17**, 1962–1977 (2016).

66. H. Sabra, M. Brunner, V. Mandati, B. Wehrle-Haller, D. Lallemand, A.-S. Ribba, G. Chevalier, P. Guardiola, M. R. Block, D. Bouvard, β1 integrin-dependent Rac/group I PAK signaling mediates YAP activation of Yes-associated protein 1 (YAP1) via NF2/merlin. *J Biol Chem*. **292**, 19179–19197 (2017).

67. F.-X. Yu, J. Luo, J.-S. Mo, G. Liu, Y. C. Kim, Z. Meng, L. Zhao, G. Peyman, H. Ouyang, W. Jiang, J. Zhao, X. Chen, L. Zhang, C.-Y. Wang, B. C. Bastian, K. Zhang, K.-L. Guan, Mutant Gq/11 promote uveal melanoma tumorigenesis by activating YAP. *Cancer Cell*. **25**, 822–830 (2014).

68. P. Tocci, R. Cianfrocca, V. Di Castro, L. Rosanò, A. Sacconi, S. Donzelli, S. Bonfiglio, G. Bucci, E. Vizza, G. Ferrandina, G. Scambia, G. Tonon, G. Blandino, A. Bagnato, β-arrestin1/YAP/mutant p53 complexes

orchestrate the endothelin A receptor signaling in high-grade serous ovarian cancer. *Nat Commun*. **10**, 3196 (2019).

69. Y. Qiao, J. Chen, Y. B. Lim, M. L. Finch-Edmondson, V. P. Seshachalam, L. Qin, T. Jiang, B. C. Low, H. Singh, C. T. Lim, M. Sudol, YAP Regulates Actin Dynamics through ARHGAP29 and Promotes Metastasis. *Cell Reports*. **19**, 1495–1502 (2017).

70. J. Shen, Q. Huang, W. Jia, S. Feng, L. Liu, X. Li, D. Tao, D. Xie, YAP1 induces invadopodia formation by transcriptionally activating TIAM1 through enhancer in breast cancer. *Oncogene*. **41**, 3830–3845 (2022).

71. J. W. Haskins, D. X. Nguyen, D. F. Stern, Neuregulin 1-activated ERBB4 interacts with YAP to induce Hippo pathway target genes and promote cell migration. *Sci Signal*. **7**, ra116 (2014).

72. J. He, Q. Bao, Y. Zhang, M. Liu, H. Lv, Y. Liu, L. Yao, B. Li, C. Zhang, S. He, G. Zhai, Y. Zhu, X. Liu, K. Zhang, X.-J. Wang, M.-H. Zou, Y. Zhu, D. Ai, Yes-Associated Protein Promotes Angiogenesis via Signal Transducer and Activator of Transcription 3 in Endothelial Cells. *Circ Res*. **122**, 591–605 (2018).

73. J. Park, D.-H. Kim, S. R. Shah, H.-N. Kim, Kshitiz, P. Kim, A. Quiñones-Hinojosa, A. Levchenko, Switch-like enhancement of epithelial-mesenchymal transition by YAP through feedback regulation of WT1 and Rho-family GTPases. *Nat Commun*. **10**, 2797 (2019).

74. D. Hanahan, R. A. Weinberg, Hallmarks of Cancer: The Next Generation. *Cell*. **144**, 646–674 (2011).

75. B. S. Wong, S. R. Shah, C. L. Yankaskas, V. K. Bajpai, P.-H. Wu, D. Chin, B. Ifemembi, K. ReFaey, P. Schiapparelli, X. Zheng, S. S. Martin, C.-M. Fan, A. Quiñones-Hinojosa, K. Konstantopoulos, A microfluidic cell-migration assay for the prediction of progression-free survival and recurrence time of patients with glioblastoma. *Nat Biomed Eng*. **5**, 26–40 (2021).

76. J. Kim, J. G. Shamul, S. R. Shah, A. Shin, B. J. Lee, A. Quinones-Hinojosa, J. J. Green, Verteporfin-Loaded Poly(ethylene glycol)-Poly(beta-amino ester)-Poly(ethylene glycol) Triblock Micelles for Cancer Therapy. *Biomacromolecules*. **19**, 3361–3370 (2018).

77. J. G. Shamul, S. R. Shah, J. Kim, P. Schiapparelli, C. A. Vazquez-Ramos, B. J. Lee, K. K. Patel, A. Shin, A. Quinones-Hinojosa, J. J. Green, Verteporfin-Loaded Anisotropic Poly(Beta-Amino Ester)-Based Micelles Demonstrate Brain Cancer-Selective Cytotoxicity and Enhanced Pharmacokinetics. *Int J Nanomedicine*. **14**, 10047–10060 (2019).

78. S. R. Shah, J. Kim, P. Schiapparelli, C. A. Vazquez-Ramos, J. C. Martinez-Gutierrez, A. Ruiz-Valls, K. Inman, J. G. Shamul, J. J. Green, A. Quinones-Hinojosa, Verteporfin-Loaded Polymeric Microparticles for Intratumoral Treatment of Brain Cancer. *Mol Pharm*. **16**, 1433–1443 (2019).

79. O. Gonzalez-Perez, H. Guerrero-Cazares, A. Quiñones-Hinojosa, Targeting of deep brain structures with microinjections for delivery of drugs, viral vectors, or cell transplants. *J Vis Exp*, 2082 (2010).

80. X. Xie, P. Rigor, P. Baldi, MotifMap: a human genome-wide map of candidate regulatory motif sites. *Bioinformatics*. **25**, 167–174 (2009).

81. M. Dai, P. Wang, A. D. Boyd, G. Kostov, B. Athey, E. G. Jones, W. E. Bunney, R. M. Myers, T. P. Speed, H. Akil, S. J. Watson, F. Meng, Evolving gene/transcript definitions significantly alter the interpretation of GeneChip data. *Nucleic Acids Res*. **33**, e175 (2005).

82. R. A. Irizarry, C. Wang, Y. Zhou, T. P. Speed, Gene set enrichment analysis made simple. *Stat Methods Med Res*. **18**, 565–575 (2009).

FIGURE LEGENDS:

Figure 1 | YAP regulates migratory capacity. a, Immunoblots of YAP expression in human non-cancer cortex and primary glioblastoma patient tissues. **b,** Migration pattern and average distance traveled by shCtrl or shYAP JHGB651 cells *in vitro* on 2D surface (n = 20 cells). **c, d,** Mean migration speed of shCtrl versus shYAP JHGBM651 cells or CONT versus YAP OE JHGBM612 cells (n=30 cells). **e,** Left: Human Nuclei/DAPI immunofluorescent images of mouse brain coronal sections after injections of shCtrl or shYAP JHGBM612 cells (i.s. = injection site). Dashed lines outline the bulk tumor margins on the ipsilateral hemisphere. White boxes outline the area magnified in the right panel. Right: magnified images of the corpus callosum in the right hemisphere (m.l. = midline, c.c. = corpus callosum, st = striatum, ctx = cortex, v = ventricle). See also *Supplemental Fig. 1j, k.* **f,** Total number of shCtrl or shYAP cells invading past the midline into the contralateral hemisphere. (n = 5 mice per group), *=P<0.05, Student's t-test. **g,** Representative Paxillin/F-actin/DAPI immunofluorescent images of shCtrl or shYAP JHGBM651 cells. **h,** Mean number of focal adhesion in shCtrl (n=25 cells) or shYAP JHGBM651 cells (n=16 cells); normalized per cell. **i,** Representative immunoblot of YAP, p-LIMK, and LIMK expression in shCtrl, shYAP-1, or -2 JHGBM651 cells. All error bars are s.e.m. Black * = P<0.05, Wilcoxon Rank-Sum test. All experiments were performed in triplicate except otherwise stated and repeated three times with similar results.

Figure 2 | YAP regulates migration through a RhoGTPase switch. a, G-LISA analysis of RhoA-GTP levels in shCtrl or shYAP JHGBM651 cells. **b,** Mean migration speed of shCtrl or shYAP JHGBM651 cells treated with increasing doses of the ROCK inhibitor Y27632 (n=30 cells). **c,** G-LISA analysis of Rac1-GTP levels in shCtrl or shYAP JHGBM651 cells. **d,** Mean migration speed of shCtrl or shYAP

JHGBM651 cells treated with increasing doses of the Rac1-GEF inhibitor NSC23766 (n=30 cells). **e,** Mean speed of shCtrl and shYAP JHGBM651 cells treated with no drug, Y27632, or NSC23766 for 3 or 6 hours as indicated (n=30 cells). Wilcoxon Rank-Sum test; Black * = P<0.05, between mean speed from hour1 to hour2 and that from hour4 to hour5 in shCtrl cells; Red * = P<0.05, between mean speed from hour1 to hour2 and that from hour4 to hour5 in shYAP cells; Red # = P<0.05, between mean speed in shYAP cells and that in shCtrl cells at corresponding time points. **f,** G-LISA analysis of Rac1-GTP levels in shCtrl or shYAP JHGBM651 cells treated with vehicle or Y27632. **g,** G-LISA analysis of RhoA-GTP levels in shCtrl or shYAP JHGBM651 cells treated with vehicle or NSC23766. **f-g,** Wilcoxon Rank-Sum test; * = P<0.05, between drug and no drug treatment in shCtrl or shYAP cells; # = P<0.05, between shYAP and shCtrl cells with no drug treatment. **h,** Representative immunoblot of YAP and RhoA expression in shCtrl or shYAP JHGBM651 cells transfected with siCtrl or siRhoA. **i,** Mean migration speed of shCtrl or shYAP JHGBM651 cells transfected with siCtrl or siRhoA (n=30 cells). Wilcoxon Rank-Sum test; * = P<0.05, between siRhoA and siCtrl in shYAP cells; # = P<0.05, between siCtrl in shYAP and that in shCtrl cells. **j,** Mean migration speed of shCtrl or shYAP GBMA172 cells transfected with pCtrl or a dominant-negative RhoA vector (pRhoA-DN). Wilcoxon Rank-Sum test; * = P<0.05, between pRhoA-DN and pCtrl in shYAP cells; # = P<0.05, between pCtrl in shYAP and that in shCtrl cells. **k,** Mean migration speed of shCtrl or shYAP GBMA172 cells transfected with pCtrl or a constitutively active Rac1 vector (pRac1-CA) (n=30 cells). Wilcoxon Rank-Sum test; * = P<0.05, between pRhoA-CA and pCtrl in shYAP cells; # = P<0.05, between pCtrl in shYAP and that in shCtrl cells. All error bars are s.e.m. All experiments were performed in triplicate except otherwise stated and repeated three times with similar results.

Figure 3 | YAP directly transactivates the Rac1-GEF TRIO. a, Representative immunoblot of TRIO expression in shCtrl or shYAP JHGBM651/JHGBM612 cells. **b,** TRIO mRNA expression in shCtrl or shYAP JHGBM651/JHGBM612 cells. **c,** Representative immunoblot of TRIO expression in CONT or

YAP OE JHGBM612 cells. **d,** YAP/TEAD4 binding to an intronic region of TRIO as observed in a publicly available ChIP-sequencing dataset using MDA-MD-231 cells(*33*). Substantial H3K4 monomethylation (H3K4me1) and H3K27 acetylation (H3K27ac), without H3K4 trimethylation (H3K4me3), indicates an active enhancer element in this locus. **e,** ChIP-PCR querying across two enhancer elements of TRIO using JHGBM612 cells. **f,** *TRIO* gene enhancer luciferase assay in using TRIO enhancer segment in cells with or without YAP OE. **g, h, i,** G-LISA analysis of Rac1-GTP levels in CONT or YAP OE JHGBM612 cells, CONT or TRIO OE JHGBM612 cells, and shCtrl or shTRIO JHGBM651 cells, respectively. **j,** Correlation plot of relative YAP and TRIO protein expression (normalized to β-actin) in patient-derived primary GBM tissues based on densitometric quantification of immunoblots in Fig. 5i and Fig. S5m. **k,** TRIO and TIAM1 expression in GB-YAP high, intermediate, or low patient groups in the REMBRANDT GBM dataset. **b, f-i, k,** * = P<0.05, Student's t-test. **l,** Percentage of patients with elevated GB-YAP signature, TRIO transcript, or both in the REMBRANDT GBM dataset. *P* = Fisher's exact test using the sizes of the shown patient groups. All error bars are s.e.m. All experiments were performed in triplicate except otherwise stated and repeated three times with similar results.

Figure 4 | YAP-TRIO signaling regulates migration. a, Left: Representative immunoblot of TRIO expression in shCtrl, shTRIO-1, or -2 JHGBM651 cells. Right: Mean migration speed of shCtrl or shTRIO JHGBM651 cells (n=30 cells). **b,** Left: Representative immunoblot of TRIO and YAP expression in CONT and TRIO OE JHGBM651 cells. Right: Mean migration speed of CONT and TRIO OE JHGBM651 cells (n=30 cells). **a-b,** * = *P*<0.05, Student's t-test. **c,** Mean migration speed of shCtrl, shYAP, and shYAP+TRIO OE JHGBM651 cells (n=30 cells). Student's t-test; * = P<0.05, between shYAP and shCtrl cells. **d,** Left: Representative immunoblot of GFP and TRIO expression in CONT, TRIO OE (wildtype), TRIO iGEF1 OE, or TRIO iGEF2 OE JHGBM612 cells. Right: Mean migration speed of CONT, TRIO OE (wildtype TRIO), TRIO iGEF1 OE, or TRIO iGEF2 OE JHGBM612 cells (n=30 cells). Student's t-test; * = P<0.05, compared to CONT. All error bars are s.e.m. All experiments

were performed in triplicate except otherwise stated and repeated three times with similar results.

Figure 5 | YAP promotes invasion by activating STAT3. a, Invasive gene signature expression in GB-YAP high, intermediate, or low patient groups in the TCGA GBM dataset. **b, c,** Matrigel Boyden invasion assay of shCtrl or shYAP JHGBM651 and CONT or YAP OE JHGBM612 cells, respectively. **d,** Expression of GB-STAT3 signatures in GB-YAP high, intermediate, or low patient samples in the TCGA GBM dataset. GB-STAT3 signatures were derived from BTIC or SNB19 GBM cells. Conserv = STAT3 signature conserved in both cell lines. **a-d,** * = $P<0.05$, Student's t-test. **e,** Percentage of patients with elevated GB-YAP signature, STAT3, or both in the REMBRANDT GBM dataset. P = Fisher's exact test using the sizes of the shown patient groups. **f, g,** Representative immunoblot of YAP and total and phospho-Tyr705 STAT3 expression in shCtrl or shYAP JHGBM651/JHGBM612 and CONT or YAP OE JHGBM612 cells, respectively. **h,** Matrigel Boyden invasion assay of shCtrl and shYAP JHGBM651 cells treated with vehicle or the STAT3 inhibitor LLL12. Student's t-test; * = P<0.05, between drug and no drug treatment; # = P<0.05 between shYAP and shCtrl cells with no drug treatment. **i,** Immunoblots of YAP and total and phospho-Tyr705 STAT3 expression in non-cancer cortex and primary glioblastoma patient tissues. **j,** Percentage of High and Low YAP expressing patients with High or Low phospho-Tyr705/total STAT3 expression ratio from immunoblots in i. All error bars are s.e.m. All experiments were performed in triplicate except otherwise stated and repeated three times with similar results.

Figure 6 | YAP potentiates invasion by activating the TRIO-mediated Rac1-STAT3 axis. a, Representative immunoblot of total and phospho-Tyr705 STAT3 expression in shCtrl, shTRIO-1, or -2 JHGBM651 and JHGBM612 cells. **b,** Matrigel Boyden invasion assay of shCtrl, shYAP, or shTRIO JHGBM651 and JHGBM612 cells. Student's t-test; * = P<0.05, compared to shCtrl cells. **c,** Representative immunoblot of total and phospho-Tyr705 STAT3 expression in CONT and TRIO OE JHGBM651 cells. **d,** Matrigel Boyden invasion assay of CONT and TRIO OE JHGBM651 cells. * =

P<0.05, Student's t-test. **e,** Representative immunoblot of total and phospho-Tyr705 STAT3 expression in shCtrl and shYAP JHGBM651 cells with or without TRIO overexpression. **f,** Representative immunoblot of total and phospho-Tyr705 STAT3 expression in shCtrl and shTRIO JHGB651 cells with or without YAP overexpression. **g,** Left: Human Nuclei/DAPI immunofluorescent images of mouse brain coronal sections after injections of CONT + shCtrl, CONT + shTRIO, YAP OE shCtrl, or YAP OE + shTRIO JHGBM612 cells (i.s. = injection site). Bulk tumor margins are indicated on the ipsilateral hemisphere. White boxes outline the area magnified in the right panel. Right: magnified images of the corpus callosum in the right hemisphere (m.l. = midline, c.c. = corpus callosum, st = striatum, ctx = cortex, v = ventricle). **h,** Total number of CONT + shCtrl, CONT + shTRIO, YAP OE shCtrl, or YAP OE + shTRIO cells invading corpus callosum into the contralateral hemisphere (*n* = 5 mice per group). Student's t-test; * = P<0.05, compared to shCtrl cells; # = P<0.05 between YAP OE shCtrl and CONT shCtrl cells. **i,** Schematic representation of YAP and TRIO modulating STAT3 phosphorylation independently of RhoA-ROCK signaling. All error bars are s.e.m. All experiments were performed in triplicate except otherwise stated and repeated three times with similar results.

Figure 7 | YAP-TRIO-STAT3 signaling predicts poor clinical outcome in glioblastoma. a, Percentage of patients with elevated GB-YAP signature expression. Patients are grouped by glioma grade in REMBRANDT and TCGA datasets. **b,** Kaplan-Meier graph of cumulative progression-free survival in patient groups defined by GB-YAP signature expression in TCGA dataset. *P*=Log-Rank test. **c,** Percentage of GBM patients with elevated GB-YAP signature expression in TCGA subtypes. P=Fisher's exact test. **d,** Expression of GBM subclass signatures in GB-YAP high, intermediate, or low patient samples in the TCGA dataset. GBM subclass signatures were derived from TCGA "Core" samples. * = P<0.05, Student's t-test between YAP high and YAP low. **e,** mRNA expression of Mesenchymal GBM subclass signature genes in shCtrl (black bars) or shYAP (red bars) JHGB651, JHGB640, and JHGB612 cells. * = P<0.05, Student's t-test between shYAP and shCtrl cells. **f,** Distribution of patient groups

expressing either one, two, or all three of GB-YAP signature, TRIO transcript, and STAT3-conserved signature expression patterns. **g-i,** Kaplan-Meier graphs of cumulative progression-free survival in patient groups defined by the GB-YAP signature, TRIO transcript, and STAT3-conserved signature expression in the TCGA dataset. *P*=Log-Rank test. **j,** Schematic of the YAP-driven pro-migratory and invasive signaling pathway in a single cell on a layer of extracellular matrix. Dashed lines demonstrate movement of the cell body during migration and invasion. Darker shading of the extracellular matrix around the invading edge of the cell represents the degradation of the surrounding tissue. All experiments were performed in triplicate except otherwise stated and repeated three times with similar results.

Materials and Methods:

Cell culture. Patient primary glioblastoma tissue specimens were obtained at the Johns Hopkins Hospital under the approval of the Institutional Review Board (IRB). All primary cell lines were established from excess tumor tissue from patients undergoing surgical resection for glioblastoma as listed in **Suppl Table 1.** GBM cell line derivation and culture protocols were as previously described(*26*), without the addition of N2 supplement and cultured on laminin-coated (1μg/cm^2) plates. Specifically, DMEM/F12 (Invitrogen) was supplemented with B27 supplement (Invitrogen), antibiotic/antimycotic (Invitrogen), human EGF (Peprotech), and FGF (Peprotech). MCF10A cells were purchased from ATCC and maintained in complete MEGM media (Lonza) supplemented with 100 ng/mL cholera toxin (Sigma) as recommended. GBMA172 cells were purchased from ATCC and maintained in DMEM (Gibco) supplemented with 10% FBS (Gibco). NHA cells were purchased from Lonza and cultured as recommended. All cell lines were tested and confirmed to be mycoplasm free using a PCR-based MycoDtect^{TM} kit from Greiner Bio-One.

Lentiviral transduction. Glycerol stocks of Human Mission TRC1 sequence-verified shRNA lentiviral plasmid vectors were obtained from the Johns Hopkins University High Throughput Biology Center (See

below). Plasmids were isolated using a Spin Miniprep kit (Qiagen). Vesicular stomatitis virus glycoprotein-pseudotyped virus was produced by co-transfecting 293T cells using Lipofectamine 2000 (Invitrogen) with an shRNA transducing vector and 2 packaging vectors, psPAX2 and pMD2.G. On days 3 and 4 post-transfection, the virus was harvested and filtered through a 0.22-μm pore cellulose acetate filter before centrifugal concentration using a Centricon Plus-70 (Millipore). An empty TRC1 lentiviral construct was used as the Control virus (Sigma).

The TRIO (pCDH1-GFP TRIO), TRIO iGEF1 (TRIO QALE), TRIO iGEF2 (TRIO L2051E), and its corresponding control lentiviral plasmids (pCDH1) were generated by the Schmidt Lab. Vesicular stomatitis virus glycoprotein-pseudotyped virus was produced by co-transfecting 293T cells using PureFection transfection reagent (Systems Biosciences) with the pCDH1-based lentiviral vector and pPACKH1 packaging plasmid mix (Systems Biosciences).

The YAP constitutively active overexpression lentiviral vector was generated using pCMV-Flag YAP127/128/131/381A plasmid (Addgene) and Duet011 lentiviral plasmid.

Primary GB, GBMA172, MCF10A, and NHA cells were transduced with equal titers of concentrated virus in complete growth media supplemented with 1 μg/ml polybrene (Sigma) for 24 hours. Following transduction, cells were given 24 hours to recover before selection in 0.25 μg/ml (JHGBM651, JHGBM640, JHGBM1A) or 0.5 μg/ml (JHGBM612, GBMA172, MCF10A, and NHA) puromycin (Sigma) for a minimum of 6 days. Minimum effective puromycin or hygromycin concentrations were determined using kill curves of non-transduced cells (data not shown).

shRNA Plasmids

Target Gene	TRC Number	TRC Version
Human YAP Clone 1	TRCN0000107265	TRC 1

Human YAP Clone 2	TRCN0000107267	TRC 1
Mouse YAP/ Human Clone 3	TRCN0000107266	TRC 1
Human YAP Clone 4	TRCN0000107268	TRC 1
Human YAP Clone 5	TRCN0000107269	TRC 1
Human TRIO Clone 1	TRCN0000195292	TRC 1
Human TRIO Clone 2	TRCN0000196250	TRC 1

Time-lapse microscopy, drug treatments, and analysis of single cell migration speed. GBM or MCF10A cells were seeded at a density of 2000-4000 cells/well in a 96-well tissue-culture polystyrene plate (BD Falcon) that was pretreated with 3 μg/cm^2 laminin for GBM cells (Sigma) or 5 μg/cm^2 collagen for MCF10A cells (Stem Cell Technologies). 48 hours after seeding, cells were fed with either control or treated complete growth medium (as indicated) and placed and imaged in a temperature- and gas-controlled environmental chamber (37 °C, 5% CO_2). Y27632 (Tocris), NSC23766 (Tocris), and ITX3 (Tocris) were resuspended in sterile PBS concentrations for the indicated times. Time-lapse microscopy was performed using a motorized inverted microscope (Olympus IX81) equipped with a Cascade 512B II CCD camera. Phase-contrast images were captured with a 10x objective (NA = 0.30) under the control of Slidebook 4.1 (Intelligent Imaging Innovations, Denver, CO) at 10–20 minute intervals for at least 6 hours. A single observer used a custom MATLAB script to view time-lapse images and manually mark cell body positions. (See **Supplemental Videos**). Due to the inhomogeneous seeding of cells throughout individual wells, care was taken to image 5-8 fields of view per well that were most comparable to other experimental conditions. Additionally, a minimum of 30 cells was tracked from 4 replicate wells for each experimental

condition. Cell migration speed was computed as displacement (between each captured time point) over time. Individual cell speeds were summarized as the average speed within one-hour intervals. Since the speeds of many cell populations failed to pass normality testing, a Wilcoxon rank-sum test was used to compare experimental conditions. Error bars represent the standard error of the mean of the cell population in a given experimental condition.

Intracranial xenograft model and immunohistochemistry. All animal protocols were approved by the Johns Hopkins Animal Care and Use Committee. Briefly, JHGBM612 cells were resuspended at 75,000 cells/µl in complete growth media and placed on ice. 1-month old male NOD-SCID gamma-null (NSG) mice were anesthetized before intracranial injections following an established protocol(*79*). 2 µl of shCtrl or shYAP cells were injected into the striatum; specifically (X: 1.5, Y: 1.34, Z: -3.5) mms from the bregma (n = 5 per group).

5 weeks post-injection, mice were anesthetized before trans-cardiac perfusion with saline followed by 10% formalin. Brains were then harvested and fixed overnight at 4 °C in 10% formalin. Fixed brains were placed in OCT compound (Tissue-Tek) overnight at 4 °C and subsequently flash-frozen. Embedded brains were cut into 10-micron coronal sections using a cryostat microtome.

Brain sections spaced every 500µm were stained with hematoxylin and eosin to identify landmark neuroanatomical structures and therefore identify comparable slides from each mouse for further analysis. Slides immediately adjacent to the identified slides were then selected for immunohistochemistry and quantification. Antigen retrieval was performed using sodium citrate (10 mM) for 30 minutes in a water bath at 95°C. Slides were rinsed in PBS and blocked in 10% normal goat serum for 1 hour. Primary antibody was diluted in PBS with 0.1% Triton X-100 and 2% normal goat serum. Slides were incubated with primary antibody overnight at 4°C. After rinsing with PBS, the slides were incubated with the appropriate anti–IgG secondary antibody (Molecular Probes, Invitrogen) conjugated with a fluorochrome

for 1 hour and rinsed. Slides were then incubated with DAPI for 30 minutes and rinsed in PBS before visualization on an Olympus IX81 inverted microscope. Antibodies are listed at the end of this section.

Immunoblotting, antibodies, and immunocytochemistry. *Immunoblotting:* Tissues from the operating room were briefly rinsed in HBSS before being flash-frozen in liquid nitrogen. Proteins were extracted using T-PER (Pierce) tissue protein extraction reagent and a tissue homogenizer. GBM, MCF10A, and NHA cells were lysed on ice with a cell scraper and radioimmunoprecipitation assay lysis buffer (Pierce) supplemented with protease inhibitor tablets (Roche) and a phosphatase inhibitor cocktail (Pierce). Extracts were incubated for 45 minutes for complete lysis and centrifuged at 10,000 RPM for 10 minutes at 4°C to pellet cell debris. Supernatant protein concentrations were quantified using a BCA Protein Assay kit (Pierce) and a spectrophotometric plate reader (BioTek). Most protein lysates were separated by running 30-100 μg of lysate on 10% Bis-Tris NuPage gels (Invitrogen) and subsequently, transferred to 0.2μm pore polyvinylidene fluoride (PVDF) membranes (BioRad). Because TRIO is an exceptionally large protein, some lysates were run on 4-12% Tris-Acetate NuPage gels and transferred to 0.45 μm pore PVDF membranes overnight. Primary antibody incubations were according to the manufacturer's recommendations in 0.1% Tween TBS supplemented with 5% non-fat dry milk or BSA, as recommended. Immunoreactive bands were visualized using the appropriate horseradish peroxidase-conjugated anti-IgG antibodies (Pierce). Bands were detected using enhanced chemiluminescence or prime detection reagent (GE Healthcare) whenever appropriate. Densitometric analysis was done with ImageJ and results are listed in **Suppl Table 3**. All immunoblotting experiments were performed in triplicate and repeated three times with similar results.

For *immunocytochemistry*, 160,000 GBM cells were seeded on laminin-coated 35-mm cell culture plates. 48 hours later, cells were washed in cold PBS and fixed in 10% formalin for 30-60 minutes. Cells were blocked in 10% normal goat serum for 1 hour. Primary antibody was diluted in PBS with 0.1% Triton X-100 and 2% normal goat serum. Cells were incubated with primary antibody overnight at 4°C. After

rinsing with cold PBS, cells were incubated with the appropriate anti–IgG secondary antibody (Molecular Probes, Invitrogen) conjugated with a fluorochrome for 1 hour. Cells were rinsed in PBS before incubation with DAPI for 30 minutes. Finally, cells were rinsed in PBS before visualization on an Olympus IX81 inverted microscope.

For *focal adhesion analysis*, high-resolution images were captured using a fluorescence microscope at 20-40X. Quantification of area or size was conducted using ImageJ.

Antibodies used for these procedures are listed at the end of this section.

Pull-down of GTP-bound Small Rho GTPases. The Rac1-GTP Assay (Cell Bio Labs) and RhoA-GTP Assay (Millipore) kits were used in accordance with the manufacturer's instructions. Briefly, 1.2 x 10^6 MCF10A or GBM cells per dish were seeded into collagen- or laminin-coated 100 mm cell culture dishes (Corning). 48 hours later, cells were rinsed twice with ice-cold PBS and placed on ice. Extracts were harvested quickly by scraping in ice-cold 1X assay buffer supplemented with protease and phosphatase inhibitors. Lysis was completed by incubation for 30 minutes on ice and vortexing every 10 minutes. Protein supernatants were isolated and quantified as above. 4 mg of shCtrl or shYAP MCF10A lysate was used as input for RhoA-GTP pull-down and 2 mg as input for Rac1-GTP pull-down. 1 mg of protein lysate was used as input for the Rac1-GTP pull-down of JHGBM651 cells. 50 μg of input lysates were kept for immunoblotting. Agarose beads conjugated with Rhotekin binding domain (RBD) were incubated with lysates for 4 hours, and p21-binding domain (PBD) agarose beads were incubated with lysates for 1 hour. Beads were rinsed three times with cold 1X assay buffer, resuspended in 2X SDS-PAGE sample buffer, and boiled for 10 minutes. Proteins were separated on 10% Bis-Tris NuPage gels, transferred to 0.2 μm pore PVDF membranes, and immunoblotted as described above. Mouse anti-RhoA antibody (26C4) was purchased from Santa Cruz. Refer to the end of this section for a listing of all antibodies used. In addition, for more quantitative analyses, G-LISA RhoA or Rac1 activation kits from Cytoskeleton were used according to the manufacturer's protocol.

Motif Search. MotifMap(*80*) was used to search 10 kilobase regions upstream of select transcription start sites in the hg19 reference genome. Significant motifs were called at a false discovery rate below 0.05.

Invasion assay. Matrigel-coated Boyden chambers (BD Biosciences) were used to assess the invasive capacity of cells. 100,000 cells were resuspended in their appropriate media supplemented with 0.5% FBS. Cell suspension aliquots were plated on the upper surface of the transwell plates with a porous PET membrane (8μm pores) pre-coated with a layer of growth factor reduced matrigel basement membrane matrix. 750 μl of 2% FBS containing DMEM media was placed in the lower chamber. Filters were incubated at 37C°, 5% CO2 for 48 hours. Invasion of cells was determined by fixing the membrane, staining the cells using the Diff-Quik® staining kit, directly counting the number of invaded cells in 9 high-power fields at 10x using an Olympus 1X81 microscope system, and calculating the mean per well. The assays were run in triplicates and at least three independent experiments were performed. See also **Supplemental Fig. 15c**.

RNA extraction and quantitative real-time PCR. Total RNA was extracted in TRIzol, phase-separated using chloroform, and precipitated overnight at 4°C in isopropanol. Further isolation of total RNA was performed using the RNeasy Mini Kit (Qiagen) according to the manufacturer's instructions. 1 μg purified RNA was reverse transcribed using the Superscript III First-Strand cDNA Synthesis Kit (Invitrogen). Quantitative real-time PCR using SYBR Green (Applied Biosystems) was performed on a 7300 Cycler (Applied Biosystems) and the included data analysis software. GAPDH primers were used as a loading control. See the table below for all primer sequences used.

Primer pairs

Target Gene	Forward Sequence (5' to 3')	Reverse Sequence (5' to 3')
YAP1	TAGCCCTGCGTAGCCAGTTA	TCATGCTTAGTCCACTGTCTGT
WWTR1	GTCCTACGACGTGACCGAC	CACGAGATTTGGCTGGGATAC
GAPDH	AAGGTGAAGGTCGGAGTCAAC	AAGGTGAAGGTCGGAGTCAAC
TRIO	CCAGGAGCGGACGATCCACCT	CCAGGAGCGGACGATCCACCT
TIAM1	GATCCACAGGAACTCCGAAGT	GCTCCCGAAGTCTTCTAGGGT
MCL-1 (Isoform 1)	TGCTTCGGAAACTGGACATCA	TAGCCACAAAGGCACCAAAAG
MMP9	GGGACGCAGACATCGTCATC	TCGTCATCGTCGAAATGGGC
CTGF	GGCAAAAAGTGCATCCGTACT	CCGTCGGTACATACTCCACA
MMP2	CTTCCAAGTCTGGAGCGATGT	TACCGTCAAAGGGGTATCCAT
FOSL2	TATCCCGGGAACTTTGACAC	TATCCCGGGAACTTTGACAC
RUNX1	CCCATCGCTTTCAAGGTG	CCCATCGCTTTCAAGGTG
CHI3L1/YKL 40	CCTGGGAGTGGAATGATGTGA	TCAGGTTGGGGTTCCTGTTCT
MET	AGCAATGGGGAGTGTAAAGAGG	CCCAGTCTTGTACTCAGCAAC
MERTK	CTCTGGCGTAGAGCTATCACT	AGGCTGGGTTGGTGAAAACA
CXCR4	ACTACACCGAGGAAATGGGCT	ACTACACCGAGGAAATGGGCT

CDH11	GTATCCTCGAAGGACAACCCT	GTATCCTCGAAGGACAACCCT
TNC	TCCCAGTGTTCGGTGGATCT	TCCCAGTGTTCGGTGGATCT
FN1	GAGAATAAGCTGTACCATCGCAA	GAGAATAAGCTGTACCATCGCAA
COL5A1	TACAACGAGCAGGGTATCCAG	TACAACGAGCAGGGTATCCAG

Biostatistical analysis. For Affymetrix data (GB-YAP, TCGA, and Rembrandt datasets), raw data files were processed in aroma.affymetrix (http://statistics.berkeley.edu/sites/default/files/tech-reports/745.pdf) using a custom CDF with updated probeset mappings(*81*) (BrainArray v15.1.0). Differential expression analysis was performed using the sam function of the siggenes package (version 1.28.0) in R 2.15.2. For Illumina beadchip data, signature probesets (GB-STAT3 and GB-C/EBPβ datasets(*47*)) were required to map to a single Entrez Gene ID. Redundant probesets mapping to the same gene were eliminated after differential expression analysis.

To derive gene signatures, each cell line was analyzed for differential expression independently (GB-YAP, GB-STAT3, and GB-C/EBPβ datasets). Genes with $q < .05$ and absolute fold-change > 1.5 were considered as differentially expressed genes, although $q < 0.1$ was used when no genes passed $q < 0.05$. This relaxed FDR was excused because the final signatures were taken as the genes significantly differentially expressed in both cell lines, at least one of which required $q < .05$.

To stratify patients into groups of low, intermediate, and high expression of a given gene signature, we used the gene set z-score(*82*). Briefly, RMA normalized data were quantile normalized, variance filtered, and log2 transformed. Gene sets were filtered to remove genes not present in the normalized, filtered data for each analysis. Each gene was converted into an expression z-score relative to other samples of the same class (e.g., other GBMs but not low-grade gliomas), and the gene set score (GSS) was computed as the sum of the member genes' z-scores divided by the square root of the size of the gene set. Samples with

GSS < -0.5 were categorized as low, samples with GSS > 0.5 were high, and those between were intermediate. Since microarray data to derive a gene signature of TRIO was unavailable, patients with a TRIO gene z-score < -0.5 were called low and those with a TRIO gene z-score > 0.5 were called high.

Antibodies

Target Protein	Company	Note
YAP p-S127	Cell Signaling	
YAP	Cell Signaling	
Beta-actin	Abcam	
Human Nuclei	Millipore	Clone 3E1.3
Paxillin	Sigma	Clone PXC10
F-actin	Sigma	
Rac1	Cell Biolabs	Included in kit
RhoA	Santa Cruz	Clone 26C4
ROCK1	Santa Cruz	Clone H-85
ROCK2	Santa Cruz	Clone C-20
LIMK1/2 p-T505/508	Cell Signaling	
LIMK1	Cell Signaling	
MLC2 p-S19	Cell Signaling	

MLC2	Cell Signaling	
TRIO	Santa Cruz	Clones H-120 and D-20
STAT3 p-Y705	Cell Signaling	Clone D3A7
STAT3	Santa Cruz	Clone H-190
TEAD4	Aviva Labs	
WWTR1/TAZ	BD Pharmingen	Clone M2-303

Accession codes. The microarray dataset of JHGBM651 and JHGBM612 cells treated with shCtrl or shYAP in triplicate will be made available on the Gene Expression Omnibus prior to publication.

SUPPLEMENTAL INFORMATION:

Supplemental Figures: The file named **"**Suppl Figs. 1-12" contains the following 12 supplemental figures with their associated legends listed below:

Supplemental Figure 1. YAP regulates migration. a, Densitometric analysis of YAP and YAP/β-actin expression in Fig. 1a. **b,** mRNA expression of YAP target genes, Mcl-1 and CTGF, in glioblastoma tissues compared to the non-cancer cortex. * = P<0.05, Student's t-test comparing to NCC. **c,** *Top:* Representative immunoblot of YAP and p-YAP expression in primary GBM cell cultures. *Bottom:* Representative immunoblot of YAP expression in nuclear and cytosolic fractions of primary GBM cells. * = cells used in functional assays. Numbers correspond to Patient Sample ID listed in Suppl Table 1. **d,** Representative immunoblot of YAP expression in wildtype (WT), shCtrl, or shYAP-1-5 JHGBM612 cells. s.e. = short exposure, l.e. = long exposure. **e,** Representative immunoblot of YAP and TAZ expression in shCtrl or shYAP-1/2 JHGBM651 cells. **f, g,** Mean

migration speed of shCtrl or shYAP-1 or -2 MCF10A, NHA, JHGBM651/612/640/1A cells (n=30 cells). * = P<0.05, Student's t-test comparing to shCtrl cells. **h-i,** *Left:* Representative immunoblot of YAP expression in CONT or YAP OE NHA, JHGBM612, and JHGBM1A cells, respectively. *Right:* Mean migration speed of CONT or YAP OE NHA, and JHGBM1A cells, respectively (n=30 cells). * = P<0.05, Student's t-test. **j,** MRI images of Patient #30/JHGBM612. **k,** Representative H&E images showing the formation of solid tumors in the in vivo GBM xenograft model used in experiments presented in Fig.1e and Fig.6g after intracranial injection of JHGBM612 cells. **l,** *Left:* Schematic of the murine intracranial xenograft model of GBM used to assess YAP's migratory and invasive capacity *in vivo. Right:* Number of cells invading past the midline into the contralateral hemisphere as presented in a. i.s. = injection site, c.c. = corpus callosum, st = striatum, ctx = cortex, v = ventricle, m.l. = midline, l.e. of brain = lateral edge of brain. (n = 5 mice per group). See also Materials and Methods for details. * = P<0.05, Student's t-test between shYAP and shCtrl cells at a corresponding distance from midline. **m-n,** Analysis of focal adhesion in shCtrl or shYAP JHGBM651 and GBMA172 cells repectively. * = P<0.05, Student's t-test. All error bars are s.e.m. All experiments were performed in triplicate except otherwise stated and repeated three times with similar results.

Supplemental Fig. 2. YAP regulates migration by inhibiting RhoA-ROCK signaling. a, Representative immunoblot of YAP, total and p-LIMK expression in shCtrl, shYAP-1, or -2 JHGBM651/612, NHA, and MCF10A cells. **b,** G-LISA analysis of Rac1-GTP levels of shCtrl or shYAP NHA cells. * = P<0.05, Wilcoxon Rank-Sum test. **c,** Mean migration speed of shCtrl, shYAP-1, or -2 JHGBM651/612/640/1A, NHA, and MCF10A cells treated with the ROCK inhibitors Y27632 or H1152 (n=30 cells). Wilcoxon Rank-Sum test; Red and black * = P<0.05, comparing to no drug treatment in shYAP-1 or -2 cells; Red # = P<0.05, comparing to shCtrl cells at corresponding drug concentration; Black # = P<0.05, comparing to shCtrl cells with no drug treatment. **d,** Representative immunoblots of JHGBM651 or JHGBM612 cells treated with vehicle or ROCK inhibitors Y27632 or

H1152. All error bars are s.e.m. All experiments were performed in triplicate except otherwise stated and repeated three times with similar results.

Supplemental Fig. 3. YAP regulates migration by activating Rac1 signaling. a, G-LISA analysis of Rac1-GTP levels of shCtrl or shYAP NHA cells. * = P<0.05, Wilcoxon Rank-Sum test. **b,** Representative immunoblot of YAP, total and p-PAK in shCtrl and shYAP GBMA172 cells. **c,** Mean migration speed of shCtrl, shYAP-1, or -2 JHGBM651/612/640, NHA, and MCF10A cells treated with the Rac1 inhibitor NSC23766 (n=30 cells). Wilcoxon Rank-Sum test; Black * = P<0.05, comparing to no drug treatment; Red # = P<0.05, between shYAP-1 or -2 and shCtrl cells at corresponding drug concentrations. **d,** Schematic representation of YAP modulating Rho-GTPases. All error bars are s.e.m. All experiments were performed in triplicate except otherwise stated and repeated three times with similar results.

Supplemental Fig. 4. YAP regulates migration by modulating a Rho-GTPase switch. a, Experimental paradigm to delineate the hierarchy of molecular events of YAP's modulation of a Rho-GTPase switch. **b,** Mean speed of shCtrl, shYAP-1, or -2 JHGBM651 and JHGBM612 cells treated with no drug/vehicle, Y27632, or NSC23766 for 3 or 6 hours as indicated (n=30 cells). Wilcoxon Rank-Sum test; Black * = P<0.05, between mean speed from hour1 to hour2 and that from hour4 to hour5 in shCtrl cells; Red * = P<0.05, between mean speed from hour1 to hour2 and that from hour4 to hour5 in shYAP-1 or -2 cells; Red # = P<0.05, between mean speed in shYAP-1 or -2 cells and that in shCtrl cells at corresponding time points. **c-e,** G-LISA analysis of Rac1-GTP or RhoA-GTP levels of shCtrl or shYAP cells treated with vehicle, ROCK inhibitors Y27632 or H1152, or Rac1-GEF inhibitor NSC23766. Wilcoxon Rank-Sum test; * = P<0.05, comparing to no drug treatment; # = P<0.05, comparing to shCtrl cells with no drug treatment. **f,** Schematic representation of the hierarchy

of YAP's modulation of a Rho-GTPase switch. All error bars are s.e.m. All experiments were performed in triplicate except otherwise stated and repeated three times with similar results.

Supplemental Fig. 5. YAP transactivates TRIO signaling. a, Representative immunoblots of YAP and TRIO expression in shCtrl, shYAP-1, or -2 JHGBM651/612/640/1A, MCF10A, and NHA cells. **b,** Relative TRIO mRNA expression in shCtrl or shYAP JHGBM651/612/640 and MCF10A cells. **c,** Representative immunoblot of YAP and TRIO expression in CONT or YAP OE MCF10A cells. **d,** Relative TIAM1 mRNA expression in shCtrl or shYAP JHGBM651/612/640 cells. **e,** ChIP-PCR querying across two enhancer elements of TRIO using JHGBM1A cells. **f,** GFP-luciferase reporter assay with the promoter sequence of TRIO and CTGF (positive control) in CONT and YAP OE GBMA172 cells. **g,** Immunoblots of pull-down analysis of Rac1-GTP levels in CONT and YAP OE JHGBM612 cells. **h,** Immunoblots of pull-down analysis of Rac1-GTP levels in CONT and TRIO OE JHGBM612 cells. **i,** Left: Immunoblots of pull-down analysis of Rac1-GTP levels in shCtrl and shTRIO JHGBM612 cells. Right: G-LISA analysis of Rac1-GTP levels in shCtrl and shTRIO NHA cells. **j,** G-LISA analysis of RhoA-GTP levels in CONT, YAP OE, and TRIO OE JHGBM651 cells. **k,** Representative immunoblots of total and p-YAP expression in shCtrl, shYAP, and shTRIO GBMA172 cells. **l,** G-LISA analysis of RhoA-GTP levels in shCtrl and shTRIO JHGBM651 and NHA cells. **b, f, i-j, l,** * = $P<0.05$, Wilcoxon Rank-Sum test. **m,** Representative immunoblot of TRIO expression in non-cancer cortex and patient-derived primary glioblastoma tissues. **n,** Expression of YAP/TAZ and YAP signatures, derived from a variety of other tissues, in GB-YAP high, intermediate, or low patient groups in the REMBRANDT and TCGA GBM datasets. All error bars are s.e.m. All experiments were performed in triplicate except otherwise stated and repeated three times with similar results.

Supplemental Fig. 6. YAP regulates migration via TRIO signaling. a, Representative immunoblots of TRIO expression in shCtrl, shTRIO-1, or -2 JHGBM612/640, MCF10A, and NHA cells. **b,** Mean migration speed of shCtrl, shTRIO-1, or -2 JHGBM651/612/1A, NHA, and MCF10A cells (n=30 cells). * = P<0.05, Wilcoxon Rank-Sum test comparing to shCtrl cells. **c,** G-LISA analysis of Rac1-GTP levels in shCtrl or shTRIO JHGBM651 cells treated with vehicle or the TRIO inhibitor of ITX3. Wilcoxon Rank-Sum test; * = P<0.05, comparing to no drug treatment; # = P<0.05, comparing to shCtrl with no drug treatment. **d,** Mean migration speed of shCtrl, shYAP-1, or -2, or shTRIO-1, or -2 JHGBM651/612/1A, NHA, and MCF10A cells treated with increasing doses of the TRIO inhibitor ITX3 (n=30 cells). Wilcoxon Rank-Sum test; Black * = P<0.05, comparing to no drug treatment in shCtrl cells; Red # = P<0.05, between shYAP and shCtrl at corresponding drug concentration; Blue # = P<0.05, between shTRIO-1 or -2 and shCtrl at corresponding drug concentration. All error bars are s.e.m. All experiments were performed in triplicate except otherwise stated and repeated three times with similar results.

Supplemental Fig. 7. YAP-TRIO signaling modulates Rac1-RhoA signaling to drive migration. a, Mean migration speed of shCtrl, shYAP-1, or -2 JHGBM651/612/640/1A, NHA, and MCF10A cells treated with increasing doses of the TRIO inhibitor ITX3 (n=30 cells). **b,** Mean migration speed of CONT or YAP OE JHGBM612 cells treated with vehicle or the TRIO inhibitor ITX3 (n=30 cells). Wilcoxon Rank-Sum test; Black * = P<0.05, comparing to no drug treatment in CONT cells; Red * = P<0.05, comparing to no drug treatment in YAP OE cells; Red # = P<0.05, between YAP OE and CONT at corresponding drug concentration. **c, d,** G-LISA analysis of Rac1-GTP or RhoA-GTP levels in shCtrl or shYAP JHGBM651 cells treated with vehicle or the TRIO inhibitor ITX3. Wilcoxon Rank-Sum test; * = P<0.05, comparing to no drug treatment in shCtrl or shYAP cells; # = P<0.05, comparing to shCtrl cells with no drug treatment. **e,** Mean migration speed of shCtrl, shYAP, or shTRIO JHGBM651/612/640 and NHA cells treated with increasing doses of the Rac1-GEF inhibitor

NSC23766 (n=30 cells). **f, h,** G-LISA analysis of Rac1-GTP or RhoA-GTP levels in shCtrl or shTRIO JHGBM651 cells treated with vehicle or the Rac1-GEF inhibitor NSC23766. **g,** Mean migration speed of shCtrl and shTRIO GBMA172 cells transfected with pCtrl or a constitutively active Rac1 vector (pRac1-CA). Wilcoxon Rank-Sum test; * = P<0.05, comparing to pCtrl in shTRIO cells; # = P<0.05, comparing to pCtrl shCtrl cells. **a, e, f, h,** Wilcoxon Rank-Sum test; Black * = P<0.05, comparing to no drug treatment in shCtrl cells; Black # = P<0.05, between shYAP-1 or -2 or shTRIO and shCtrl cells with no drug treatment; Red # = P<0.05, between shYAP-1 or -2 and shCtrl cells at corresponding drug concentration; Blue # = P<0.05, between shTRIO-1 or -2 and shCtrl cells at corresponding drug concentration. All error bars are s.e.m. All experiments were performed in triplicate except otherwise stated and repeated three times with similar results.

Supplemental Fig. 8. YAP-TRIO signaling regulates migration by modulating Rac1-RhoA crosstalk. a, G-LISA analysis of RhoA-GTP levels in shCtrl or shTRIO JHGBM651 cells treated with vehicle or the TRIO inhibitor ITX3. **b,** Mean migration speed of shCtrl and shTRIO GBMA172 cells transfected with pCtrl or a dominant-negative RhoA vector (pRhoA-DN) (n=30 cells). Wilcoxon Rank-Sum test; * = P<0.05, comparing to pCtrl in shTRIO cells; # = P<0.05, comparing to pCtrl shCtrl cells. **c,** Mean migration speed of shCtrl, shYAP, or shTRIO JHGBM651/612/1A, and NHA cells treated with increasing doses of the ROCK inhibitor Y27632 or H1152 (n=30 cells). **d,** G-LISA analysis of Rac1-GTP or RhoA-GTP levels in shCtrl or shTRIO JHGBM651 cells treated with vehicle or the ROCK inhibitor Y27632 or H1152 (n=30 cells). Wilcoxon Rank-Sum test; * = P<0.05, comparing to pCtrl in shTRIO cells; # = P<0.05, comparing to pCtrl shCtrl cells. **e,** *Left*: Representative immunoblot of TRIO and YAP expression in CONT of TRIO OE MCF10A cells. *Right*: Mean migration speed of CONT or TRIO OE MCF10A cells. Wilcoxon Rank-Sum test, * = P<0.05, comparing to CONT cells. **a, c-d,** Wilcoxon Rank-Sum test; Black * = P<0.05, comparing to no drug treatment in shCtrl or shTRIO cells; Black # = P<0.05, comparing to shCtrl cells with no drug

treatment. Red * = P<0.05, comparing to no drug treatment in shYAP cells; Blue * = P<0.05, comparing to no drug treatment in shTRIO cells; Red # = P<0.05, between shYAP and shCtrl cells at corresponding drug concentration; Blue # = P<0.05, between shTRIO and shCtrl cells at corresponding drug concentration. **f,** Mean migration speed of shCtrl, shYAP-2, and shYAP-2+TRIO OE JHGBM651 cells (n=30 cells). Wilcoxon Rank-Sum test, * = P<0.05, comparing to shCtrl cells. All error bars are s.e.m. All experiments were performed in triplicate except otherwise stated and repeated three times with similar results.

Supplemental Fig. 9. YAP activates STAT3 to drive invasion. a, Expression of the Invasive signatures in GB-YAP high, intermediate, or low patient groups in the REMBRANDT GBM dataset. **b,** Percentage of patients with elevated GB-YAP signature, Invasive signature, or both in the REMBRANDT GBM dataset. P = Fisher's exact test using the sizes of the shown patient groups. **c,** Matrigel Boyden invasion assay of shCtrl, shYAP-1, or -2 JHGBM651/612, NHA, MCF10A cells and CONT or YAP OE MCF10A cells. **d,** Relative MMP2, MMP9, and CTGF mRNA expression in shCtrl or shYAP JHGBM651/612 cells. **e,** Expression of different STAT3 signatures in GB-YAP high, intermediate, or low patient groups in the REMBRANDT GBM dataset. **a, e,** Student's t-test, * = P<0.05, between YAP high and YAP low. **c-d,** Wilcoxon Rank-Sum test, * = P<0.05, comparing to shCtrl or CONT cells. **f,** Representative immunoblot of YAP, total and phospho-Tyr705 STAT3 expression in shCtrl, shYAP-1, or -2 JHGBM651/612/640/1A, NHA, and MCF10A cells and CONT or YAP OE MCF10A cells. **g,** Matrigel Boyden invasion assay of shCtrl and shYAP JHGBM612 cells treated with vehicle or the STAT3 inhibitor LLL12. Wilcoxon Rank-Sum test; * = P<0.05, comparing to no drug treatment in shCtrl cells; # = P<0.05, comparing to shCtrl cells with no drug treatment. **h,** Mean migration speed of shCtrl, shYAP-1, or -2 JHGBM651 cells treated with increasing doses of the STAT3 inhibitor LLL12 (n=30 cells). Wilcoxon Rank-Sum test; Black * = P<0.05, comparing to no drug treatment in shCtrl cells; Red * = P<0.05, comparing to no drug treatment in shYAP cells; Red

= P<0.05, between shYAP and shCtrl cells at corresponding drug concentration. All error bars are s.e.m. All experiments were performed in triplicate except otherwise stated and repeated three times with similar results.

Supplemental Fig. 10. YAP-TRIO signaling regulate invasion through the Rac1-STAT3 axis. a, Representative immunoblot of TRIO, total and phosphor-Tyr705 STAT3 expression in shCtrl, shTRIO-1, or -2 JHGBM1A, NHA, and MCF10A cells. **b,** Matrigel Boyden invasion assay of shCtrl, shYAP, shTRIO-1, or -2 JHGBM651/640 and NHA cells. Wilcoxon Rank-Sum test; * = P<0.05, comparing to shCtrl cells. **c,** Representative immunoblot of total and phosphor-Tyr705 STAT3 expression in JHGBM651/612 cells treated with the Rac1-GEF inhibitor NSC23766 or TRIO inhibitor ITX3. **d,** Matrigel Boyden invasion assay of shCtrl, shYAP, or shTRIO JHGBM651/612/640 and NHA cells treated with the TRIO inhibitor ITX3. **e,** Matrigel Boyden invasion assay of shCtrl, shYAP-1/2, or shTRIO1/2 JHGBM651/612 and NHA cells treated with the ROCK inhibitors Y26732 or H1152. **d-e,** Wilcoxon Rank-Sum test; * = P<0.05, comparing to no drug treatment in shCtrl cells; # = P<0.05, comparing to shCtrl cells with no drug treatment. **f,** *Left*, Representative immunoblot of MMP2 expression in shCtrl, shYAP, shTRIO, and shSTAT3 GBMA172 cells. *Right*, Relative MMP2 mRNA expression in shCtrl, shYAP, shTRIO, and shSTAT3 GBMA172 cells. Wilcoxon Rank-Sum test, * = P<0.05, ** = P<0.01, comparing to shCtrl cells. All error bars are s.e.m. All experiments were performed in triplicate except otherwise stated and repeated three times with similar results.

Supplemental Fig. 11. Elevated YAP signaling predicts poor clinical outcome in all GBM subtypes. a, Expression of GB-YAP signature expression across different glioma grades in REMBRANDT dataset. **b,** Kaplan-Meier graph of cumulative overall survival in patient groups defined by GB-YAP signature expression in REMBRANDT dataset. *P* = Log-Rank test. **c-e,** Kaplan-Meier graphs of cumulative overall survival in patient groups defined by GB-YAP signature

expression in each indicated GBM subclass in the TCGA dataset. P=Log-Rank test. **f,** Kaplan-Meier graph of cumulative overall survival in patient groups defined by GB-STAT3 signature expression in REMBRANDT dataset. P=Log-Rank test. **g,** Kaplan-Meier graph of cumulative overall survival in patient groups defined by both the GB-YAP and STAT3 signature expression in the REMBRANDT dataset. *P* = Log-Rank test. All error bars are s.e.m. All experiments were performed in triplicate except otherwise stated and repeated three times with similar results.

Supplemental Fig. 12. Each component of the YAP-TRIO-STAT3 network is indispensable to promoting poor clinical outcome in GBM patients. Kaplan-Meir graphs of all combinations of mixed expression groups of YAP, TRIO, STAT3 in TCGA microarray dataset. Tables include p-value of comparisons between different combination groups. YAP-TRIO survival combinations were also evaluated in RNA-seq expression data from TCGA (table shown). *P* = Log-Rank test.

Supplemental Movies: Seven (7) movies show migration of shCtrl, shYAP, or shTRIO JHGBM651 cells with different treatments (i.e., inhibitors against ROCK, Rac1-GEF, TRIO, or STAT3). Each movie is listed and described below:

Supplemental Movie 1. Migration of shCtrl and shYAP GBM cells. A representative time-lapse video of shCtrl (left) and shYAP (right) JHGBM651 cells. Images captured at 20-minute intervals for 6 hours. Each colored line represents the migration pattern of each cell. Scale bar = 100 μm.

Supplemental Movie 2. Migration of shCtrl and shYAP GBM cells with vehicle or ROCK inhibitor treatment. A representative time-lapse video of shCtrl (left) and shYAP (right) JHGBM651 cells with vehicle (top) or treatment with the ROCK inhibitor Y27632 (bottom). Images are captured

at 20-minute intervals for 6 hours. Each colored line represents the migration pattern of each cell. Scale bar = 100 μm.

Supplemental Movie 3. Migration of shCtrl and shYAP GBM cells with vehicle or Rac1-GEF inhibitor treatment. A representative time-lapse video of shCtrl (left) and shYAP (right) JHGBM651 cells with vehicle (top) or treatment with the Rac1-GEF inhibitor NSC23766 (bottom). Images are captured at 20-minute intervals for 6 hours. Each colored line represents the migration pattern of each cell. Scale bar = 100 μm.

Supplemental Movie 4. Migration of shCtrl and shYAP GBM cells with vehicle or TRIO inhibitor treatment. A representative time-lapse video of shCtrl (left) and shYAP (right) JHGBM651 cells with vehicle (top) or treatment with TRIO inhibitor ITX3 (bottom). Images are captured at 20-minute intervals for 6 hours. Each colored line represents the migration pattern of each cell. Scale bar = 100 μm.

Supplemental Movie 5. Migration of shCtrl and shTRIO GBM cells. A representative time-lapse video of shCtrl (left) and shtTRIO (right) JHGBM651 cells. Images captured at 20-minute intervals for 6 hours. Each colored line represents the migration pattern of each cell. Scale bar = 100 μm.

Supplemental Movie 6. Migration of shCtrl and shTRIO GBM cells with vehicle or ROCK inhibitor treatment. A representative time-lapse video of shCtrl (left) and shTRIO (right) JHGBM651 cells with vehicle (top) or treatment with ROCK inhibitor Y27632 (bottom). Images are captured at 20-minute intervals for 6 hours. Each colored line represents the migration pattern of each cell. Scale bar = 100 μm.

Supplemental Movie 7. Migration of shCtrl and shYAP GBM cells with vehicle or STAT3 inhibitor treatment.

A representative time-lapse video of shCtrl (left) and shYAP (right) JHGBM651 cells with vehicle (top) or treatment with STAT3 inhibitor LLL12 (bottom). Images are captured at 20-minute intervals for 6 hours. Each colored line represents the migration pattern of each cell. Scale bar = 100 μm.

Supplemental Tables: Three tables are submitted separately. **Supplemental** Table 1 contains a table in PDF format. **Supplemental** Table 2 and 3 are MS Excel files. Descriptions/titles for each Table are listed below:

Supplemental Table 1. Annotation of intraoperatively obtained human GBM tissues and cells with corresponding clinical characteristics of donor patient.

This table contains GBM tissue and cell ID numbers with their corresponding de-identified patient IDs, age, gender, and final pathology diagnosis.

Supplemental Table 2. Microarray data of shCtrl or shYAP JHGBM651 and JHGBM612 cells.

Supplemental Table 3. Densitometric quantification of all immunoblotting results included in this paper.

Figure 1| YAP regulates migratory capacity

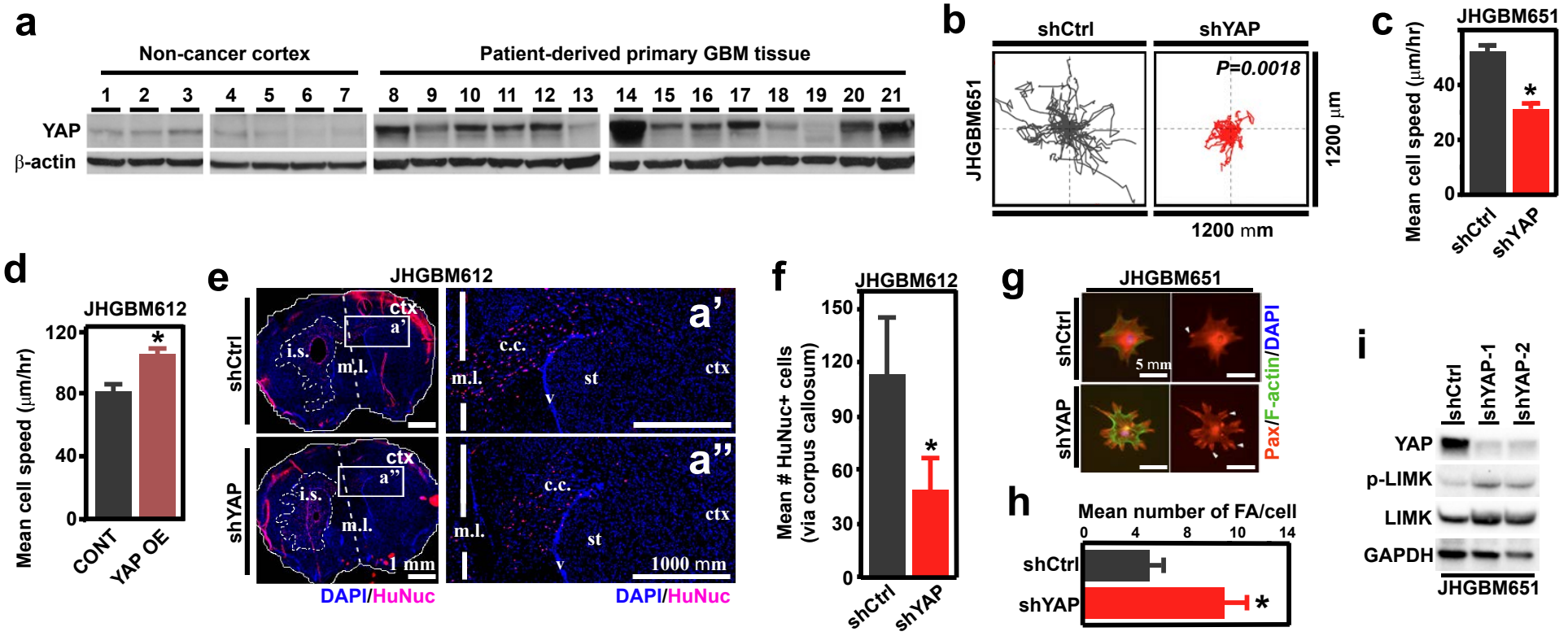

Figure 2| YAP regulates migration through a Rho-GTPase Switch

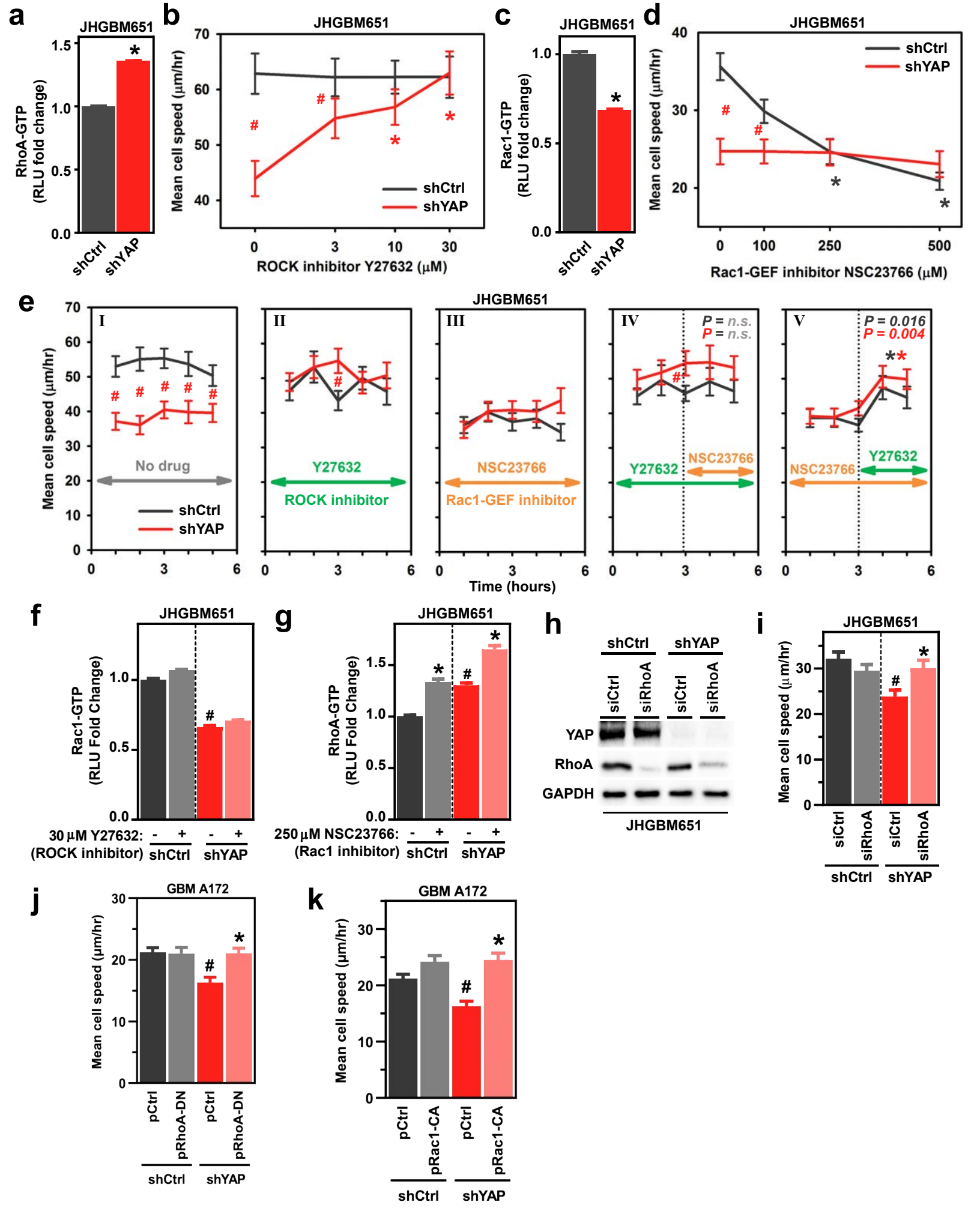

Figure 3| YAP directly transactivates the Rac1-GEF TRIO

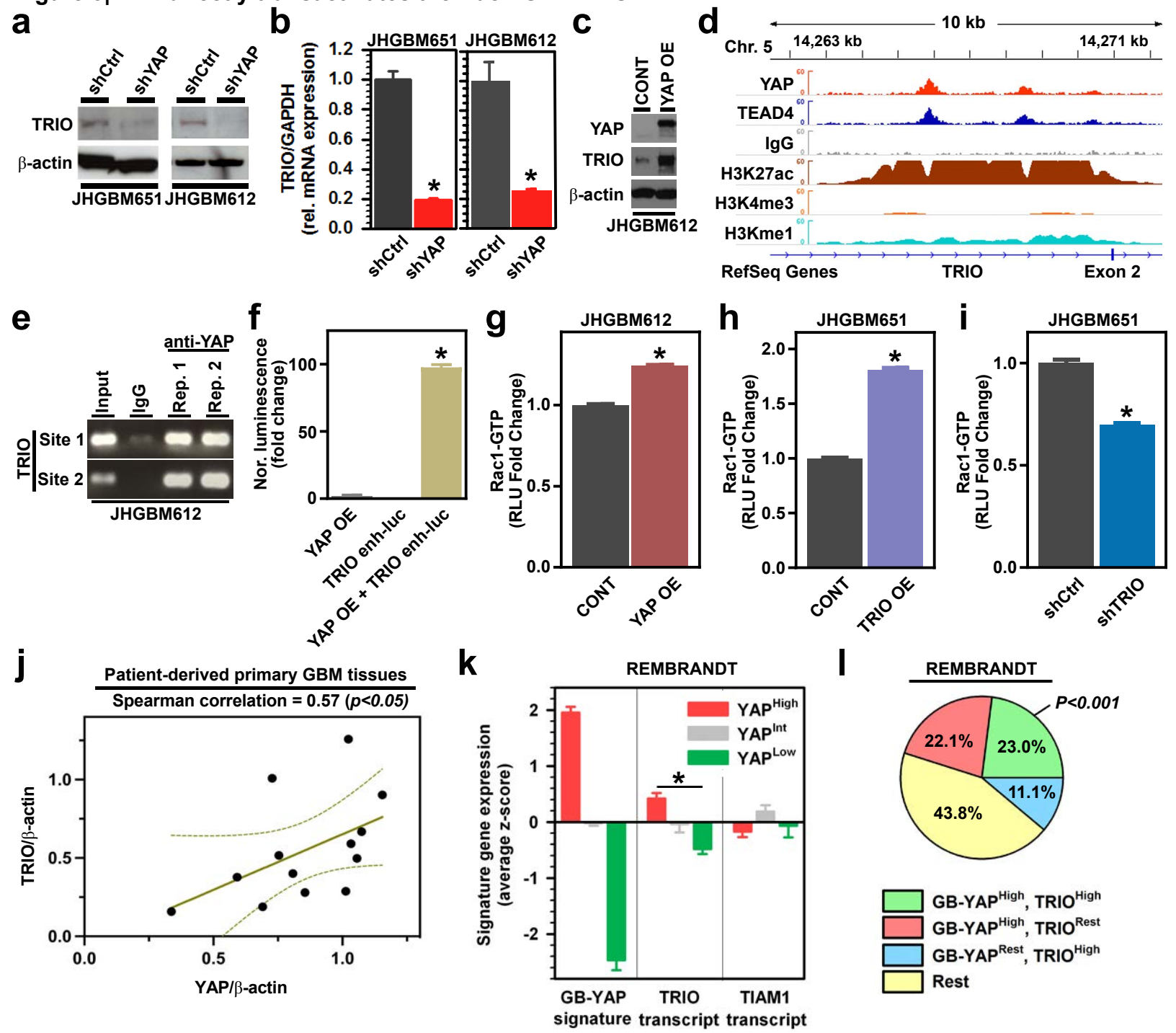

Figure 4| YAP-TRIO signaling regulates migration

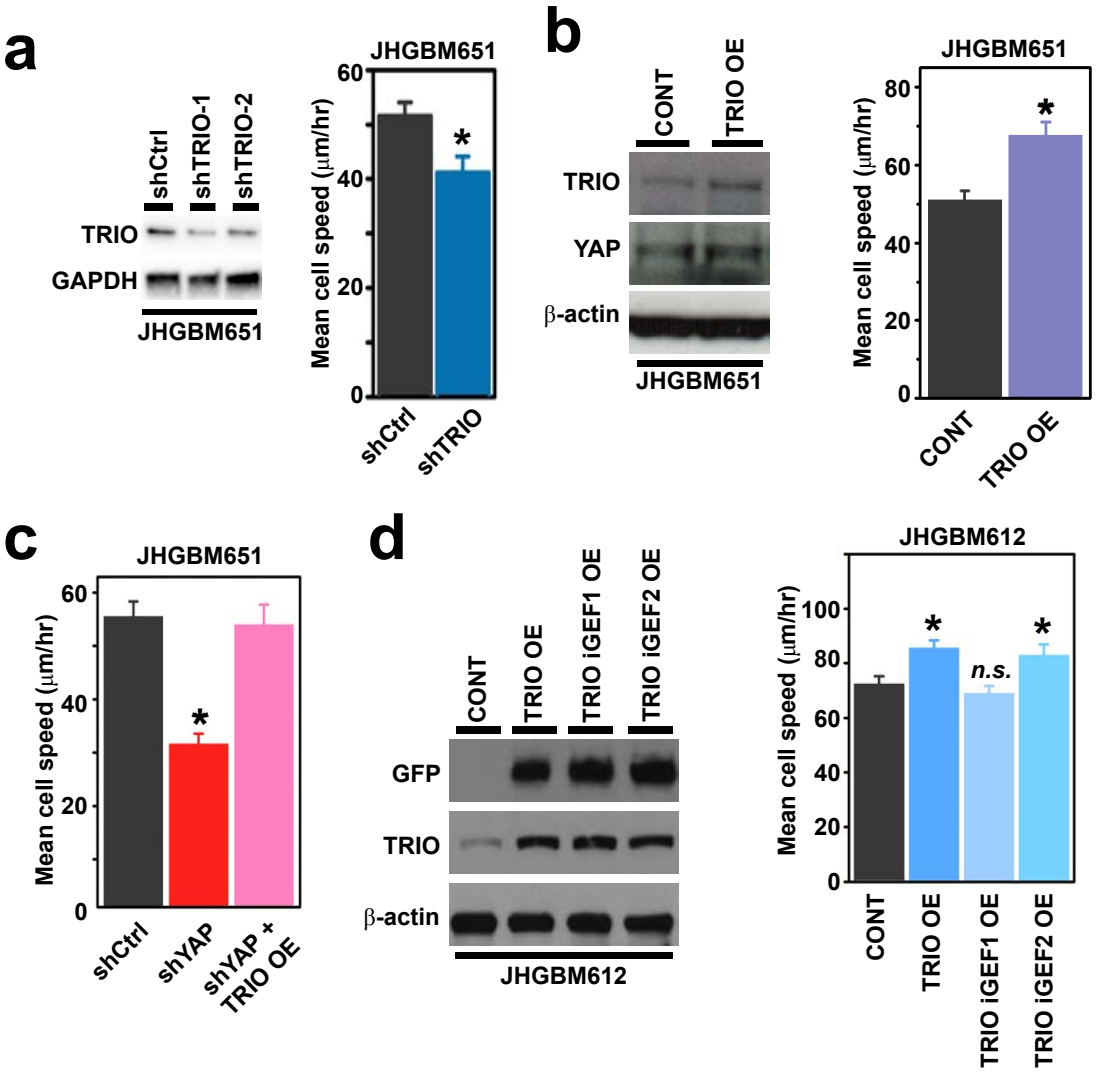

Figure 5| YAP promotes invasion by activating STAT3

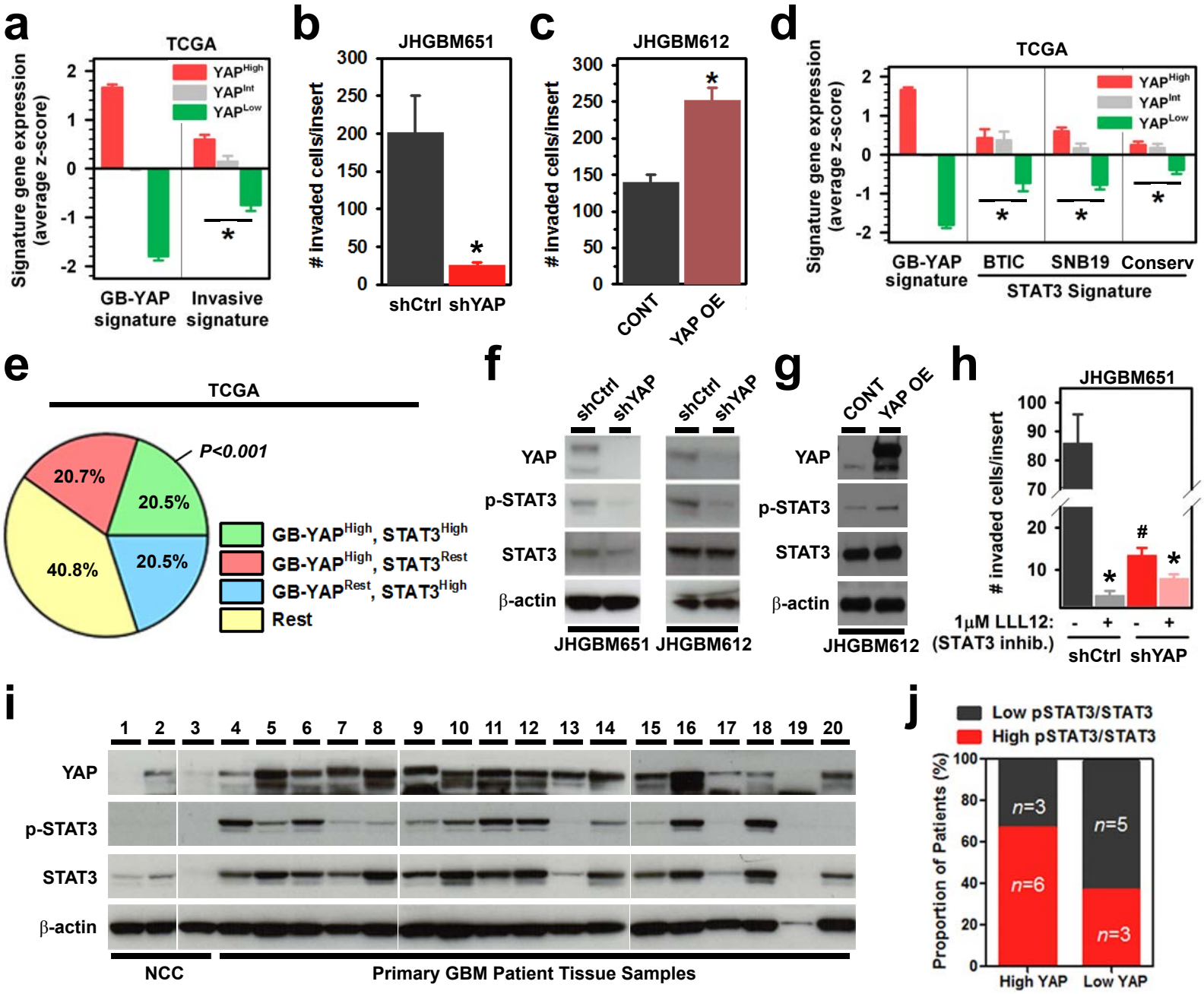

Figure 6| YAP potentiates invasion by activating the TRIO mediated Rac1-STAT3 axis

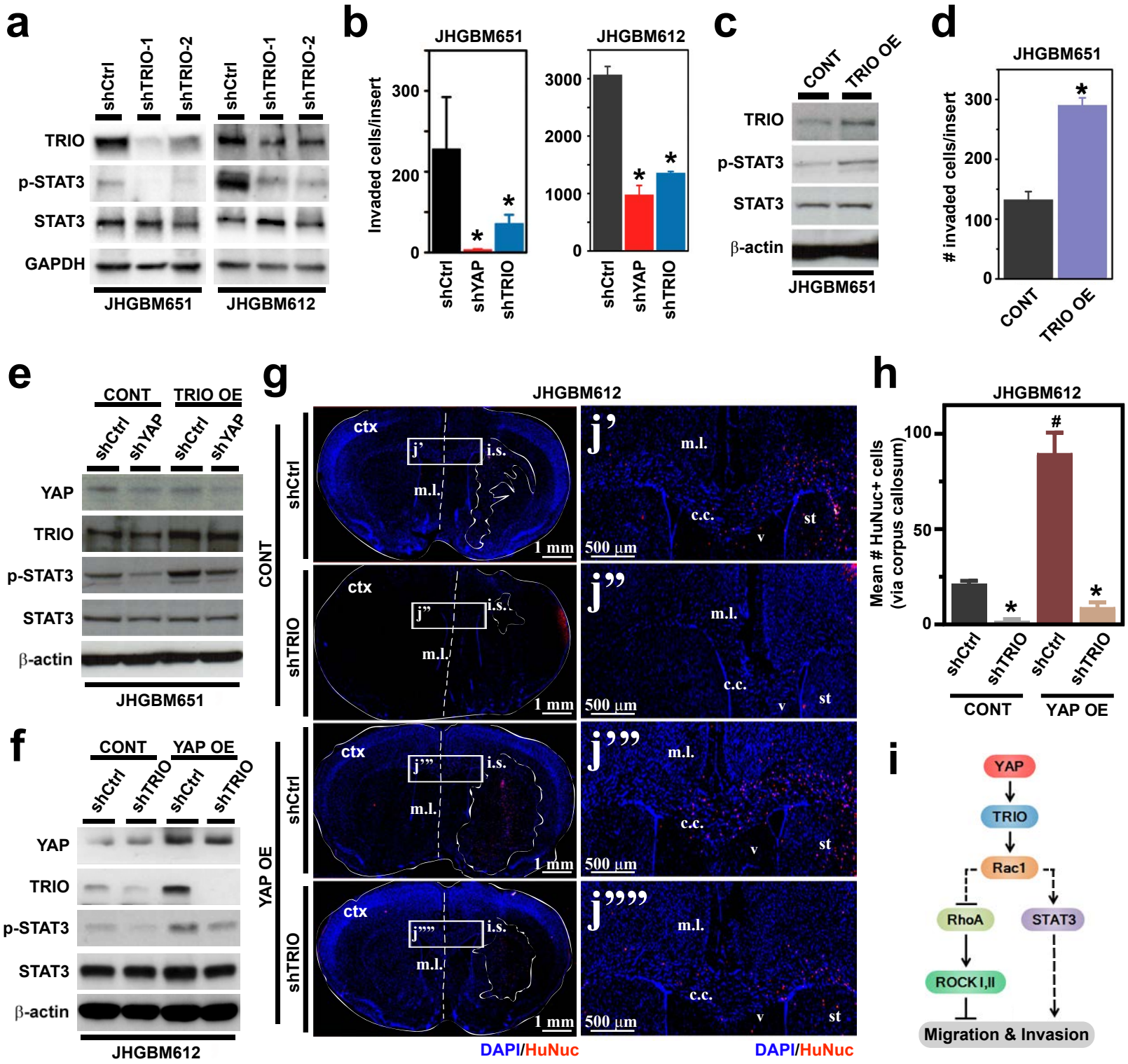

Figure 7| YAP-TRIO-STAT3 signaling predicts poor clinical outcome in glioblastoma

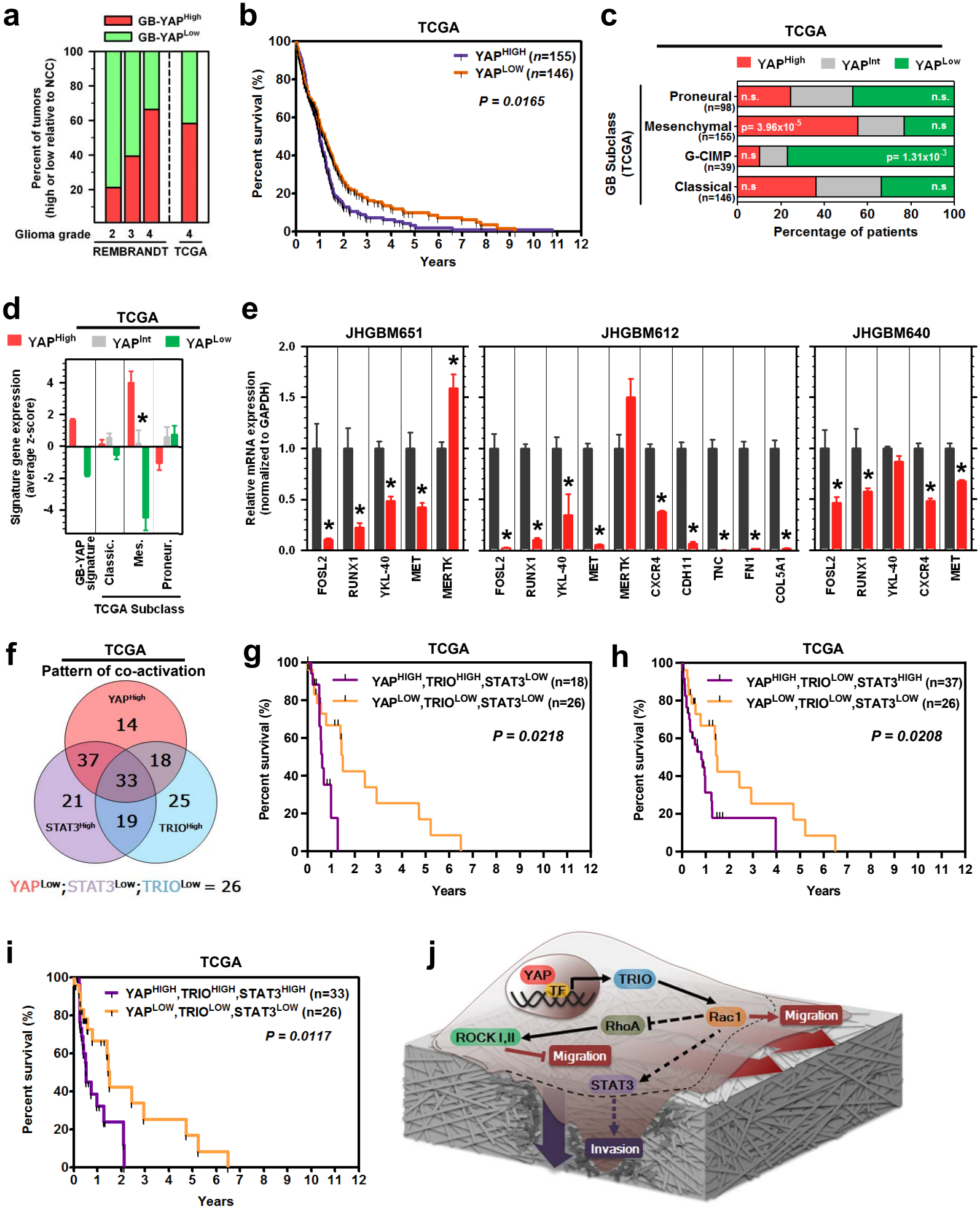

Supplementary Figure 1| YAP regulates migration

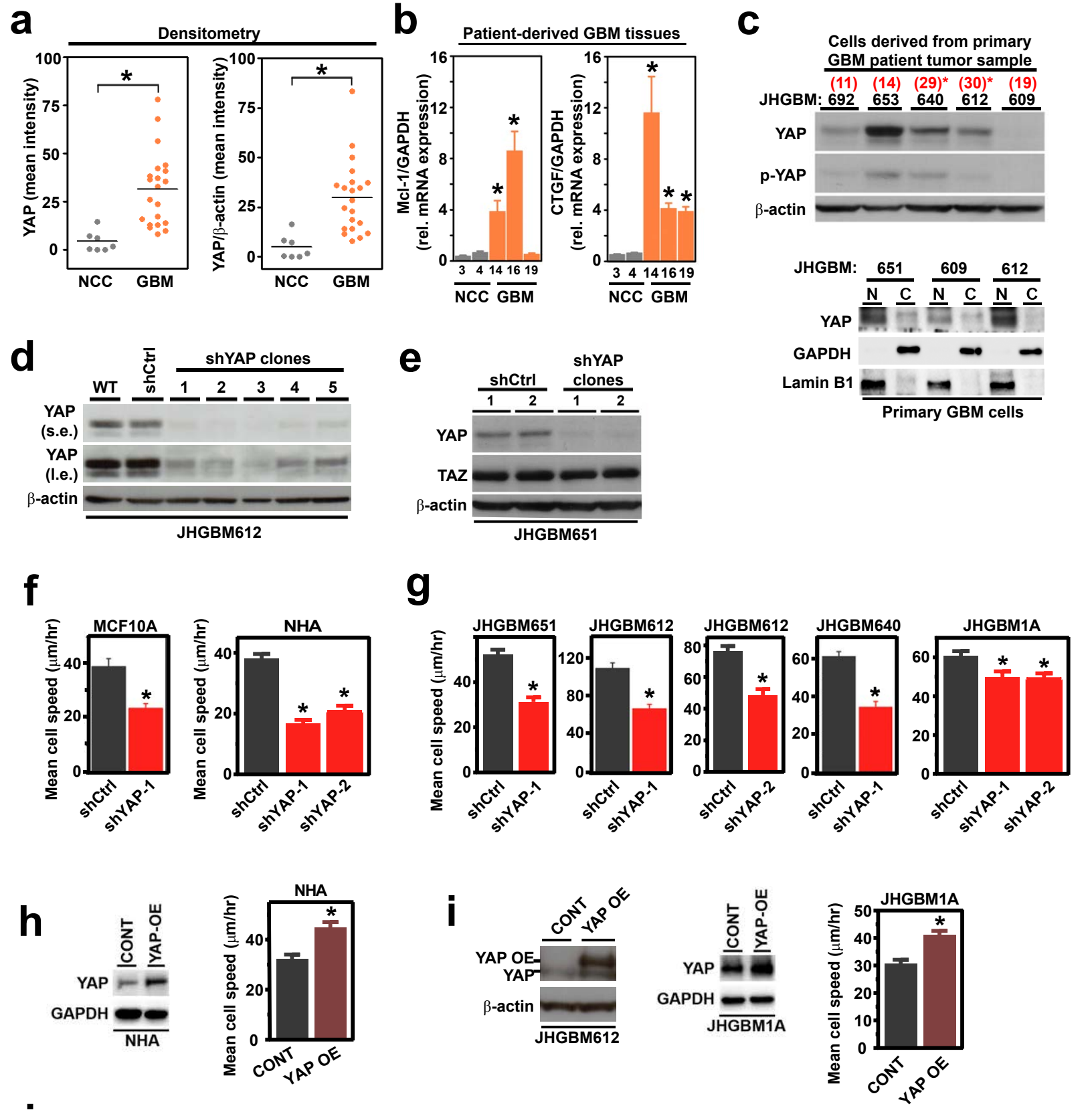

Supplemental Figure 1| YAP regulates migration

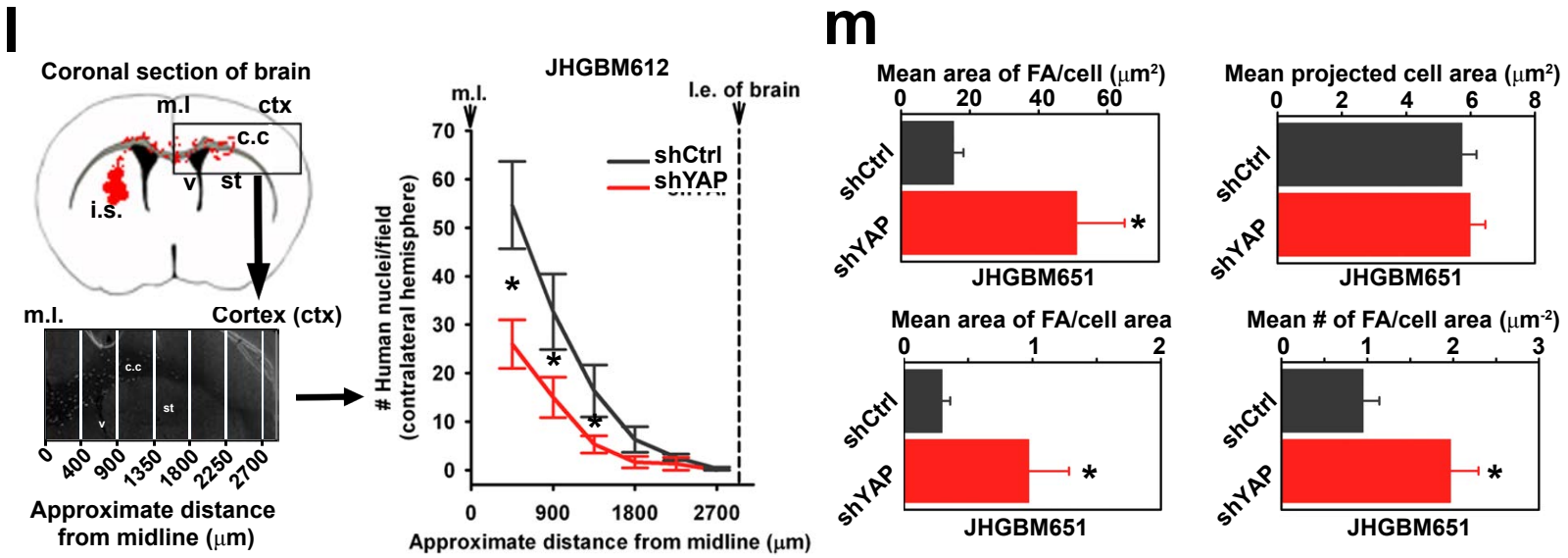

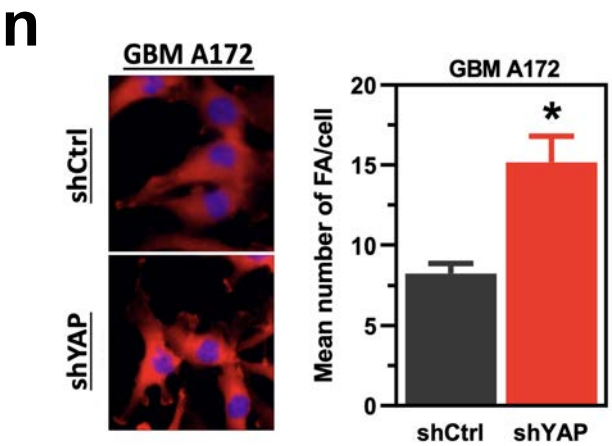

Supplemental Figure 2| YAP regulates migration by inhibiting RhoA-ROCK signaling

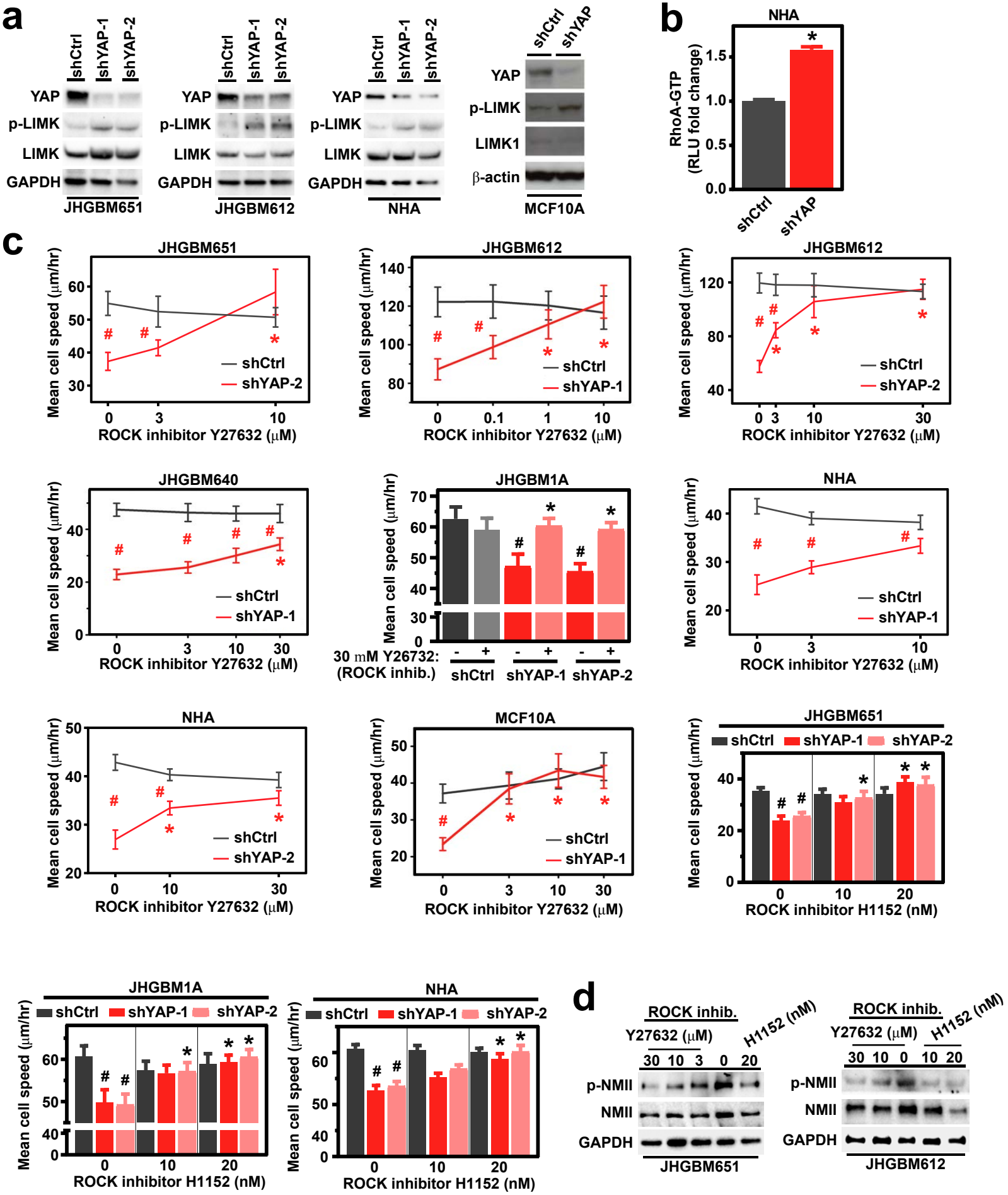

Supplemental Figure 3| YAP regulates migration by activating Rac1 signaling

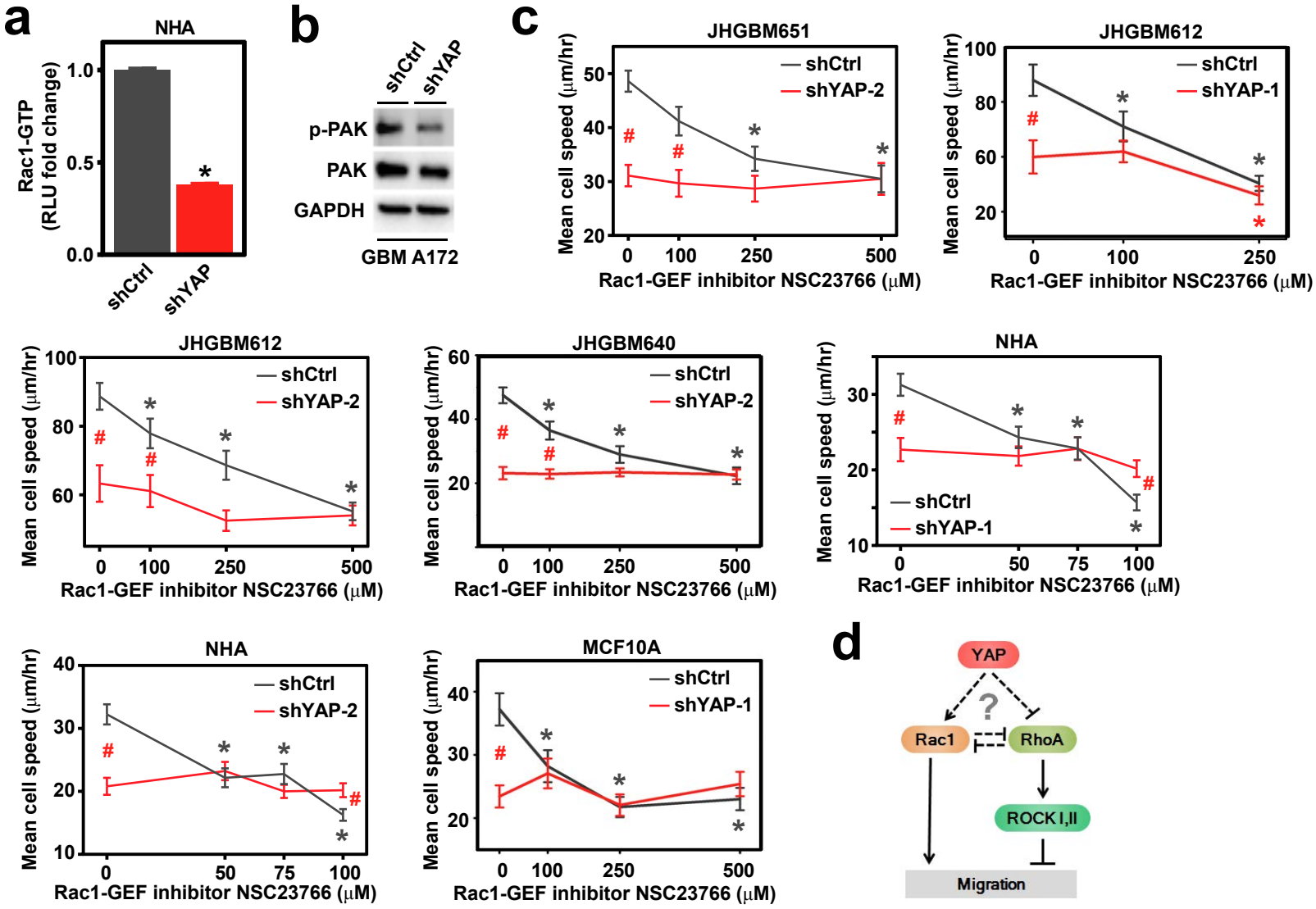

Supplemental Figure 4| YAP regulates migration by modulating a Rho-GTPase switch

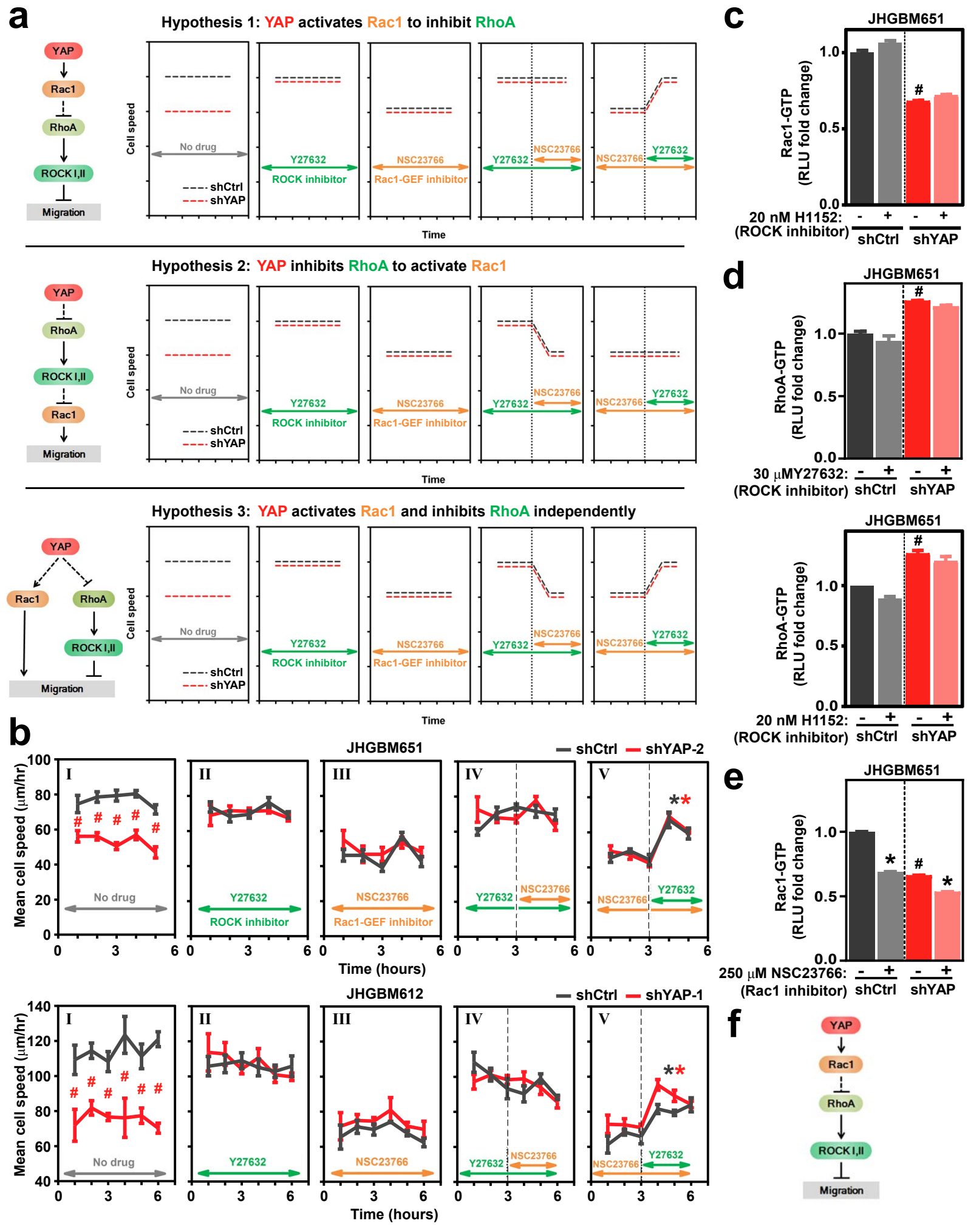

Supplemental Figure 5| YAP transactivates TRIO signaling

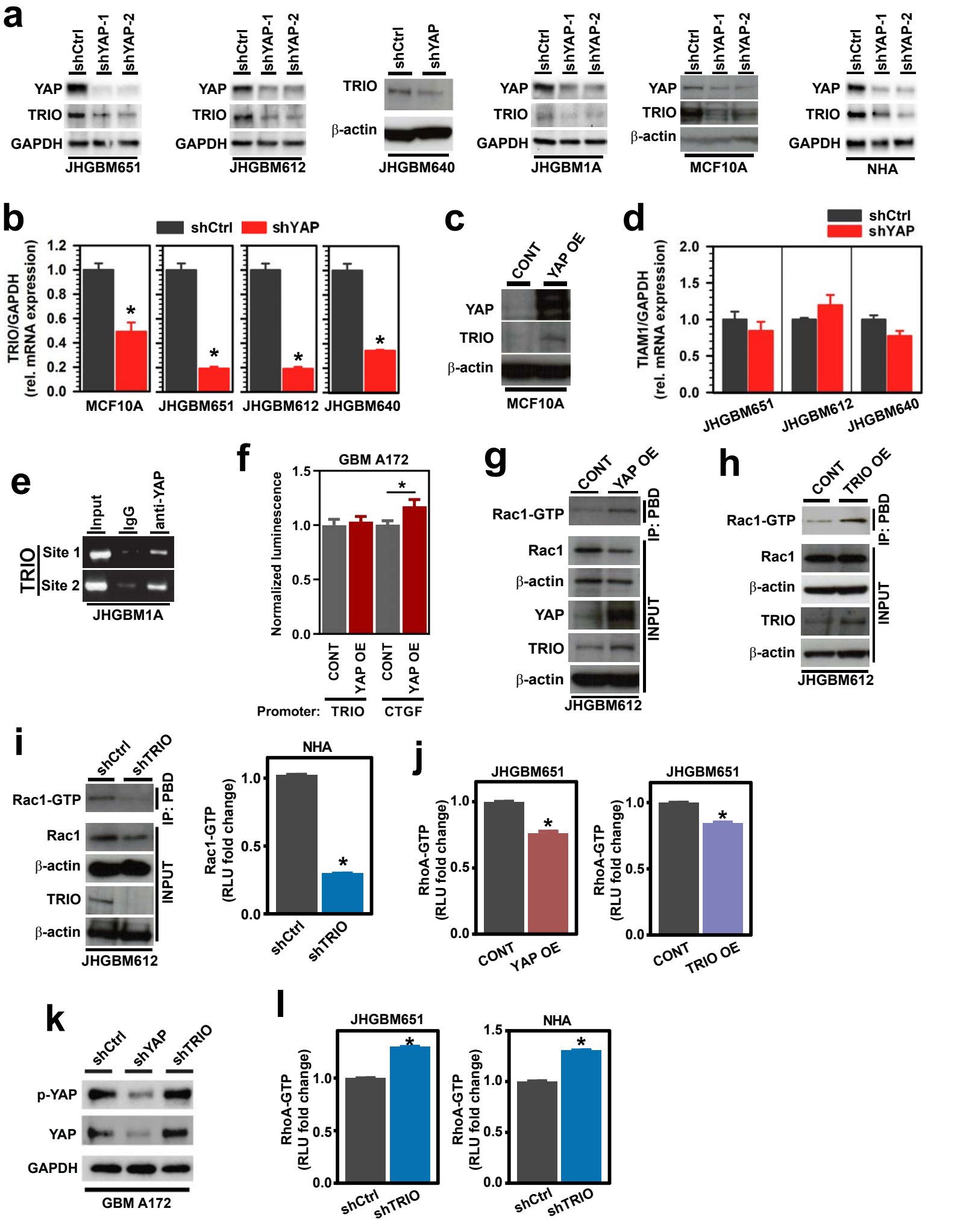

Supplemental Figure 5| YAP transactivates TRIO signaling

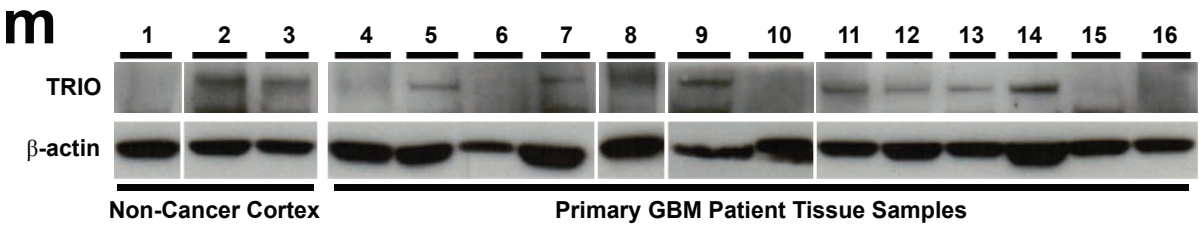

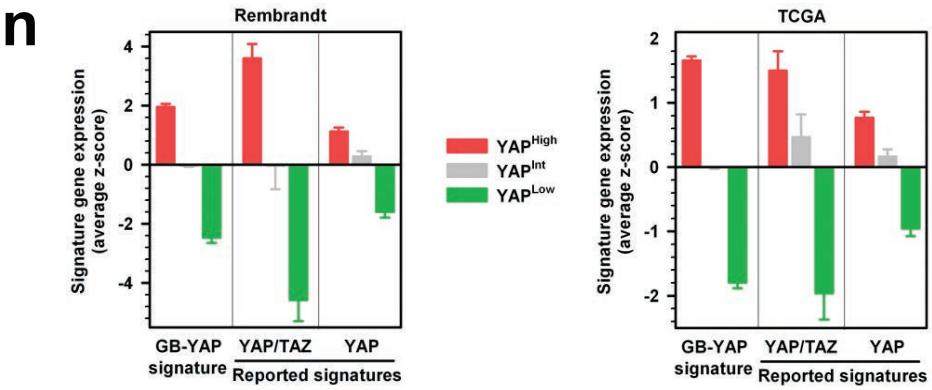

Supplemental Figure 6| YAP regulates migration via TRIO signaling

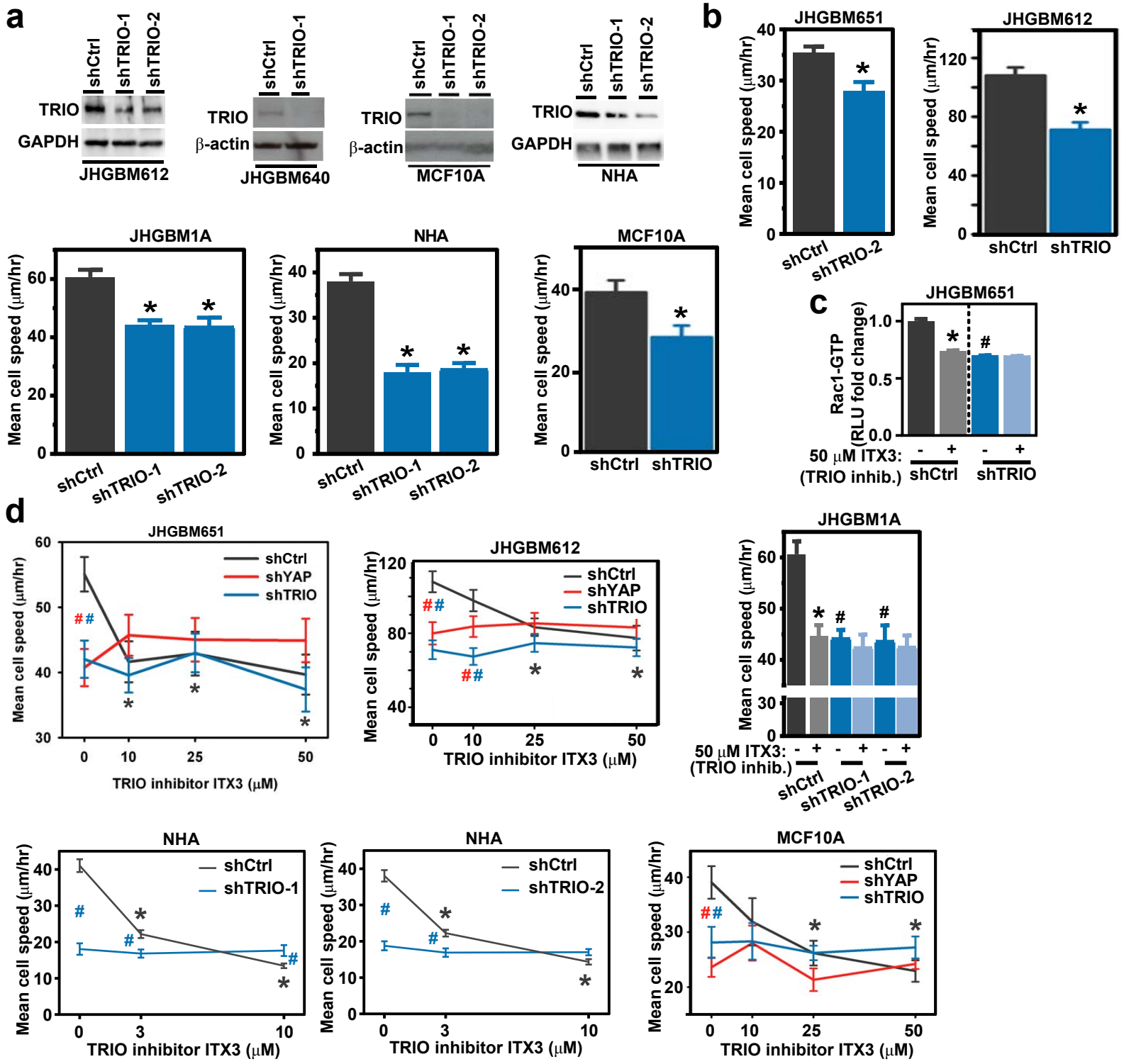

Supplemental Figure 7| YAP-TRIO signaling modulates Rac1-RhoA signaling to drive migration

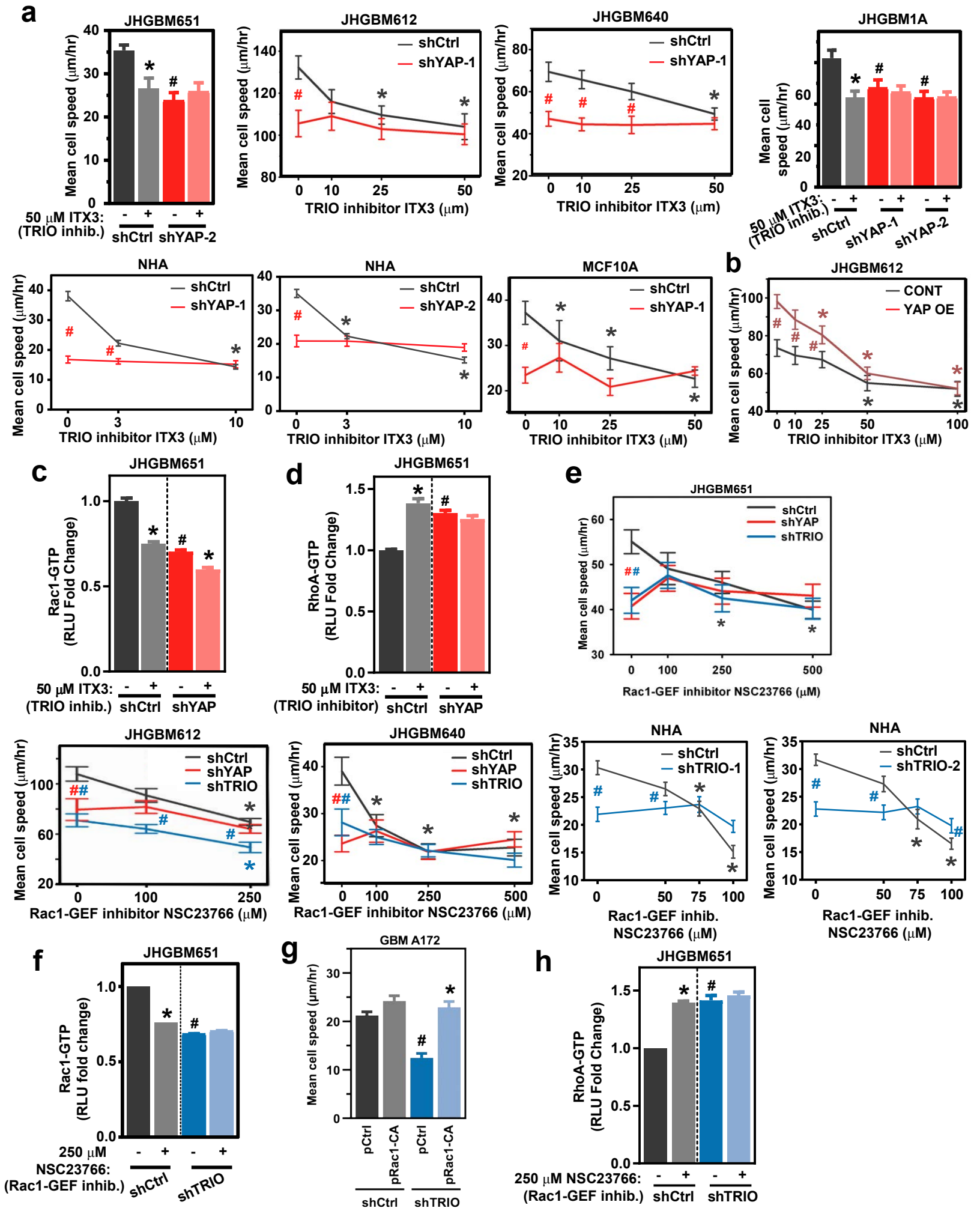

Supplemental Figure 8| YAP-TRIO signaling regulates migration by modulating Rac1-RhoA crosstalk

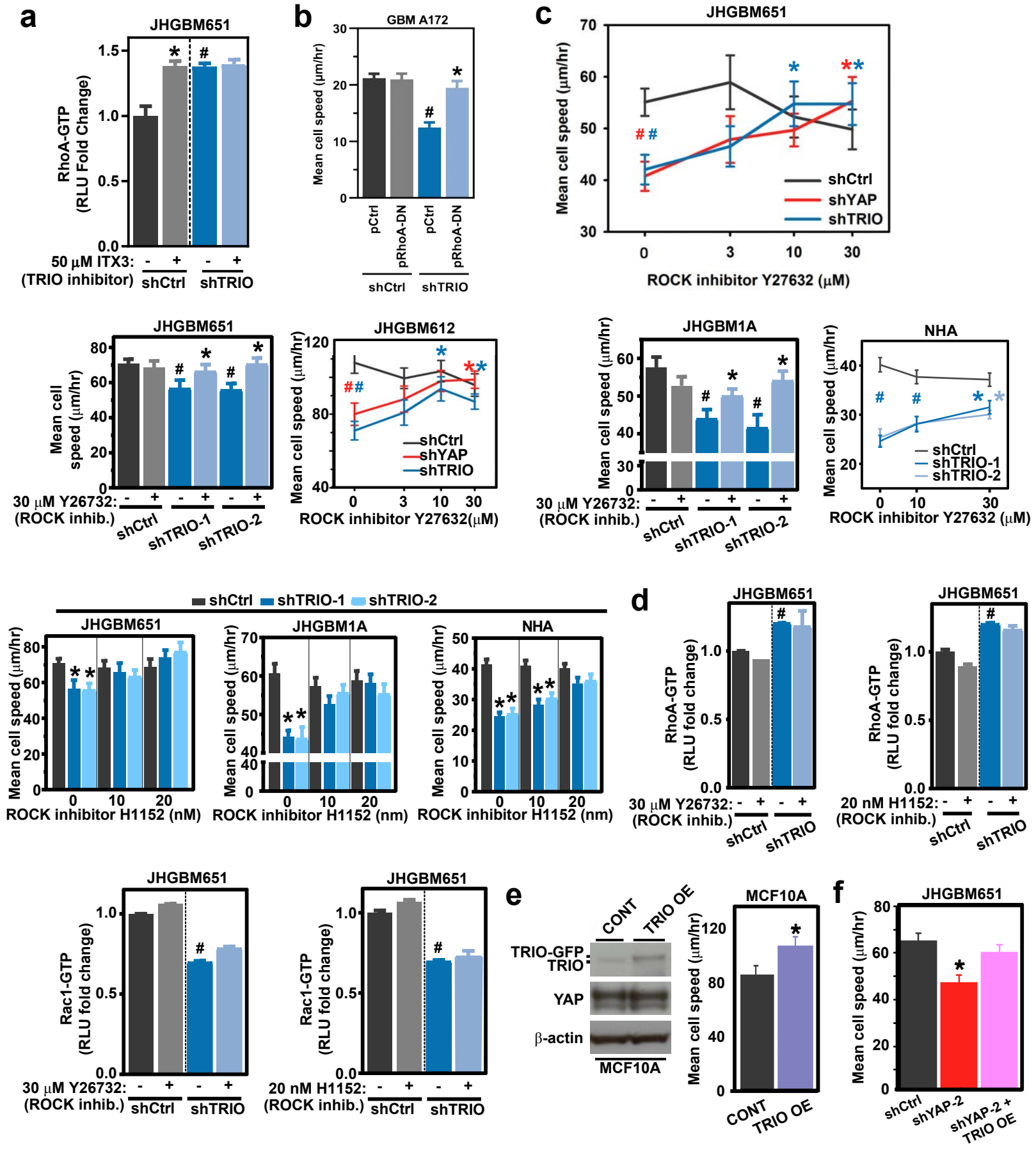

Supplemental Figure 9| YAP activates STAT3 to drive invasion

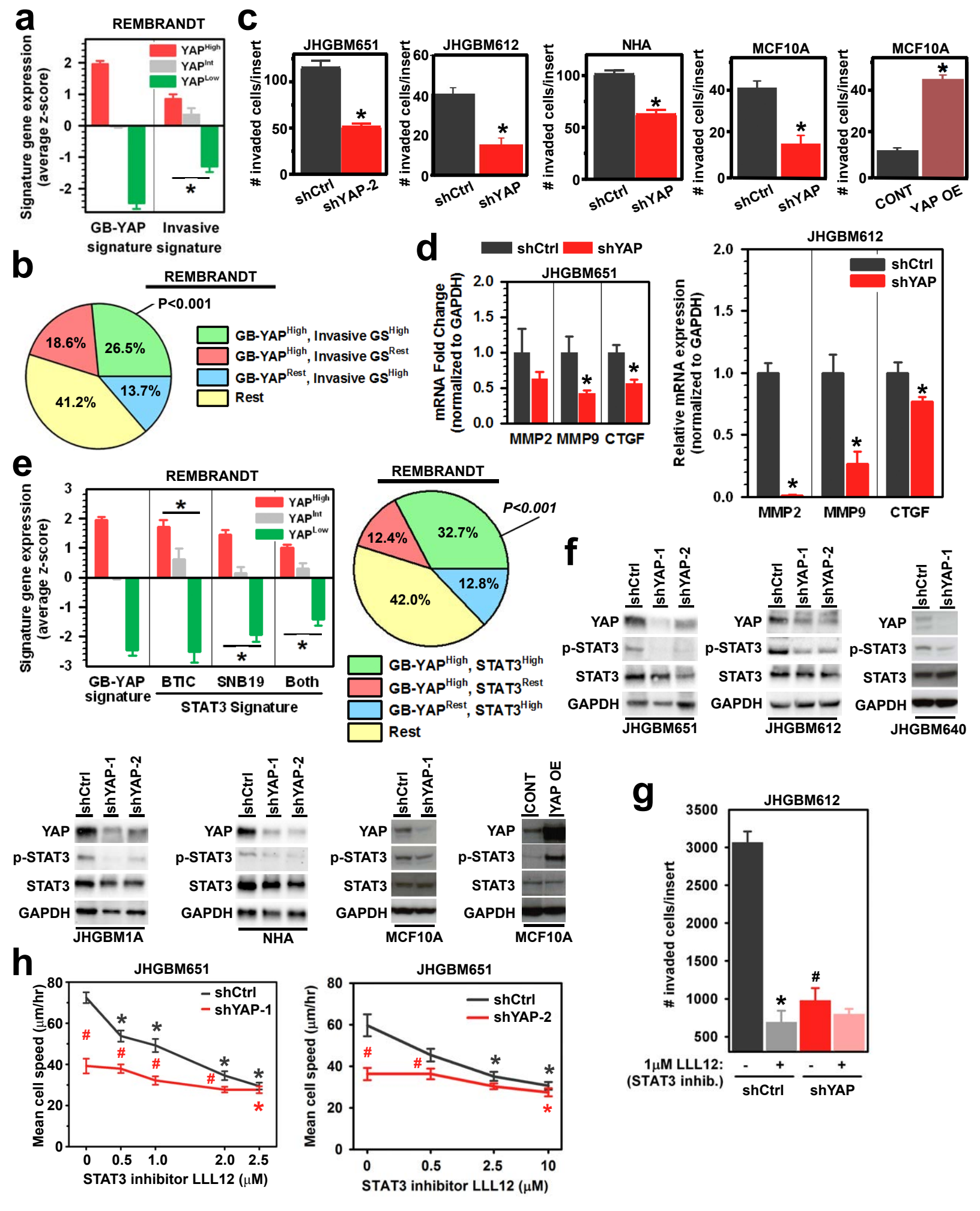

Supplemental Figure 10| YAP-TRIO signaling regulate invasion through the Rac1-STAT3 axis

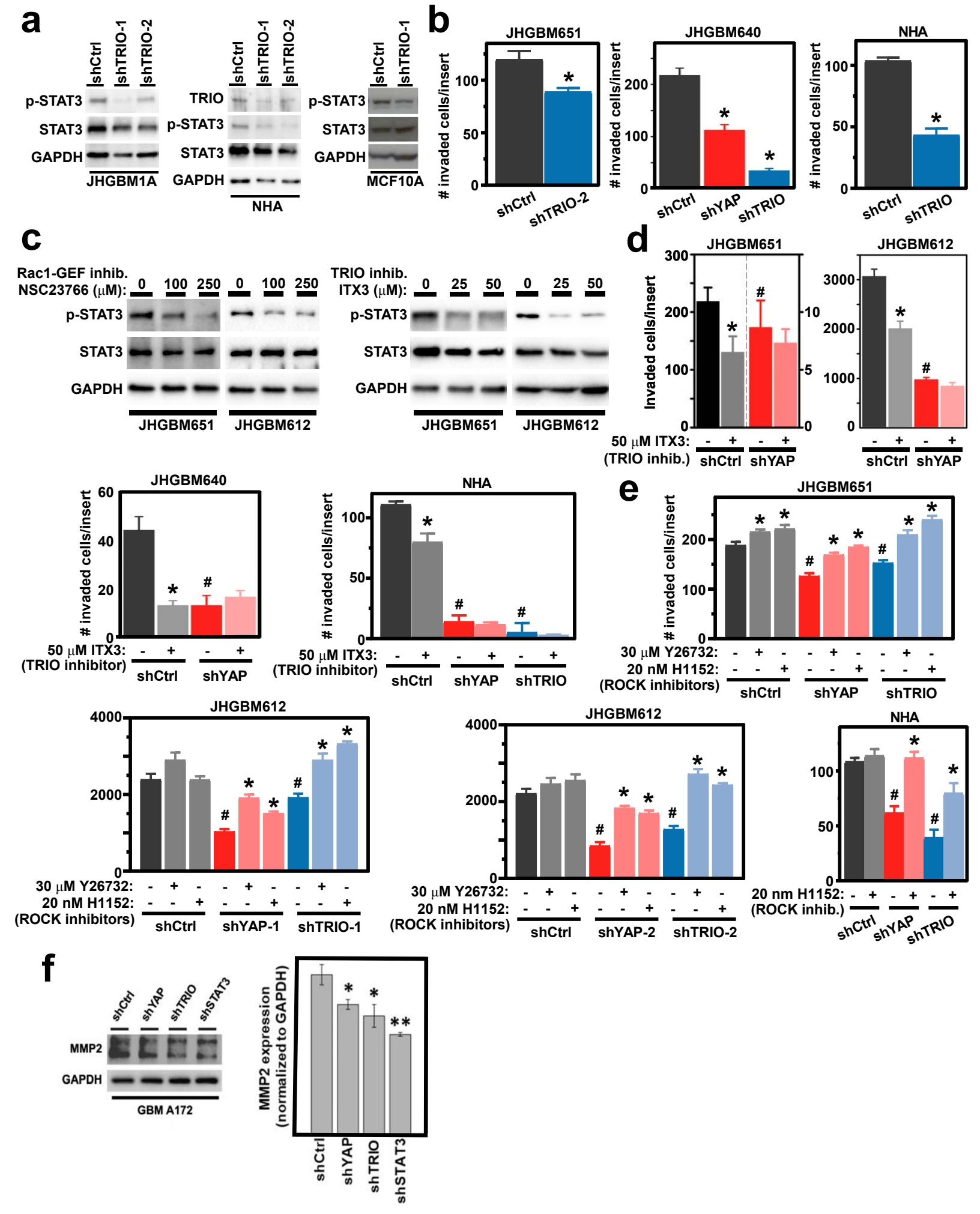

Supplemental Figure 11| Elevated YAP signaling predicts poor clinical outcome in all GBM subtypes

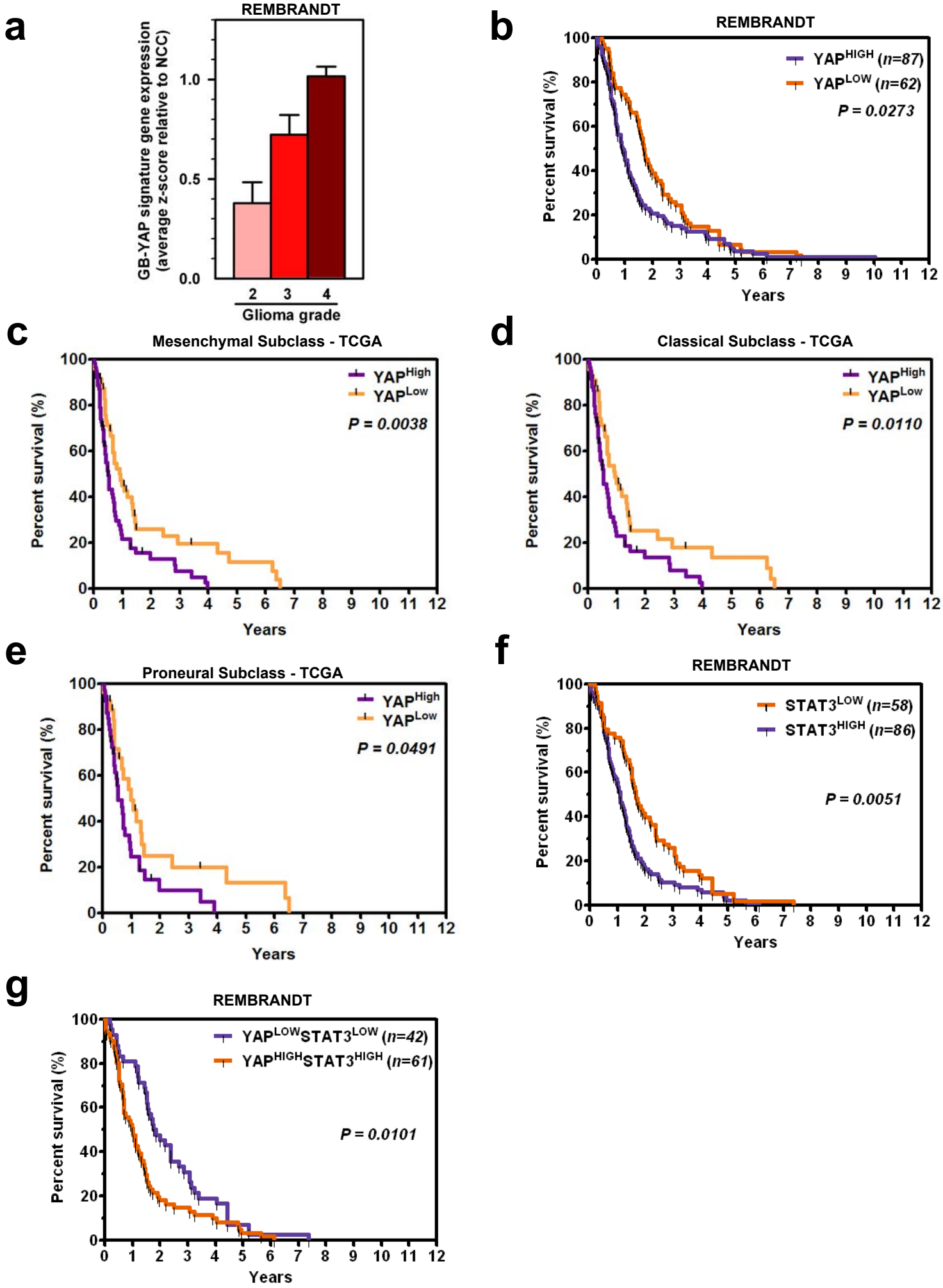

Supplemental Figure 12| Each component of the YAP-TRIO-STAT3 network is indispensable to promoting poor clinical outcome in GBM patients

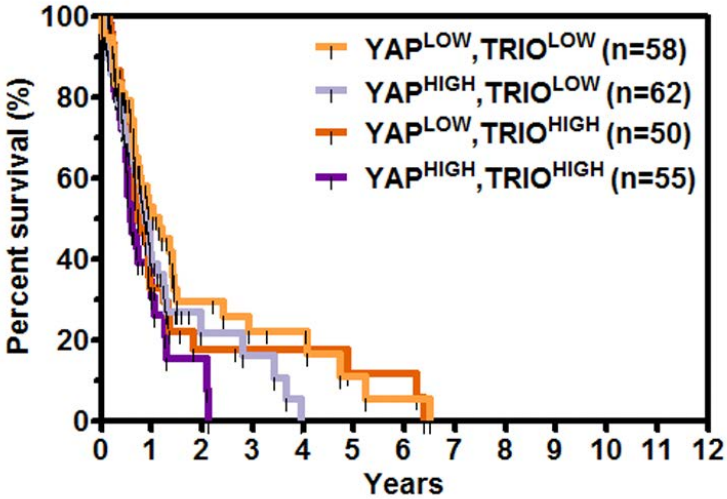

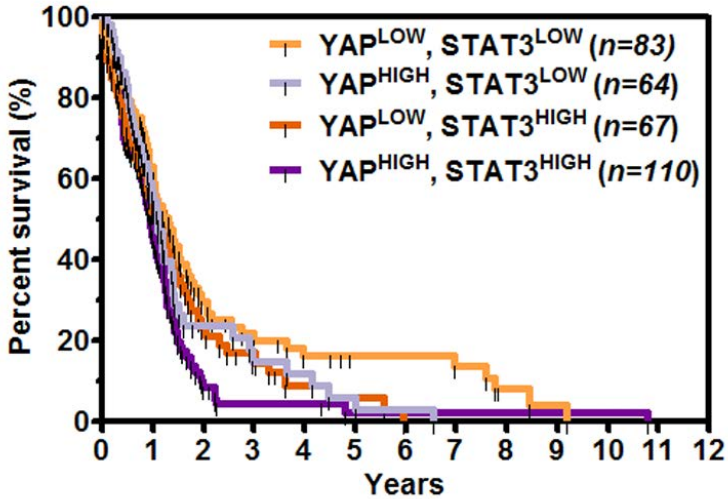

YAP-TRIO (microarray)		
	Hi.Lo	Lo.Hi
Lo.Lo	0.151	0.32
Hi.Hi	0.17	0.184

YAP-TRIO (RNA-Seq)		
	Hi.Lo	Lo.Hi
Lo.Lo	0.08	0.191
Hi.Hi	0.1032	0.52

YAP-STAT3 (microarray)		
	Hi.Lo	Lo.Hi
Lo.Lo	0.1394	0.0856
Hi.Hi	0.1019	0.1105

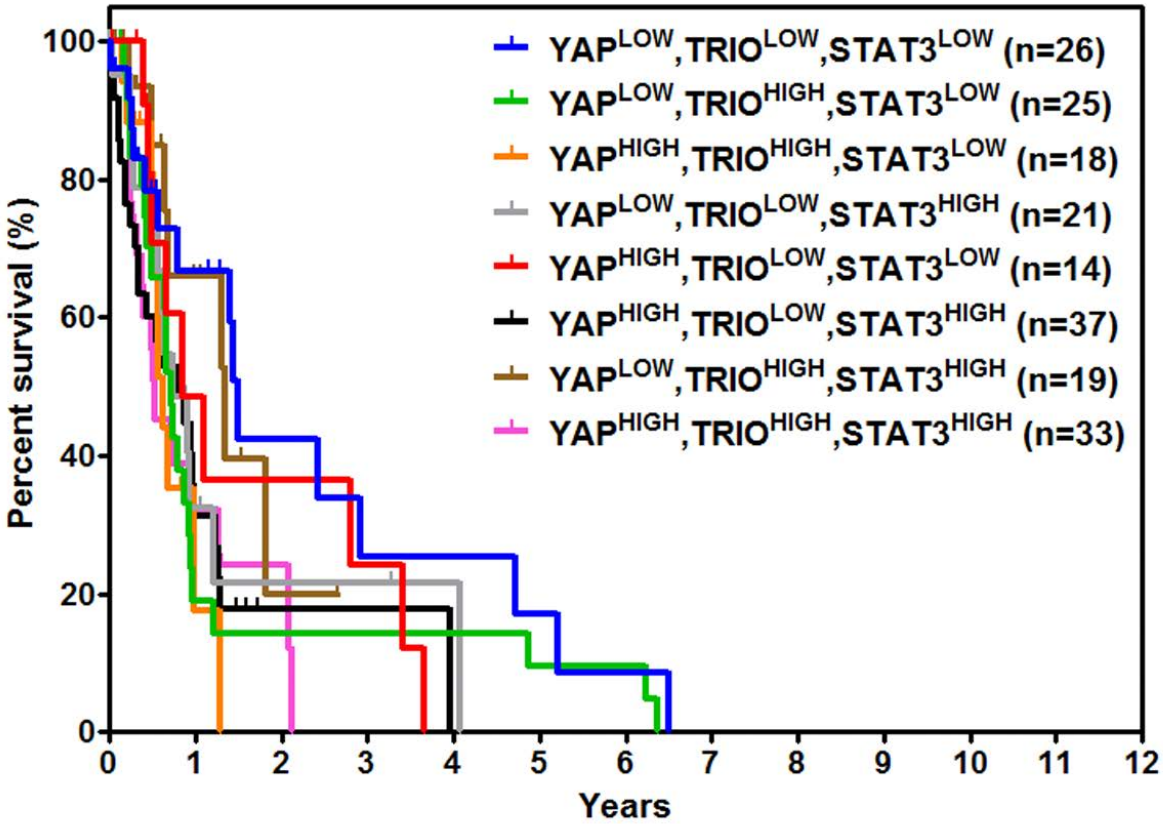

YAP-TRIO-STAT3 (microarray)							
	Hi.Lo.Lo.	Lo.Hi.Lo	Lo.Lo.Hi	Lo.Hi.Hi	Hi.Lo.Hi	Hi.Hi.Lo	
Lo.Lo.Lo	0.3869	0.0688	0.1452	0.7766	0.0208	0.0218	Lo.Lo.Lo
Hi. Hi. Hi	0.0823	0.6775	0.3479	0.058	0.9496	0.9977	Hi. Hi. Hi

Supplemental Table 1

Sample #	Identifier	Sex	Age	Pathology
1	JHNC693	F	57	Normal neocortex (meningioma; WHO grade I)
2	JHNC574	F	53	Normal neocortex (mesial temporal sclerosis; hippocampus)
3	JHNC557	M	29	Normal neocortex (mesial temporal sclerosis; hippocampus)
4	JHNC533	M	49	Normal neocortex (mesial temporal sclerosis; hippocampus)
5	JHNC503	M	28	Normal neocortex (mesial temporal sclerosis; hippocampus)
6	JHNC482	F	31	Normal neocortex (mesial temporal sclerosis; hippocampus)
7	JHNC399	F	48	Normal neocortex (mesial temporal sclerosis; hippocampus)
8	JHGB698	F	76	Glioblastoma
9	JHGB697	F	60	Glioblastoma (recurrent)
10	JHGB695	F	63	Glioblastoma
11	JHGB692	M	56	Glioblastoma
12	JHGB661	M	41	Glioblastoma (primitive neuroectodermal + oligodendroglial features)
13	JHGB658	F	58	Glioblastoma
14	JHGB653	M	74	Glioblastoma
15	JHGB652	M	34	Glioblastoma
16	JHGB651	M	49	Glioblastoma
17	JHGB620	F	73	Glioblastoma
18	JHGB615	F	76	Glioblastoma
19	JHGB609	M	42	Glioblastoma
20	JHGB608	M	69	Glioblastoma
21	JHGB579	M	73	Glioblastoma
22	JHGB577	F	57	Glioblastoma
23	JHGB576	M	80	Glioblastoma
24	JHGB567	M	48	Glioblastoma
25	JHGB549	F	83	Glioblastoma
26	JHGB547	M	64	Glioblastoma (recurrent)
27	JHGB544	M	70	Glioblastoma
28	JHGB529	M	86	Glioblastoma
29	JHGB640	F	49	Glioblastoma
30	JHGB612	F	56	Glioblastoma
31	JHGB531	F	77	Glioblastoma
32	JHGB496	F	53	Glioblastoma (recurrent, secondary gliosarcoma)

Supplemental Table 2

Entrez	Symbol	612-pval	651-pval	612-qval	651-qval	612-FoldChange	651-FoldChange	MeanFoldChange	612Ctrl1	612Ctrl2	612Ctrl3	612shYAP1	612shYAP2	612shYAP3	651Ctrl1	651Ctrl2	651Ctrl3	651shYAP1	651shYAP2	651shYAP3
399694	**SHC4**	0.00205	0.00010	0.07301	0.04276	-1.379	-3.106	-2.243	7.4839551	7.6177382	7.7319358	7.310804549	7.129080319	7.193321714	9.7397266	9.7441781	9.8435432	8.223703611	8.058281136	8.140098627
214	**ALCAM**	0.00704	0.00013	0.09841	0.04276	-1.304	-3.047	-2.176	9.8157206	9.7756539	9.9871523	9.558015416	9.439270874	9.497994935	9.9814406	9.9381418	10.084188	8.516085208	8.341517059	8.323442948
9341	**VAMP3**	0.00016	0.00024	0.06179	0.04276	-1.629	-2.660	-2.144	9.9855156	9.9817084	9.9368992	9.326053627	9.207660509	9.232860477	11.006444	10.939156	11.135149	9.636865756	9.588839508	9.620774008
79912	**PYROXD1**	0.00015	0.00028	0.06179	0.04276	-1.610	-2.557	-2.084	7.1071245	7.9997996	7.9442894	7.322652717	7.287247233	7.244410149	8.3042687	8.2966904	8.4197855	7.043257961	6.931401838	6.982812406
100507127	**LOC100507127**	0.00031	0.00039	0.06562	0.04276	-1.522	-2.583	-2.052	5.5913921	5.6240831	5.560639	4.984319969	5.040367321	4.93571711	9.5281243	9.5769733	9.8635548	8.292791886	8.168023685	8.401048633
54537	**FAM35A**	0.00054	0.00055	0.06562	0.04276	-1.722	-2.304	-2.013	9.0934122	9.3848512	9.4824813	8.885760412	8.554159168	8.508022985	8.890006	8.9405053	9.0434088	7.781954963	7.761690511	7.717281899
85465	**EPT1**	0.00161	0.00032	0.07166	0.04276	-1.444	-2.579	-2.012	8.7685883	8.744747	8.9095922	8.357113139	8.186151124	8.347739356	8.7658713	8.699322	8.8539976	7.494616846	7.414741616	7.309180864
9331	**B4GALT6**	0.00035	0.00058	0.06562	0.04276	-1.719	-2.304	-2.011	8.8737758	9.1588506	9.2433925	8.606717071	8.316198654	8.336829461	9.4204637	9.460288	9.5640861	8.34814582	8.232451084	8.251992303
88455	**ANKRD13A**	0.00109	0.00026	0.06926	0.04276	-1.344	-2.607	-1.975	9.0917385	9.3384377	9.2953219	8.924296039	8.859900704	8.886246287	10.549071	10.736302	10.641882	9.245705308	9.242990887	9.292209277
9926	**LPGAT1**	0.00024	0.00108	0.06179	0.04276	-1.744	-2.150	-1.947	9.5903735	9.6892349	9.859977	9.038550818	8.913690561	8.964833328	8.5765853	8.5497591	8.7095286	7.710005624	7.417877876	7.394594052
9582	**APOBEC3B**	0.00051	0.00115	0.06562	0.04276	-1.641	-2.214	-1.927	7.4284248	7.8658312	7.7211098	7.155608689	7.139660324	6.942671815	8.7359234	8.5639751	9.0460884	7.58147817	7.526519775	7.797250972
23625	**FAM89B**	0.00076	0.00083	0.06883	0.04276	-1.639	-2.178	-1.908	10.066334	10.331978	10.127884	9.606722154	9.379872634	9.564406304	10.913588	10.84968	10.943138	9.790737557	9.648251802	9.898942958
93487	**MAPK1IP1L**	0.00061	0.00053	0.06571	0.04276	-1.390	-2.346	-1.868	10.576874	10.675327	10.643927	10.21607412	10.16722303	10.17145949	10.124633	10.274753	10.186438	9.016103164	8.969775844	8.909012813
84247	**LDOC1L**	0.00043	0.00076	0.06562	0.04276	-1.579	-2.146	-1.862	8.9256663	9.02934	8.9145271	8.354613799	8.231416325	8.353881643	9.2282188	9.1919293	9.263601	8.078974267	8.096701162	8.202380491
56951	**C5orf15**	0.00097	0.00073	0.06888	0.04276	-1.405	-2.307	-1.856	9.1348288	9.1011502	9.1289935	8.71504733	8.599702788	8.559047824	10.018111	9.9198543	10.201327	8.774815908	8.773901311	8.972760552
151246	**SGOL2**	0.00151	0.00066	0.07079	0.04276	-1.390	-2.306	-1.848	8.2303945	8.2294854	8.3384442	7.893309216	7.762117393	7.770092505	7.8455595	7.9532648	8.0516162	6.843153167	6.635113618	6.756808657
56062	**KLHL4**	0.00648	0.00037	0.09679	0.04276	-1.323	-2.345	-1.834	8.1508742	8.2871546	8.4883354	8.108811086	7.896825632	7.94571146	10.004036	10.029543	10.047863	8.812451338	8.780734387	8.79859095
345778	**MTX3**	0.00046	0.00109	0.06562	0.04276	-1.546	-2.114	-1.830	8.7691455	8.8098541	8.8578778	8.231524726	8.091562258	8.292268125	8.4885268	8.2979862	8.4789104	7.475413083	7.308471662	7.241865496
55076	**TMEM45A**	0.00153	0.00103	0.07079	0.04276	-1.408	-2.242	-1.825	7.3261748	7.6350792	7.7711607	7.25836547	7.132852691	7.237784867	7.8707265	7.7500605	8.0796724	6.929015988	6.488372681	6.788812209
80219	**COQ10B**	0.00038	0.00150	0.06562	0.04276	-1.617	-1.978	-1.798	9.3573365	9.4956854	9.5863705	8.928336651	8.723672921	8.889990807	10.156523	10.132899	10.390842	9.272151916	9.231229239	9.224452629
3037	**HAS2**	0.00087	0.00106	0.06883	0.04276	-1.522	-2.073	-1.798	9.2720524	9.585015	9.7254466	9.129636766	8.948973775	9.068962247	9.0056138	8.8125625	8.9135018	7.842212019	7.921479412	7.812270941
84061	**MAGT1**	0.00048	0.00092	0.06562	0.04276	-1.459	-2.120	-1.790	8.2508761	8.5052824	8.4784429	8.017960873	7.92145544	7.901209409	8.7751912	8.8560834	8.9445105	7.699763694	7.819505242	7.803660135
348995	**NUP43**	0.00100	0.00079	0.06920	0.04276	-1.369	-2.207	-1.788	9.7397359	9.7463318	9.810127	9.352987806	9.310011385	9.312868141	9.7927993	9.6243496	9.8319552	8.626167771	8.515651239	8.680501607
91947	**ARRDC4**	0.00056	0.00117	0.06562	0.04276	-1.547	-2.001	-1.774	6.9035405	7.3871558	7.3211491	6.684968153	6.636079262	6.85429886	10.250461	10.218934	10.252135	9.172802572	9.292253237	9.254413494
25923	**ATL3**	0.00073	0.00111	0.06783	0.04276	-1.400	-2.130	-1.765	9.0660034	9.3476683	9.3326617	8.89823722	8.79463222	8.872037831	9.7364654	9.9762267	10.104287	8.815587636	8.845142766	8.882770369
10413	**YAP1**	0.00075	0.00094	0.06883	0.04276	-1.445	-2.084	-1.765	9.3916559	9.3303555	9.2408421	8.744918298	8.807209761	8.711084022	10.190925	10.315098	10.298026	9.173052305	9.242577527	9.210528665
55872	**PBK**	0.00338	0.00100	0.08213	0.04276	-1.302	-2.212	-1.757	8.6720372	9.0516428	9.0756159	8.80214763	8.640204108	8.607566237	8.6595668	8.5870228	8.9539319	7.502599116	7.506872065	7.754903809
84002	**B3GNT5**	0.00318	0.00110	0.08109	0.04276	-1.328	-2.178	-1.753	9.4549366	9.5104457	9.5890234	9.217666665	9.016778199	9.18771316	8.8608708	8.7275344	9.1463796	7.871710883	7.808561441	7.684858926
84912	**SLC35B4**	0.00036	0.00143	0.06562	0.04276	-1.531	-1.970	-1.751	9.8523506	9.8527764	9.8738423	9.277901456	9.152377228	9.315534631	8.9405956	8.8864907	8.98928	8.064963584	7.877352666	7.939269464
127933	**UHMK1**	0.00198	0.00078	0.07301	0.04276	-1.361	-2.134	-1.747	8.8923281	8.9124736	8.9865117	8.58810361	8.399470257	8.528287649	9.5431163	9.4651403	9.442488	8.424067848	8.345528289	8.399950912
56990	**CDC42SE2**	0.00149	0.00108	0.07079	0.04276	-1.418	-2.046	-1.732	9.4535385	9.3786325	9.5125082	8.945468484	8.858216391	9.019944772	9.5680404	9.5128062	9.5604617	8.601286461	8.495502885	8.446960221
8803	**SUCLA2**	0.00092	0.00129	0.06883	0.04276	-1.452	-2.011	-1.731	9.310234	9.7375302	9.6437577	9.229878778	9.078516504	9.150270085	9.2304173	9.3134587	9.4319664	8.370487872	8.251714413	8.329784296
6884	**TAF13**	0.00188	0.00136	0.07232	0.04276	-1.380	-2.078	-1.729	8.9082147	9.2402039	9.1512289	8.823904024	8.619625919	8.749339568	9.1284024	9.2657939	9.5020033	8.332136145	8.198931623	8.19958893
7706	**TRIM25**	0.00049	0.00206	0.06562	0.04289	-1.524	-1.872	-1.698	9.0105973	9.2840377	9.1834203	8.666891225	8.5583594	8.651850756	8.77973	8.7521333	8.9292175	7.844882726	7.865899934	8.035997827
9221	**NOLC1**	0.00273	0.00118	0.07878	0.04276	-1.316	-2.053	-1.684	9.1531142	9.4079728	9.3739168	9.092911471	8.901027435	8.990966421	8.9861161	9.1440936	9.1124855	8.086206052	7.937189526	8.106787673
197021	**LCTL**	0.00119	0.00129	0.06926	0.04276	-1.343	-2.008	-1.676	6.4860431	6.4860282	6.4936377	6.087841396	6.104104409	6.000070511	7.4652952	7.4627247	7.6133636	6.479070222	6.45532722	6.589082819
2925	**GRPR**	0.00114	0.00684	0.06926	0.04386	-1.748	-1.577	-1.663	7.7096661	7.5919371	7.9634969	6.885627678	7.015080659	7.015450444	7.2269273	7.12793	7.054371	6.52804281	6.590288934	6.318299379
4644	**MYO5A**	0.00039	0.00247	0.06562	0.04289	-1.550	-1.772	-1.661	9.5039371	9.7922985	9.8214133	9.252717254	9.064218614	9.206881412	9.863231	9.9444041	9.980076	9.147956226	9.082452491	9.080334973
157567	**ANKRD46**	0.00045	0.00242	0.06562	0.04289	-1.514	-1.803	-1.658	8.1930777	8.487629	8.4838155	7.948063463	7.783605272	7.931799112	8.0558338	7.938472	8.1420813	7.204352184	7.200191297	7.180145453
6385	**SDC4**	0.00081	0.00291	0.06883	0.04289	-1.483	-1.781	-1.632	8.1901956	8.2734993	8.1551224	7.665478295	7.702525603	7.570228172	11.382157	11.362968	11.463579	10.42734149	10.57907731	10.70401622
64924	**SLC30A5**	0.00292	0.00166	0.08009	0.04276	-1.352	-1.903	-1.628	8.290301	8.406542	8.4454913	8.112531775	7.841953465	8.019055342	8.2491017	8.1678337	8.3331153	7.371582179	7.295560445	7.297190706
79188	**TMEM43**	0.00211	0.00127	0.07358	0.04276	-1.314	-1.939	-1.627	9.7728368	9.77829	9.7357266	9.440996113	9.316548642	9.330171499	10.027031	10.022538	10.024859	9.057553363	9.053009585	9.097025043
199857	**ALG14**	0.00041	0.00491	0.06562	0.04328	-1.601	-1.642	-1.622	8.1301503	8.1677882	8.1198946	7.570445457	7.326333199	7.497365564	7.3132617	7.1647389	7.3601485	6.551210468	6.618309656	6.521298385
196527	**ANO6**	0.00281	0.00177	0.07913	0.04276	-1.362	-1.874	-1.618	9.5453517	9.700377	9.8090154	9.440841167	9.253050514	9.233189869	10.198185	10.304437	10.351324	9.360421544	9.377079435	9.398011148
2013	**EMP2**	0.00295	0.00160	0.08009	0.04276	-1.305	-1.890	-1.597	8.2418603	8.272072	8.3583653	7.998538784	7.911372237	7.883964577	7.8983724	7.8533761	7.9104371	7.014742784	6.964837734	6.928569337
1948	**EFNB2**	0.00202	0.00239	0.07301	0.04289	-1.395	-1.783	-1.589	9.693586	10.02835	9.9697433	9.661023888	9.384028794	9.510936888	10.153686	10.244266	10.265109	9.419737388	9.385013452	9.356166485
7852	**CXCR4**	0.00065	0.00603	0.06571	0.04337	-1.546	-1.630	-1.588	7.9291132	7.8328654	7.9045929	7.38072448	7.17094003	7.167750114	8.8103058	8.5771344	8.8456445	8.151179474	8.095062632	7.872372596
10162	**LPCAT3**	0.00018	0.00365	0.06179	0.04319	-1.475	-1.689	-1.582	10.343602	10.421968	10.42531	9.877597746	9.862152642	9.85041664	10.633544	10.708349	10.758526	9.893937869	9.950370431	9.988150017
89782	**LMLN**	0.00127	0.00310	0.06999	0.04300	-1.364	-1.758	-1.561	8.7840778	8.8900735	8.9575244	8.45444138	8.434595143	8.538227659	8.3018001	8.2036467	8.2368068	7.577929641	7.382373889	7.339488089
5834	**PYGB**	0.00165	0.00198	0.07166	0.04289	-1.310	-1.810	-1.560	10.724798	10.810042	10.786993	10.44414174	10.34466204	10.43663085	11.738603	11.749702	11.748031	10.85188245	10.89308587	10.92302638
4734	**NEDD4**	0.00245	0.00417	0.07578	0.04319	-1.426	-1.682	-1.554	6.9731822	7.4611237	7.528352	7.191976534	6.84554116	6.910006947	8.3241417	8.4527426	8.5474706	7.739359841	7.64614139	7.689042054
23545	**ATP6V0A2**	0.00162	0.00298	0.07166	0.04289	-1.344	-1.747	-1.545	9.6172218	9.8578311	9.8802349	9.51923707	9.350909515	9.458553302	8.8841845	8.9707284	8.9648275	8.035036499	8.154682621	8.215833052
5481	**PPID**	0.00256	0.00635	0.07659	0.04360	-1.442	-1.646	-1.544	7.2500425	7.5208774	7.6438237	7.171793586	6.838394338	7.15323472	7.3138349	7.3301274	7.7555142	6.840556665	6.770714396	6.631082335
51633	**OTUD6B**	0.00457	0.00399	0.08767	0.04319	-1.309	-1.757	-1.533	9.4284657	9.605622	9.6874723	9.279537188	9.118190033	9.377484204	9.1731045	9.0395127	9.2811612	8.578559847	8.244738075	8.231711774
36	**ACADSB**	0.00058	0.00798	0.06562	0.04426	-1.555	-1.507	-1.531	7.008503	7.6665594	7.7553504	7.162985002	6.951913327	7.106969095	7.5846162	7.5991657	7.6803445	7.094271346	7.038375322	6.955968839
6605	**SMARCE1**	0.00023	0.00725	0.06179	0.04408	-1.533	-1.529	-1.531	10.372795	10.773426	10.773656	10.2271388	10.10647045	10.1385254	10.493414	10.487286	10.633775	9.919997956	9.937713607	9.919362282
9488	**PIGB**	0.00094	0.00624	0.06888	0.04354	-1.437	-1.614	-1.525	7.378349	7.711361	7.6508042	7.229415581	7.061138613	7.184123653	8.2951877	8.5391756	8.6687381	7.768096469	7.8289337	7.834611951
167153	**PAPD4**	0.00118	0.00358	0.06926	0.04319	-1.327	-1.710	-1.519	9.3268	9.4583565	9.4838268	9.08773734	9.020230895	9.079950375	9.6932873	9.6629132	9.8605518	9.00360901	8.934751518	8.956454416
394	**ARHGAP5**	0.00220	0.00416	0.07405	0.04319	-1.338	-1.691	-1.515	8.2384438	8.6385584	8.6834438	8.346161876	8.215453015	8.160488668	8.3227245	8.3233208	8.4899901	7.560867247	7.565925551	7.734978101
51762	**RAB8B**	0.00186	0.00411	0.07232	0.04319	-1.319	-1.681	-1.500	9.5381304	9.810321	9.8264435	9.501730057	9.371347137	9.384665592	10.694504	10.795227	10.868443	9.970469741	10.03396753	10.10626915
100506658	**OCLN**	0.00052	0.00809	0.06562	0.04433	-1.488	-1.511	-1.500	7.7301334	7.8970887	7.8736762	7.360858066	7.209616377	7.365864522	10.540653	10.554273	10.515033	9.947591015	9.831564813	10.04293847
10495	**ENOX2**	0.00101	0.00582	0.06920	0.04337	-1.421	-1.572	-1.497	8.2143673	8.4320182	8.3986179	7.976188431	7.79769467	7.950223305	8.2084923	8.2729222	8.3220969	7.639312001	7.586368633	7.619639686
10282	**BET1**	0.00112	0.00460	0.06926	0.04323	-1.318	-1.670	-1.494	7.8822672	7.9899181	7.9885401	7.616174701	7.55875024	7.598795721	8.3764044	8.1820274	8.3701588	7.66695676	7.524807111	7.518257424
6388	**SDF2**	0.00155	0.00465	0.07079	0.04323	-1.347	-1.640	-1.494	8.9550953	9.1101071	9.0692449	8.663343325	8.579776168	8.735551479	9.1849944	9.1107602	9.1605855	8.368291703	8.425209627	8.521938364
23767	**FLRT3**	0.00079	0.00665	0.06883	0.04379	-1.386	-1.596	-1.491	9.6687216	9.8649663	9.8541902	9.450245705	9.364640315	9.351382221	9.3785663	9.3896446	9.5662498	8.640915346	8.729827435	8.939042534
25937	**WWTR1**	0.00279	0.00422	0.07913	0.04319	-1.315	-1.666	-1.490	8.6439291	8.4702743	8.5034901	8.166029576	7.982861399	8.127402444	11.505706	11.504408	11.638802	10.80966687	10.75367114	10.87693299
113201	**CASC4**	0.00175	0.00529	0.07180	0.04337	-1.339	-1.626	-1.482	10.09057	10.586896	10.592008	10.26900351	10.11883876	10.11779543	10.60797	10.758757	10.831813	9.971134969	10.06131136	10.06294568
29982	**NRBF2**	0.00354	0.00408	0.08287	0.04319	-1.303	-1.661	-1.482	8.3957115	8.5334034	8.420791	8.159320579	8.076688238	8.050457995	8.6545258	8.5570882	8.6566313	7.926947709	7.839994049	7.904580878
79693	**YRDC**	0.00272	0.00514	0.07878	0.04334	-1.341	-1.608	-1.474	9.4903434	9.5385494	9.4334455	9.114752221	8.962823212	9.110207847	8.8966602	8.8428744	8.9386534	8.212699718	8.152369959	8.2578584
138151	**NACC2**	0.00098	0.00801	0.06888	0.04426	-1.436	-1.506	-1.471	9.4610497	9.5629954	9.4469986	8.969268378	8.951739417	9.027446755	9.558457	9.5835633	9.6070022	8.903238109	9.01415689	9.060175422
63877	**FAM204A**	0.00163	0.00767	0.07166	0.04410	-1.409	-1.524	-1.466	8.0738516	8.4551445	8.3521138	7.923150639	7.790079086	8.014453527	8.3873991	8.517363	8.5808799	7.9346449	7.88500694	7.842768593
53344	**CHIC1**	0.00332	0.00444	0.08203	0.04323	-1.304	-1.615	-1.460	8.0210211	8.2926947	8.1690942	7.84586328	7.840818254	7.858095424	8.7831226	8.8011779	8.7755021	8.091481068	8.088398609	8.104434471
8795	**TNFRSF10B**	0.00240	0.00655	0.07498	0.04369	-1.376	-1.537	-1.457	9.626713	9.8224705	9.7300569	9.429956295	9.186097006	9.329896637	10.389213	10.390515	10.44708	9.766303547	9.800140373	9.80068794
439949	**LOC439949**	0.00442	0.00727	0.08700	0.04408	-1.350	-1.553	-1.452	6.8404969	7.2425918	7.1381615	6.938366108	6.728111401	6.604364891	6.431959	6.2341532	6.2602647	5.776419377	5.592445175	5.653477628
10123	**ARL4C**	0.00288	0.00819	0.08009	0.04440	-1.371	-1.501	-1.436	9.3399578	9.3253554	9.3671136	9.069347818	8.812743431	8.789871498	10.872076	10.736221	10.857059	10.1891029	10.22902531	10.28803892
9303	**SNORD25**	0.00317	0.01236	0.08109	0.04548	-1.327	-1.509	-1.418	7.47757	8.1993953	8.2557619	7.84591916	7.692964488	7.920729926	6.1016079	6.4620837	6.4583613	5.735480826	6.106820254	5.400332245

Supplemental Table 3_Primary Figures

Fig1i			
	shCtrl	shYAP-1	shYAP-2
YAP	141.125	27.541	28.154
p-LIMK	18.036	54.357	40.939
LIMK	60.438	99.252	82.768
GAPDH	115.745	88.375	57.237
YAP/GAPDH	1.22	0.31	0.49
p-LIMK/GAPDH	0.16	0.62	0.72
LIMK/GAPDH	0.52	1.12	1.45
p-LIMK/LIMK	0.30	0.55	0.49

Fig2h	shCtrl		shYAP	
	siCtrl	siRhoA	siCtrl	siRhoA
YAP	176.721	166.417	8.1	4.51
RhoA	101.008	10.538	76.226	24.604
GAPDH	110.198	128.052	102.517	102.344
YAP/GAPDH	1.60	1.30	0.08	0.04
RhoA/GAPDH	0.92	0.08	0.74	0.24

Fig3a					
JHGBM651	shCtrl	shYAP	**JHGBM612**	shCtrl	shYAP
TRIO	24.956	10.395	TRIO	24.956	10.395
beta-actin	102.941	131.231	beta-actin	102.941	131.231
TRIO/beta-actin	0.24	0.08	TRIO/beta-actin	0.24	0.08

Fig3c		
	CONT	YAP OE
YAP	0.058	82.742
TRIO	18.662	78.619
beta-actin	72.004	72.93
YAP/beta-actin	0.00	1.13
TRIO/beta-actin	0.26	1.08

Fig4a			
	shCtrl	shTRIO-1	shTRIO-2
TRIO	68.643	29.038	47.59
GAPDH	124.355	101.905	141.841
TRIO/GAPDH	0.55	0.28	0.34

Fig4b		
	CONT	TRIO OE
TRIO	14.946	26.206
YAP	34.74	48.424
beta-actin	120.517	123.4
TRIO/beta-actin	0.12	0.21
YAP/beta-actin	0.29	0.39

Fig4d				
	CONT	TRIO OE	TRIO iGEF1 OE	TRIO iGEF2 OE
GFP	0.13	49.922	62.237	66.997
TRIO	9.328	48.081	54.59	48.045
beta-actin	69.044	61.61	63.869	65.607
GFP/beta-actin	0.00	0.81	0.97	1.02
TRIO/beta-actin	0.14	0.78	0.85	0.73

Fig5f					
JHGBM651	shCtrl	shYAP	**JHGBM612**	shCtrl	shYAP
YAP	30.262	3.169	YAP	24.727	14.477
p-STAT3	14.792	1.94	p-STAT3	19.739	3.942
STAT3	41.294	23.248	STAT3	42.675	40.783
beta-actin	132.773	125.338	beta-actin	70.827	99.512
YAP/beta-actin	0.23	0.03	YAP/beta-actin	0.35	0.15
p-STAT3/beta-actin	0.11	0.02	p-STAT3/beta-actin	0.28	0.04
STAT3/beta-actin	0.31	0.19	STAT3/beta-actin	0.60	0.41
p-STAT3/STAT3	0.36	0.08	p-STAT3/STAT3	0.46	0.10

Fig5g		
	CONT	YAP OE
YAP	3.821	68.639
p-STAT3	8.784	24.172
STAT3	64.219	71.537
beta-actin	88.372	86.475
YAP/beta-actin	0.04	0.79
p-STAT3/beta-actin	0.10	0.28
STAT3/beta-actin	0.73	0.83
p-STAT3/STAT3	0.14	0.34

Fig5i	NCC			GBM																
	1	2	3	4	5	6	7	8	9	10	11	12	13	14	15	16	17	18	19	20
YAP	4.015	41.293	11.949	35.221	121.956	81.38	99.655	121.354	121.132	96.62	116.498	92.813	64.676	73.232	68.79	123.841	33.955	31.936	14.9	59.158
p-STAT3	1.97	1.301	2.812	56.529	22.878	42.685	6.759	9.551	17.894	31.936	54.703	48.193	2.23	20.323	9.326	56.909	4.062	60.492	2.584	0.148
STAT3	12.885	21.157	3.385	47.564	66.976	54.502	40.235	79.05	52.491	89.12	68.375	79.371	12.816	63.098	51.585	73.856	19.681	80.28	3.213	44.018
beta-actin	116.996	118.051	91.952	104.555	120.422	111.822	96.444	114.892	118.42	128.255	108.473	108.613	93.614	90.662	116.191	107.241	93.102	99.054	22.274	108.723
YAP/beta-actin	0.03	0.35	0.13	0.34	1.01	0.73	1.03	1.06	1.02	0.75	1.07	0.85	0.69	0.81	0.59	1.15	0.36	0.32	0.67	0.54
p-STAT3/beta-actin	0.02	0.01	0.03	0.54	0.19	0.38	0.07	0.08	0.15	0.25	0.50	0.44	0.02	0.22	0.08	0.53	0.04	0.61	0.12	0.00
STAT3/beta-actin	0.11	0.18	0.04	0.45	0.56	0.49	0.42	0.69	0.44	0.69	0.63	0.73	0.14	0.70	0.44	0.69	0.21	0.81	0.14	0.40
p-STAT3/STAT3	0.15	0.06	0.83	1.19	0.34	0.78	0.17	0.12	0.34	0.36	0.80	0.61	0.17	0.32	0.18	0.77	0.21	0.75	0.80	0.00

Fig6a							
JHGBM651	shCtrl	shTRIO-1	shTRIO-2	**JHGBM612**	shCtrl	shTRIO-1	shTRIO-2
TRIO	147.544	30.888	78.723	TRIO	106.195	53.859	64.128
p-STAT3	52.077	3.638	25.484	p-STAT3	145.091	48.283	29.594
STAT3	128.141	123.455	106.034	STAT3	125.342	162.726	129.16
GAPDH	123.818	91.695	112.235	GAPDH	96.205	73.07	77.935
TRIO/GAPDH	1.19	0.34	0.70	TRIO/GAPDH	1.10	0.74	0.82
p-STAT3/GAPDH	0.42	0.04	0.23	p-STAT3/GAPDH	1.51	0.66	0.38
STAT3/GAPDH	1.03	1.35	0.94	STAT3/GAPDH	1.30	2.23	1.66
p-STAT3/STAT3	0.41	0.03	0.24	p-STAT3/STAT3	1.16	0.30	0.23

Fig6c		
	CONT	TRIO OE
TRIO	16.976	38.916
p-STAT3	17.906	40.779
STAT3	38.501	46.809
beta-actin	142.561	141.885
TRIO/beta-actin	0.12	0.27
p-STAT3/beta-actin	0.13	0.29
STAT3/beta-actin	0.27	0.33
p-STAT3/STAT3	0.47	0.87

Fig6e	CONT		TRIO OE	
	shCtrl	shYAP	shCtrl	shYAP
YAP	17.993	13.131	16.241	6.126
TRIO	47.372	37.35	58.73	55.491
p-STAT3	44.747	21.003	74.526	51.987
STAT3	51.65	36.026	44.648	40.416
beta-actin	170.537	170.407	167.262	165.059
YAP/beta-actin	0.11	0.08	0.10	0.04
TRIO/beta-actin	0.28	0.22	0.35	0.34
p-STAT3/beta-actin	0.26	0.12	0.45	0.31
STAT3/beta-actin	0.30	0.21	0.27	0.24
p-STAT3/STAT3	0.87	0.58	1.67	1.29

Fig6f	CONT		YAP OE	
	shCtrl	shTRIO	shCtrl	shTRIO
YAP	33.087	53.715	122.319	102.196
TRIO	27.317	19.217	73.412	2.394
p-STAT3	19.542	9.267	54.212	30.537
STAT3	126.356	126.214	147.092	123.965
beta-actin	153.99	146.765	160.185	154.18
YAP/beta-ac	0.21	0.37	0.76	0.66
TRIO/beta-a	0.18	0.13	0.46	0.02
p-STAT3/bet	0.13	0.06	0.34	0.20
STAT3/beta-	0.82	0.86	0.92	0.80
p-STAT3/STA	0.15	0.07	0.37	0.25

Supplemental Table 3_Supplemental Figures

FigS1c					
JHGBM	692	653	640	612	609
YAP	17.685	70.238	38.446	25.119	0.249
p-YAP	8.259	26.748	19.402	7.072	0.253
beta-actin	68.194	49.784	69.108	74.113	69.044
YAP/beta-actin	0.26	1.41	0.56	0.34	0.00
p-YAP/beta-actin	0.12	0.54	0.28	0.10	0.00
p-YAP/YAP	0.47	0.38	0.50	0.28	1.02

	651		609		612	
	N	C	N	C	N	C
YAP	146.984	40.055	75.641	26.678	162.119	28.765
GAPDH		95.043		87.719		76.633
Lamin B1	152.916		102.394		137.902	
YAP/GAPDH		0.42		0.30		0.38
YAP/Lamin B1	0.96		0.74		1.18	

FigS1d			shYAP				
	WT	shCtrl	1	2	3	4	5
YAP (s.e.)	40.408	35.222	5.632	2.237	0.999	5.281	6.813
YAP (l.e.)	96.041	95.629	31.417	19.946	12.739	31.707	35.051
beta-actin	63.367	50.34	49.963	53.25	36.732	52.079	58.804
YAP (s.e.)/beta-actin	0.64	0.70	0.11	0.04	0.03	0.10	0.12
YAP (l.e.)/beta-actin	1.52	1.90	0.63	0.37	0.35	0.61	0.60

FigS1e	shCtrl		shYAP	
	1	2	1	2
YAP	24.218	24.179	2.916	1.999
TAZ	87.671	96.498	84.646	88.76
beta-actin	75.314	84.541	77.693	74.939
YAP/beta-actin	0.32	0.29	0.04	0.03
TAZ/beta-actin	1.16	1.14	1.09	1.18

FigS1h		
	CONT	YAP OE
YAP	37.555	76.988
GAPDH	156.038	130.802
YAP/GAPDH	0.24	0.59

FigS1i					
JHGBM612	CONT	YAP OE	**JHGBM1A**	CONT	YAP OE
YAP	18.788	67.519	YAP	112.802	139.74
beta-actin	60.217	65.388	GAPDH	140.688	136.007
YAP/beta-ac	0.31	1.03	YAP/GAPDH	0.80	1.03

FigS2a													
JHGBM651	shCtrl	shYAP-1	shYAP-2	**JHGBM612**	shCtrl	shYAP-1	shYAP-2	**NHA**	shCtrl	shYAP-1	shYAP-2	**MCF10A**	shCtrl	shYAP
YAP	138.875	28.324	30.206	YAP	121.042	67.514	76.781	YAP	77.018	40.724	22.392	YAP	34.966	5.245
p-LIMK	18.439	52.428	40.579	p-LIMK	27.281	71.903	91.444	p-LIMK	8.303	30.931	37.13	p-LIMK	16.574	26.922
LIMK	66.33	106.35	89.517	LIMK	51.479	33.336	52.382	LIMK	83.642	83.808	61.658	LIMK1	7.148	7.042
GAPDH	113.456	86.812	54.397	GAPDH	87.224	94.765	91.387	GAPDH	82.882	68.303	51.773	beta-actin	99.726	90.785
YAP/GAPDH	1.22	0.33	0.56	YAP/GAPDH	1.39	0.71	0.84	YAP/GAPDH	0.93	0.60	0.43	YAP/beta-actin	0.35	0.06
p-LIMK/GAPDH	0.16	0.60	0.75	p-LIMK/GAPDH	0.31	0.76	1.00	p-LIMK/GAPDH	0.10	0.45	0.72	p-LIMK/beta-actin	0.17	0.30
LIMK/GAPDH	0.58	1.23	1.65	LIMK/GAPDH	0.59	0.35	0.57	LIMK/GAPDH	1.01	1.23	1.19	LIMK1/beta-actin	0.07	0.08
p-LIMK/LIMK	0.28	0.49	0.45	p-LIMK/LIMK	0.53	2.16	1.75	p-LIMK/LIMK	0.10	0.37	0.60	p-LIMK/LIMK1	2.32	3.82

FigS2d											
JHGBM651	Y27632 (μM)				H1152 (nM)	**JHGBM612**	Y27632 (μM)				H1152 (nM)
	30	10	3	0	20		30	10	3	0	20
p-NMII	33.104	54.273	97.281	135.309	64.758	p-NMII	14.379	49.728	109.499	26.947	22.335
NMII	70.549	75.771	81.588	121.884	80.991	NMII	114.812	103.029	143.234	118.372	51.188
GAPDH	68.715	108.789	92.332	81.722	62.631	GAPDH	63.076	75.055	56.253	68.29	57.036
p-NMII/GAPDH	0.48	0.50	1.05	1.66	1.03	p-NMII/GAPDH	0.23	0.66	1.95	0.39	0.39
NMII/GAPDH	1.03	0.70	0.88	1.49	1.29	NMII/GAPDH	1.82	1.37	2.55	1.73	0.90
p-NMII/NMII	0.47	0.72	1.19	1.11	0.80	p-NMII/NMII	0.13	0.48	0.76	0.23	0.44

FigS3b		
	shCtrl	shYAP
p-PAK	73.18	36.68
PAK	116.29	92.89
GAPDH	90.68	89.37
p-PAK/GAPD	0.81	0.41
PAK/GAPDH	1.28	1.04
p-PAK/PAK	0.63	0.39

FigS5a																						
JHGBM651	shCtrl	shYAP-1	shYAP-2	**JHGBM612**	shCtrl	shYAP-1	shYAP-2	**JHGBM640**	shCtrl	shYAP	**JHGBM1A**	shCtrl	shYAP-1	shYAP-2	**MCF10A**	shCtrl	shYAP-1	shYAP-2	**NHA**	shCtrl	shYAP-1	shYAP-2
YAP	138.23	21.83	21.99	YAP	136.24	75.93	85.47	TRIO	32.018	14.077	YAP	127.486	74.335	69.837	YAP	29.034	12.648	15.841	YAP	114.588	38.462	34.244
TRIO	129.16	79.98	60.56	TRIO	108.14	50.09	38.02	beta-actin	158.083	157.61	TRIO	67.203	20.982	34.358	TRIO	91.485	45.354	46.971	TRIO	152.005	102.648	43.334
GAPDH	111.27	89.00	99.07	GAPDH	115.08	103.60	104.12	TRIO/beta-actin	0.20	0.09	GAPDH	102.23	80.67	86.304	beat-actin	25.723	30.256	37.235	GAPDH	143.091	110.337	127.06
YAP/GAPDH	1.24	0.25	0.22	YAP/GAPDH	1.18	0.73	0.82				YAP/GAPDH	1.25	0.92	0.81	YAP/beta-actin	1.13	0.42	0.43	YAP/GAPDH	0.80	0.35	0.27
TRIO/GAPDH	1.16	0.90	0.61	TRIO/GAPDH	0.94	0.48	0.37				TRIO/GAPDH	0.66	0.26	0.40	TRIO/beta-actin	3.56	1.50	1.26	TRIO/GAPDH	1.06	0.93	0.34

FigS5g		
	CONT	YAP OE
Rac1-GTP	13.65	30.37
Rac1	76.94	43.21
Rac1-GTP/Rac1	0.18	0.70
YAP	31.86	87.38
TRIO	26.87	49.91
beta-actin	105.56	108.51
YAP/beta-actin	0.30	0.81
TRIO/beta-actin	0.25	0.46

FigS5h		
	CONT	TRIO OE
Rac1-GTP	15.33	62.00
Rac1	66.62	70.15
Rac1-GTP/Rac1	0.23	0.88
TRIO	13.04	24.22
beta-actin	97.70	116.41
TRIO/beta-actin	0.13	0.21

FigS5i		
	CONT	shTRIO
Rac1-GTP	34.24	12.80
Rac1	59.93	40.76
Rac1-GTP/Rac1	0.57	0.31
TRIO	45.10	2.54
beta-actin	80.94	72.83
TRIO/beta-actin	0.56	0.03

FigS5k			
	shCtrl	shYAP	shTRIO
p-YAP	81.801	26.077	88.539
YAP	48.263	12.511	56.999
GAPDH	104.667	113.338	91.109
p-YAP/GAPDH	0.78	0.23	0.97
YAP/GAPDH	0.46	0.11	0.63
p-YAP/YAP	1.69	2.08	1.55

FigS5m	NCC			GBM												
	1	2	3	4	5	6	7	8	9	10	11	12	13	14	15	16
TRIO	6.41	64.194	36.047	15.739	27.024	54.159	64.712	55.084	98.667	51.777	57.126	27.302	17.071	51.372	35.667	69.719
beta-actin	97.886	107.091	94.067	99.436	93.921	53.721	109.492	110.626	78.433	100.343	85.576	97.811	90.413	128.259	94.422	77.268
TRIO/beta-actin	0.07	0.60	0.38	0.16	0.29	1.01	0.59	0.50	1.26	0.52	0.67	0.28	0.19	0.40	0.38	0.90

FigS6a														
JHGBM612	shCtrl	shTRIO-1	shTRIO-2	**JHGBM640**	shCtrl	shTRIO-1	**MCF10A**	shCtrl	shTRIO-1	shTRIO-2	**NHA**	shCtrl	shTRIO-1	shTRIO-2
TRIO	100.702	47.841	56.635	TRIO	11.142	5.02	TRIO	32.558	10.725	9.92	TRIO	82.961	48.675	21.715
GAPDH	90.501	83.96	69.85	beta-actin	49.213	67.514	beta-actin	24.264	22.589	33.255	GAPDH	96.252	104.152	105.622
TRIO/GAPDH	1.11	0.57	0.81	TRIO/beta-actin	0.23	0.07	TRIO/beta-actin	1.34	0.47	0.30	TRIO/GAPDH	0.86	0.47	0.21

FigS8e		
	CONT	TRIO OE
TRIO-GFP(TRIO	5.939	21.555
YAP	55.494	59.367
beta-actin	59.052	58.301
TRIO-GFP(TRIO	0.10	0.37
YAP/beta-actin	0.94	1.02

FigS9f																							
JHGBM651	shCtrl	shYAP-1	shYAP-2	**JHGBM612**	shCtrl	shYAP-1	shYAP-2	**JHGBM640**	shCtrl	shYAP-1	**JHGBM1A**	shCtrl	shYAP-1	shYAP-2	**NHA**	shCtrl	shYAP-1	shYAP-2	**MCF10A**	shCtrl	shYAP-1	**MCF10A**	CONT	YAP OE
YAP	95.272	21.598	55.081	YAP	62.62	43.004	47.273	YAP	16.161	1.059	YAP	132.935	60.595	78.628	YAP	97.445	28.285	21.469	YAP	29.924	5.839	YAP	14.691	76.148
p-STAT3	30.78	0.53	14.831	p-STAT3	93.494	36.759	39.051	p-STAT3	24.828	12.093	p-STAT3	44.215	6.651	18.404	p-STAT3	29.084	13.756	11.246	p-STAT3	32.691	21.508	p-STAT3	2.887	44.857
STAT3	115.366	87.591	63.304	STAT3	114.217	106.351	96.107	STAT3	55.421	65.067	STAT3	116.103	84.367	90.627	STAT3	139.189	120.107	100.928	STAT3	16.427	19.23	STAT3	36.018	28.424
GAPDH	74.911	44.446	85.352	GAPDH	58.216	73.538	72.436	GAPDH	109.164	108.789	GAPDH	101.519	54.579	69.205	GAPDH	104.155	83.628	94.481	GAPDH	90.943	83.222	GAPDH	87.16	76.136
YAP/GAPDH	1.27	0.49	0.65	YAP/GAPDH	1.08	0.58	0.65	YAP/GAPDH	0.15	0.01	YAP/GAPDH	1.31	1.11	1.14	YAP/GAPDH	0.94	0.34	0.23	YAP/GAPDH	0.33	0.07	YAP/GAPDH	0.17	1.00
p-STAT3/GAPDH	0.41	0.01	0.17	p-STAT3/GAPDH	1.61	0.50	0.54	p-STAT3/GAPDH	0.23	0.11	p-STAT3/GAPDH	0.44	0.12	0.27	p-STAT3/GAPDH	0.28	0.16	0.12	p-STAT3/GAPDH	0.36	0.26	p-STAT3/GAPDH	0.03	0.59
STAT3/GAPDH	1.54	1.97	0.74	STAT3/GAPDH	1.96	1.45	1.33	STAT3/GAPDH	0.51	0.60	STAT3/GAPDH	1.14	1.55	1.31	STAT3/GAPDH	1.34	1.44	1.07	STAT3/GAPDH	0.18	0.23	STAT3/GAPDH	0.41	0.37
p-STAT3/STAT3	0.27	0.01	0.23	p-STAT3/STAT3	0.82	0.35	0.41	p-STAT3/STAT3	0.45	0.19	p-STAT3/STAT3	0.38	0.08	0.20	p-STAT3/STAT3	0.21	0.11	0.11	p-STAT3/STAT3	1.99	1.12	p-STAT3/STAT3	0.08	1.58

FigS10a									
JHGBM1A	shCtrl	shTRIO-1	shTRIO-2	**NHA**	shCtrl	shTRIO-1	shTRIO-2	**MCF10A**	shCtrl	shTRIO-1
p-STAT3	45.256	8.218	23.371	TRIO	48.506	20.333	31.984	p-STAT3	33.364	23.305
STAT3	132.462	91.64	81.075	p-STAT3	28.362	14.159	5.226	STAT3	22.289	24.591
GAPDH	97.314	47.547	74.14	STAT3	157.598	124.81	97.943	GAPDH	36.966	50.31
p-STAT3/GAPDH	0.47	0.17	0.32	GAPDH	80.574	49.009	52.761	p-STAT3/GAPDH	0.90	0.46
STAT3/GAPDH	1.36	1.93	1.09	TRIO/GAPDH	0.60	0.41	0.61	STAT3/GAPDH	0.60	0.49
p-STAT3/STAT3	0.34	0.09	0.29	p-STAT3/GAPDH	0.35	0.29	0.10	p-STAT3/STAT3	1.50	0.95
				STAT3/GAPDH	1.96	2.55	1.86			
				p-STAT3/STAT3	0.18	0.11	0.05			

Supplemental Table 3_Supplemental Figures

FigS10c	JHGBM651			JHGBM612		
NSC23766 (μM)	0	100	250	0	100	250
p-STAT3	64.104	38.587	22.891	64.823	32.275	31.595
STAT3	82.301	63.209	62.567	106.979	124.166	107.226
GAPDH	88.939	87.097	90.958	90.061	81.6	71.147
p-STAT3/GAPDH	0.72	0.44	0.25	0.72	0.40	0.44
STAT3/GAPDH	0.93	0.73	0.69	1.19	1.52	1.51
p-STAT3/STAT3	0.78	0.61	0.37	0.61	0.26	0.29

	JHGBM651			JHGBM612		
ITX3 (μM)	0	25	50	0	25	50
p-STAT3	109.047	64.387	74.242	70.654	13.828	24.198
STAT3	151.622	109.045	88.823	107.862	92.877	79.166
GAPDH	83.224	77.834	93.567	105.414	97.531	140.533
p-STAT3/GAPDH	1.31	0.83	0.79	0.67	0.14	0.17
STAT3/GAPDH	1.82	1.40	0.95	1.02	0.95	0.56
p-STAT3/STAT3	0.72	0.59	0.84	0.66	0.15	0.31

FigS10f	shCtrl	shYAP	shTRIO	shSTAT3
MMP2	65.232	48.242	40.202	39.084
GAPDH	65.092	72.417	74.906	76.695
MMP2/GAPDH	1.00	0.67	0.54	0.51